

Code 5340

NRL Report 7221

A VHF Thomson Scatter Radar Study of the Midlatitude Ionosphere Using the Faraday Effect

JOHN M. GOODMAN

*Radar Geophysics Branch
Radar Division*

April 21, 1971



NAVAL RESEARCH LABORATORY
Washington, D.C.

Approved for public release; distribution unlimited.

DOCUMENT CONTROL DATA - R & D

(Security classification of title, body of abstract and indexing annotation must be entered when the overall report is classified)

1. ORIGINATING ACTIVITY (Corporate author) Naval Research Laboratory Washington, D. C. 20390		2a. REPORT SECURITY CLASSIFICATION Unclassified	
		2b. GROUP	
3. REPORT TITLE A VHF THOMSON SCATTER STUDY OF THE MIDLATITUDE IONOSPHERE USING THE FARADAY EFFECT			
4. DESCRIPTIVE NOTES (Type of report and inclusive dates) An interim report on one phase of the NRL Problem			
5. AUTHOR(S) (First name, middle initial, last name) John M. Goodman			
6. REPORT DATE April 21, 1971		7a. TOTAL NO. OF PAGES 98	7b. NO. OF REFS 80
8a. CONTRACT OR GRANT NO. NRL Problem R02-05		9a. ORIGINATOR'S REPORT NUMBER(S) NRL Report 7221	
b. PROJECT NO. RF 05-151-402-4001		9b. OTHER REPORT NO(S) (Any other numbers that may be assigned this report)	
c.			
d.			
10. DISTRIBUTION STATEMENT Approved for public release; distribution unlimited.			
11. SUPPLEMENTARY NOTES		12. SPONSORING MILITARY ACTIVITY Department of the Navy Office of Naval Research Arlington, Virginia 22217	
13. ABSTRACT <p>In recent years Thomson scatter radars have provided the upper-air physicist with a detailed view of the topside ionosphere. These instruments are generally capable of providing continuous information about the electron concentration between a height of roughly 100 km and the base of the exosphere. This report describes some results obtained with the Randle Cliff Radar, a new midlatitude Thomson scatter facility which utilizes Faraday rotation for the purpose of deducing electron density. An operating frequency of 140 MHz is employed at Randle Cliff, and this frequency is about optimum for making such measurements.</p> <p>In this report an investigation of Faraday dispersion is detailed, and this usually deleterious phenomenon is utilized in an alternative scheme to determine electron density profiles. Other features of the study include: a comparison of Thomson scatter results with total electron content deduced from ATS-5 satellite transmissions, a detection of quasi-periodicities over Randle Cliff and their relationship to internal gravity waves, and discussions of the midday biteout and F region response to solar eclipse.</p> <p>It is determined that quasi-periodicities are regular features of the midlatitude ionosphere. It is also suggested that the layer height fluctuations induced by these disturbances may be useful under some conditions in deducing characteristics of the neutral atmosphere. A study of the March 7, 1970 solar eclipse disclosed a 27% decrease in the total content in conjunction with a generally enhanced slab thickness during the biteout period. Furthermore, it can be deduced that during the reported solar eclipse the ionic movement term in the continuity equation was not as important as attachment in affecting the electron density below 300 km.</p>			

14. KEY WORDS	LINK A		LINK B		LINK C	
	ROLE	WT	ROLE	WT	ROLE	WT
Thomson scatter						
Midlatitude ionosphere						
Randle Cliff Radar						
Faraday effect						
Electron density						
F region						
Ionospheric quasi-periodicities						
Layer height fluctuations						
Traveling ionospheric disturbances						
Solar eclipse ionospheric response						
Faraday rotation angle						
Faraday dispersion						
Ionosonde						
Faraday rotation contours						
Electron density contours						
Attachment coefficient						
Ray path orientation						
Continuity equation						
Midday biteout						
Electron loss coefficient						
Magnetoionic medium						

CONTENTS

Abstract	ii
Problem Status	ii
Authorization	ii
CHAPTER 1 - INTRODUCTION	1
CHAPTER 2 - BRIEF REVIEW OF THOMSON SCATTER THEORY	4
CHAPTER 3 - FARADAY ROTATION AND THOMSON SCATTER	10
CHAPTER 4 - RANDLE CLIFF RADAR FACILITY	17
CHAPTER 5 - CONSTRAINTS UPON THOMSON SCATTER MEASUREMENTS USING FARADAY ROTATION	25
Ray Path Orientation	25
Pulse Length Effects and Faraday Dispersion	29
CHAPTER 6 - SPATIAL AND TEMPORAL DEPENDENCE OF THE ELECTRON DENSITY OVER RANDLE CLIFF	36
Comparison of Randle Cliff Data with Wallops Island Ionosonde	36
Comparison of Total Content Fluctuations Observed via ATS-5 with Thomson Scatter	39
Quasi-periodicities Observed at Randle Cliff	44
The Midday Biteout Over Randle Cliff	58
CHAPTER 7 - RESPONSE OF THE IONOSPHERE TO A SOLAR ECLIPSE	62
Introduction	62
Geometry of the Eclipse	62
Measurements	64
Electron Density Distribution	64
Estimation of the Electron Loss Coefficient	70
Concluding Remark	74
EPILOGUE	76
APPENDIX - Derivation of the Polarization Rotation in a Magneto-ionic Medium	79
REFERENCES	89

ABSTRACT

In recent years Thomson scatter radars have provided the upper-air physicist with a detailed view of the topside ionosphere. These instruments are generally capable of providing continuous information about the electron concentration between a height of roughly 100 km and the base of the exosphere. This report describes some results obtained with the Randle Cliff Radar, a new midlatitude Thomson scatter facility which utilizes Faraday rotation for the purpose of deducing electron density. An operating frequency of 140 MHz is employed at Randle Cliff, and this frequency is about optimum for making such measurements.

In this report an investigation of Faraday dispersion is detailed, and this usually deleterious phenomenon is utilized in an alternative scheme to determine electron density profiles. Other features of the study include: a comparison of Thomson scatter results with total electron content deduced from ATS-5 satellite transmissions, a detection of quasi-periodicities over Randle Cliff and their relationship to internal gravity waves, and discussions of the midday biteout and F region response to solar eclipse.

It is determined that quasi-periodicities are regular features of the midlatitude ionosphere. It is also suggested that the layer height fluctuations induced by these disturbances may be useful under some conditions in deducing characteristics of the neutral atmosphere. A study of the March 7, 1970 solar eclipse disclosed a 27% decrease in the total content in conjunction with a generally enhanced slab thickness during the biteout period. Furthermore, it can be deduced that during the reported solar eclipse the ionic movement term in the continuity equation was not as important as attachment in affecting the electron density below 300 km.

PROBLEM STATUS

This is an interim report on one phase of the problem.

AUTHORIZATION

NRL Problem R02-05
Project RF 05-151-402-4001

Manuscript Submitted October 27, 1970

CHAPTER 1

INTRODUCTION

The earth's lower ionosphere has been the subject of widespread investigation for several decades. The electron densities of the lower ionospheric layers have been monitored on a routine basis by vertical incidence ionosonde, but until the advent of rather powerful radar sets from which moon reflections could be obtained, the upper ionosphere had largely been the subject of speculation. Browne et al. [1956] and Evans [1956, 1957] using a moon-radar at 120 MHz found that regular fluctuations in the lunar echo strength were due to a variable polarization arising from the effect of the cis-lunar electron content acting in concert with the geomagnetic field. They concluded that the amount of polarization rotation was to first order proportional to the product of the electron content $\int N_{dh}$ and the magnetic field B, and was inversely proportional to the square of the radar frequency f. Thus was born a powerful technique to study the total electron content of the ionosphere, and with the exception of relatively infrequent rocket probes, it provided the only sampling of the topside ionosphere until the age of artificial earth satellites. The first satellite investigations of the ionosphere also made use of the polarization rotation phenomenon which is now referred to as the Faraday effect by virtue of the optical analog, and the subsatellite electron content has been measured by numerous investigators including the author of this manuscript (see for example, Goodman [1966a, 1967, 1969]).

It was Gordon [1958] who first postulated that radars were sufficiently powerful to investigate the ionosphere by means of incoherent backscatter (Thomson scatter), and in that same year the feasibility of the technique was experimentally established by Bowles [1958]. Approximately fifteen years following the initial lunar work of Brown et al. and Evans, Millman et al. [1961] found that Thomson scattered signals were not sufficiently depolarized upon reflection to prevent Faraday rotation from being observed. Subsequently Greenhow et al. [1963] and Millman et al. [1964] conducted Faraday-rotation/Thomson-scatter measurements at UHF. Due to the high frequencies employed by these groups, however, the electron density profiles so obtained were relatively inaccurate. They did nevertheless show that the use of the Thomson scattering mechanism is in principle an exceedingly advantageous way to study Faraday rotation, since the rotational derivative with respect to height is directly proportional to electron density. (Although the measurement of the total power associated with incoherent-backscatter echoes and a companion measurement of the backscatter spectrum will yield an electron density profile, it is noteworthy that this profile is only relative and must be normalized by an independent measurement such as that obtained from a colocated ionosonde. The use of Faraday rotation obviates this necessity. The accuracy of the electron density measurements via the Faraday rotation technique, however, does depend upon a precise knowledge of the magnetic field vector in the ionosphere.)

The Jicamarca Radar Observatory near Lima, Peru, on the magnetic equator has been utilized in an interesting fashion to determine Faraday profiles, and the technique has been discussed by Cohen [1967a, 1967b] and Farley [1969]. Rather than measure the Faraday rotation angle Ω , the Jicamarca system has been instrumented so that the phase difference between the two circularly polarized modes, which is equal to twice the Faraday rotation angle, is measured directly. Prior to 1970 the Jicamarca Radar

Observatory run by ESSA was the only Thomson scatter facility to use Faraday rotation as a routine way to deduce electron density profiles. A frequency of 50 MHz is employed. This rather low frequency is necessary for studies over the magnetic equator because the angle between the ray path and the magnetic field vector \mathbf{B} is quite close to 90 degrees for zenithal propagation. Under these circumstances a frequency as low as is practical (and yet not in contradiction to the high frequency approximation) is required to enhance the Faraday effect. At midlatitudes, where \mathbf{B} makes an appreciable angle with the horizontal and where as a result the ray path departs substantially from perpendicularity, a somewhat higher frequency is desirable. The higher frequency lessens the problem of Faraday dispersion while still maintaining a sufficient amount of Faraday rotation.

The Randle Cliff Radar*, shown in Fig. 1.1, is operated by NRL and located at $38^{\circ}39'37.1''\text{N}$ latitude and $76^{\circ}32'9.4''\text{W}$ longitude. It operates at a frequency of ≈ 140 MHz which is advantageous for studies of Faraday rotation for the midlatitude ionosphere using Thomson scatter. The support of this statement may be found in remarks by Evans [1967a] and in a paper by Farley [1969]. As of this writing the RCR is the only Thomson scatter facility in the United States conducting Faraday rotation measurements.

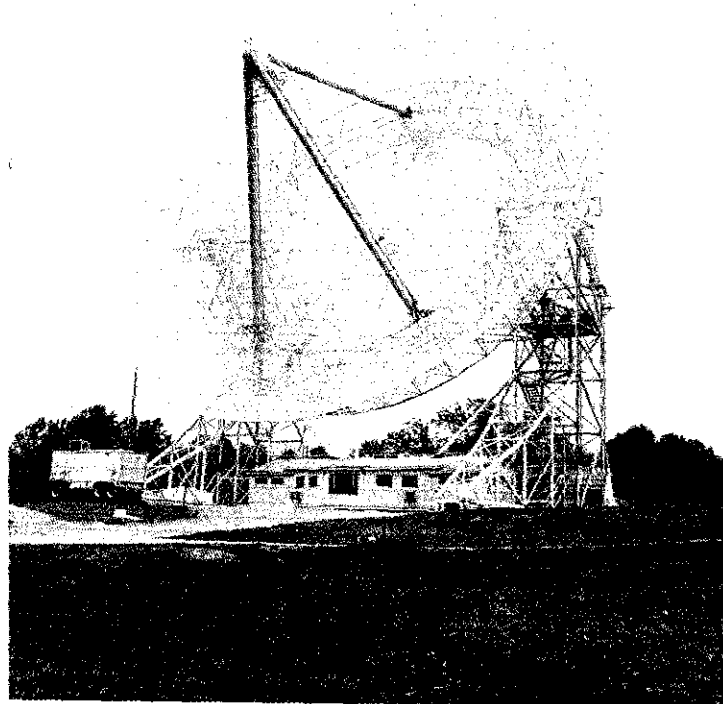


Fig. 1.1 - Randle Cliff Radar Antenna

*The Randle Cliff Radar (RCR) is located at the Chesapeake Bay Division of the Naval Research Laboratory near a village called Randle Cliff overlooking the Chesapeake Bay.

Preliminary profiles and analysis techniques have been described by the author in two recent unpublished presentations [1970a, 1970b].

Presently the RCR is among a fraternity of nine major Thomson scatter facilities which have been utilized for the study of the ionosphere. Its operating frequency of 138.6 MHz is, as has been implied, unique among these facilities, and its full-steerability enables the scientist to illuminate portions of the ionosphere under a variety of magnetic field configurations.

In this report the techniques employed at Randle Cliff to measure Faraday rotation and the use to which these measurements are put will be discussed. The utility of Faraday rotation at 140 MHz will be demonstrated, and the phenomenon of Faraday dispersion will be used as an alternative method to deduce electron density. An important feature of the study will be the discussion of medium-period traveling ionospheric disturbances (TID) which have been detected over Randle Cliff. These irregularities will be reviewed in the light of existing theory with particular emphasis on internal atmospheric gravity waves. Some additional subjects given attention include the midday bite-out and total electron content using a synchronous satellite. Of special interest perhaps is the RCR study of the March 7, 1970, solar eclipse to which Chapter 7 of this report is devoted.

CHAPTER 2

BRIEF REVIEW OF THOMSON SCATTER THEORY

In accordance with standard radar terminology, one finds for a monostatic, pulsed radar that the echo power returned from a discrete target is given by (Skolnik [1962]).

$$S = (P_t G_t G_r \sigma \lambda^2) / R^4 (4\pi)^3, \quad (2.1)$$

where P_t is the pulse power transmitted, R is the range of the target, λ is the wavelength employed, σ is the target cross section, and G_t and G_r are the antenna gains for the transmission and reception conditions respectively. It is well known that the antenna gain is connected to the effective aperture of the antenna by the relation

$$G = \frac{4\pi A_e}{\lambda^2} \quad (2.2a)$$

In addition one has the useful relation that

$$G = \frac{4\pi}{\theta^2}, \quad (2.2b)$$

where θ is so-called half-power antenna beamwidth.

For the situation described in this manuscript, the reciprocity theorem holds, and hence one may assume $G_t = G_r = G$. (That is, there is a common antenna for both transmit and receive conditions.) Thus one may write Eq. 2.1 as follows:

$$S = \frac{P_t A_e}{4\pi\theta^2 R^4} \sigma \quad (2.3)$$

Hence, if T is the radar system noise temperature and B is the system bandwidth, one concludes that the signal-to-noise ratio associated with a discrete target of cross section σ at a range R is given by

$$(S/N) = \frac{P_t A_e}{4\pi\theta^2 R^4 kTB} \sigma \quad (2.4)$$

For a distributed target such as the ionosphere it is convenient to define a new cross section Σ which is the average cross section per unit volume and will have units of cm^{-1} . Furthermore, since scattering may be considered to originate within a certain resolution cell of volume V such that $\sigma = V\Sigma$, it may be shown that the signal-to-noise ratio is actually proportional to R^{-2} rather than R^{-4} . This is apparent when the mathematical formulation of the resolution cell is considered. Assuming a symmetrical antenna beam and taking θ to be the half-power beamwidth, it is seen that the required scattering volume is proportional to R^2 so that Eq. (2.4) becomes

$$(S/N) = \frac{P_t c \tau N \sigma_e}{32 R^2 (kTB)}, \quad (2.5)$$

where

$$V = \left(\frac{\pi}{4}\right) R^2 \theta^2 \left(\frac{c\tau}{2}\right),$$

Σ has been replaced by $N\sigma_e$, N is the total number of scatterers within the scattering volume, τ is the pulse length, and the particulate radar cross section denoted by σ_e is tacitly assumed to be associated with free electrons. The scattering process of concern here is frequently termed incoherent scatter. That is, the individual particles (electrons) are undergoing random thermal motion, and the scattered power is proportional to the total number of particles.

For a situation in which the radar frequency is in the lower HF domain, say 5 MHz, it is generally found that the electronic plasma frequency exceeds this figure at some location in the ionosphere. This results in a coherent return from the scattering region and an associated radar cross section which yields a difference of many decibels from that given by Eq. (2.5). In the VHF domain, however, the Born scattering theory is appropriate, and the scattering process suggested by Eq. (2.5) predominates. There are occasions when coherent or quasi-coherent echoes contaminate the Thomson scatter returns, and this contamination is most troublesome when the radar beam is directed perpendicular to magnetic field lines. Under this condition, the field-aligned ionization associated with the radio aurora gives rise to unusually large returns. The scattering from radio aurora is of the underdense variety. Theories have been advanced which describe field-aligned ionization in terms of ion acoustic waves (Farley [1963]), and these theories are capable of explaining the quasi-coherence which results in a large radar signature.

Sporadic and shower meteors are also potentially quite troublesome in studies of the E region. Although radar echoes may be obtained from both underdense and overdense trails, the electron density of the overdense variety may be sufficient to generate a long-duration echo persistent at essentially a fixed range. Since Thomson scatter signals are inherently quite weak and meteor trails may exhibit relatively large echoes, the presence of meteors often makes low-altitude data unusable.*

At Randle Cliff it has been found that the adverse effect of meteors is most pronounced when viewing perpendicularly to the field lines. This is probably due to preferential diffusion along magnetic field lines thus producing a greater radar cross section for the perpendicular aspect (Goodman and Rutiser [1967]). Other coherent signals which must be separated from the incoherent Thomson scatter echoes result from aircraft targets which pass through sidelobes of the antenna pattern and thus appear virtually at ionospheric heights.

The electronic radar cross section is defined by (Evans [1967b]) the relation

$$\sigma_e = 4\pi \left(\frac{e^2}{m c^2}\right)^2 \sin^2 \xi.$$

In this relation ξ is the angle between the incident electron field E_0 and the scattered field wave vector \mathbf{k} , e is the electronic charge, m is the electronic mass, and c is the free-space velocity of light. (Note that σ_e is 10^{-24} cm² or 1 barn in nuclear terminology.) For

*Meteor echoes are often the order of a second in duration at 138.6 MHz, the Randle Cliff frequency. They may be ≈ 20 dB above noise level at nominal ranges for most radar systems. On the other hand, for the same system, Thomson scatter signals are equal to or less than the noise level on a single-pulse basis.

a monostatic radar $\sin^2 \xi = 1$, and e^2/mc^2 is recognized as the classical electron radius and its square as the Thomson cross section of the electron. Thus the radar cross section σ_e is simply 4π times the Thomson cross section for electrons, assuming a monostatic radar. (It is worth noting that although there is in principle an ionic component to Thomson scattering, it is always too small to consider. In fact for the lightest ion H^+ one has an effective cross section of $\sigma_e/(1840)^2$, and the principal constituents between 200 and 600 km, viz., O_2^+ and O^+ , are much heavier.)

Therefore, it can be seen that by replacing the radar cross section σ by $4\pi VN$ times the Thomson cross section, an estimate may be extracted for the signal-to-noise ratio which would be obtained by a radar illuminating the earth's ionosphere. Thus it is quite natural to refer to the process as Thomson scattering, even though in the earlier literature it is referred to as incoherent scattering. It was Gordon who first suggested that radar systems had become sufficiently powerful to measure the weak scattering effect, and it has since become a subject of rich theoretical and experimental interest (Gordon [1958]). Perhaps it should be referred to as Thomson-Gordon scattering.

Rewriting Eq. (2.5) we have

$$(S/N) = CN\sigma_e/R^2 = C\Sigma/R^2, \quad (2.6)$$

where C is a constant as long as the transmitter power, antenna aperture, wavelength, bandwidth, and the system noise temperature are invariant. It is seen that (S/N) is apparently independent of frequency and directly proportional to the electron density. Actually Eq. (2.6) is good only to a first approximation for radar frequencies of interest. In the following discussion it will be seen that $\Sigma = N\sigma_e/2$ rather than $N\sigma_e$ at VHF.

To deduce the relationship between σ_e and the cross section per unit volume Σ , the scattered field associated with dielectric fluctuations in the ionosphere must be considered. First it is assumed that the ionosphere has within a scattering volume V an average dielectric constant ϵ . In addition fluctuations $\Delta\epsilon$ are allowed to exist, and the scattered field E_s at a great range R from the scattering center is desired assuming that the incident field is a plane wave $E_0 \exp(i\omega_0 t - i\mathbf{k}_0 \cdot \mathbf{r})$. This calculation has been carried out by Booker and Gordon [1950] using the Born approximation, and may be written

$$E_s = \frac{E_0 K^2 \sin \xi \exp(i\omega_0 t - iKR)}{4\pi R \epsilon} \int_V \Delta\epsilon e^{i(\mathbf{K} - \mathbf{K}_0) \cdot \mathbf{r}} d\mathbf{r} \quad (2.7)$$

where \mathbf{k}_0 and \mathbf{k} are the incident and scattered wave vectors respectively, ξ is the angle between \mathbf{E}_0 and \mathbf{k} , K is the wave number in the medium, t is time, ω_0 is the angular wave frequency, \mathbf{r} is the radius vector, and $d\mathbf{r}$ is the volume element. Now ϵ can be written in terms of the electron density N through use of the collisionless Appleton-Hartree formula (Lawrence et al. [1964]):

$$n^2 = 1 - \frac{X}{(1 - Y_T^2 (1 - X)^2) \pm \sqrt{Y_T^4 / (1 - X)^2 + Y_L^2}}, \quad (2.8)$$

where n is the real refractive index, $X = Ne^2/\epsilon_0 m \omega_0^2$, $Y_T = e\mu_0 H \sin\theta/m\omega_0$, $Y_L = e\mu_0 H \cos\theta/m\omega_0$, ω_0 is the angular radio frequency, H is the magnetic field intensity, μ_0 is the free-space permeability, m and e are the electronic mass and charge respectively, and θ is the angle between the wave vector \mathbf{k} and the geomagnetic field vector \mathbf{H} . If ω_0 is sufficiently large (i. e., high frequency approximation, implying $\omega_0 \gg Ne^2/\epsilon_0 m$) and the effects of the magnetic field may be ignored, then

$$n^2 \approx 1 - X \quad (2.9)$$

or

$$n^2 \approx 1 - \left(Ne^2 / \epsilon_0 m \omega_0^2 \right) \quad (2.10)$$

Recalling that $n^2 = \epsilon / \epsilon_0$, one sees that Eq. (2.10) implies

$$\epsilon = \epsilon_0 \left(1 - \frac{Ne^2}{\epsilon_0 m \omega_0^2} \right) \quad (2.11)$$

and thus

$$\Delta \epsilon = - \Delta N e^2 / m \omega_0^2, \quad (2.12)$$

from which it is apparent that fluctuations in the dielectric constant are the direct result of fluctuations in the electron density. It is also seen that fluctuations in the dielectric constant of the medium are reduced as the exploring radio frequency ω_0 is increased. However, it will be seen that this frequency dependence will not appear in the final result for the scattered field E_s due to the presence of κ^2 in the numerator of Eq. (2.7). Therefore,

$$E_s = - \frac{E_0 (e^2/mc^2) \sin \zeta \exp(i\omega_0 t - iKR)}{4\pi \epsilon_0 R} \int_V \Delta N e^{i(\mathbf{\kappa} - \mathbf{\kappa}_0) \cdot \mathbf{r}} d\mathbf{r}, \quad (2.13)$$

where E_s has been expressed in terms of the three-dimensional Fourier transform of the electron density fluctuations ΔN , and R has been replaced by ω_0/c . But what gives rise to the fluctuations in electron density ΔN ? Clearly if turbulence exists, one would expect irregularities in the electron density. However, this is not necessary. Even for a gas in thermal equilibrium, one finds from elementary statistical mechanics that if within a volume V the average number of particles is NV , then the probable error (0.67 times the standard deviation) in measurement of the number of particles in the subvolume V is proportional to $(NV)^{1/2}$. Thus fluctuations in electron density arise quite naturally but are affected by the nonideal nature of the electron-ion gas and by thermal nonequilibrium. The integral in Eq. (2.13) is undetermined, but its mean-square value may be derived on the basis of a Maxwell-Boltzmann energy distribution assuming thermal equilibrium between electrons and ions. Fejer [1960] finds

$$\left| \int \Delta N e^{i(\mathbf{\kappa} - \mathbf{\kappa}_0) \cdot \mathbf{r}} d\mathbf{r} \right|^2 = \frac{1}{2} VN \left\{ 1 + \frac{|\mathbf{\kappa} - \mathbf{\kappa}_0|^2}{(Ne^2/\epsilon_0 kT) + |\mathbf{\kappa} - \mathbf{\kappa}_0|^2} \right\} \quad (2.14)$$

Now if ϕ is defined to be the angle between $\mathbf{\kappa}$ and $\mathbf{\kappa}_0$ the following identity may be used:

$$|\mathbf{\kappa} - \mathbf{\kappa}_0| = \frac{4\pi}{\lambda} \sin(\phi/2). \quad (2.15)$$

For radar backscatter and in particular at Randle Cliff, the situation is monostatic, $\phi/2 = 90^\circ$, and Eq. (2.14) becomes

$$\left| \int_V \Delta N e^{i(\mathbf{K} - \mathbf{K}_0) \cdot \mathbf{r}} d\mathbf{r} \right|^2 = \frac{1}{2} VN \left[1 + \frac{(4\pi/\lambda)^2}{(Ne^2/\epsilon_0 kT) + (4\pi/\lambda)^2} \right] \quad (2.16)$$

where $(\epsilon_0 kT/Ne^2)^{1/2} = l_D$ is the Debye shielding distance. Furthermore, Σ may now be found since there is now an expression for E_s . Thus,

$$\Sigma = \frac{|E_s|^2 R^2}{E_0^2 V} \quad (2.17)$$

The conclusion like that of Fejer [1960] is that

$$\Sigma = N\sigma_e \left[\frac{(4\pi l_D)^2 + (\lambda^2/2)}{(4\pi l_D)^2 + \lambda^2} \right] \quad (2.18)$$

The Debye shielding distance l_D which appears in Eq. (2.18) is physically the distance over which an ionized gas may be nonneutral. That is, within every Debye sphere there exist a sufficient number of electrons to render the Coulomb field of the ion negligible at the distance l_D . Therefore, although electrons possess a high mobility, it may not manifest itself except within a small sphere of radius l_D in order to preserve charge neutrality. Hence, one anticipates that if the exploring wavelength is less than l_D , one would see a fundamentally different picture than if the wavelength were greater than l_D . Referring back to Eq. (2.18), it is found that

$$\Sigma = N\sigma_e/2 \text{ when } \lambda/l_D \gg 1, \quad (2.19a)$$

and

$$\Sigma = N\sigma_e \text{ when } \lambda/l_D \ll 1. \quad (2.19b)$$

At Randle Cliff $\lambda \approx 2.16$ meters, and l_D is less than a centimeter at ionospheric heights of interest here. So Eq. (2.19a) is the appropriate selection to make, and it is found that at thermal equilibrium the cross section Σ is proportional to the electron density. With the proviso that the magnetic field be neglected and operation is in the VHF band and above (but less than the frequency corresponding to l_D), Σ is proportional to $1/2$ the electronic radar cross section (i. e., $\sigma_e/2$).

It has been shown by Buneman [1962] that if an ionosphere is allowed in which $T_e/T_i \neq 1$, it is found that

$$\Sigma = N\sigma_e \left\{ 1 - \frac{1}{1 + (4\pi l_D/\lambda)^2} + \frac{1}{[1 + (4\pi l_D/\lambda)^2] [1 + (4\pi l_D/\lambda)^2 + T_e/T_i]} \right\}, \quad (2.20)$$

provided $T_e \leq 3 T_i$. Here again it is seen that if $l_D \ll \lambda$,

$$\Sigma = N\sigma_e \left[\frac{1}{1 + (T_e/T_i)} \right], \quad (2.21)$$

which reduces to Eq. (2.19a) for $T_e = T_i$ as expected. As noted by Evans [1967^b], Eq. (2.21) is accurate in most instances, but Farley [1966] has determined a more exact expression to be used if the need arises.

It was concluded earlier (Eq. (2.6)) that (S/N) , or equivalently the power profile, is proportional to Σ/R^2 , and thus it is clear from Eq. (2.21) that if N is to be determined from a measurement of (S/N) , then it will be necessary to deduce T_e/T_i at the same time. In short, it will be necessary to examine the spectrum of the backscattered signals, since it may be shown that certain characteristics of the spectrum (e. g., its width and its wing-to-valley ratio) are related to the pertinent temperatures. The analysis of the spectra obtained from Thomson scatter echoes is usually laborious unless the operation is sufficiently computerized. In addition, it is essential to employ relatively long pulses so that the transmitted power spectrum will not appreciably distort the ionospheric spectrum. This is generally incompatible with the desire for good altitude resolution when conducting profile measurements. Thus, one is unable to make both spectrum and profile measurements simultaneously. Also, these two measurements do not associate common scattering volumes in view of their differing pulse-length requirements. Furthermore, even if these difficulties are overcome, it is found that N is determined only to within a multiplicative constant which must be deduced from a third measurement. In practice this constant is found only implicitly; relative electron density profiles are deduced and normalization is accomplished through ionosonde determination of the F2-layer maximum electron density.

At Randle Cliff a measurement of (S/N) per se is not made, and thus the circuitous procedure described in the previous paragraph is not followed. Instead another observable is operated on: the polarization of the scattered wave. Thomson scatter may be regarded as only the mechanism by which a signal may be obtained from discrete heights in the ionosphere. The scattered field once obtained is analyzed for its polarization orientation, which may be regarded as independent of power. The height derivative of this orientation angle may be shown to be proportional to N , with the proportionality constant being known. A discussion of the general procedure followed at Randle Cliff is presented in the following chapter.

CHAPTER 3

FARADAY ROTATION AND THOMSON SCATTER

It has been mentioned that Thomson scatter measurements which do not make use of Faraday rotation require an independent measurement to normalize the electron density profiles. In addition, since the ratio of electron-to-ion temperature T_e/T_i is not constant throughout the ionosphere, a spectral measurement is also necessary to deduce the altitude dependent relationship between echo power and electron density. (That is, the returned signal power is approximately proportional to $N/[1 + T_e/T_i]$ rather than N alone.) It may be safely assumed that at 140 MHz the polarization associated with the mechanism of Thomson scatter is not appreciably destroyed, thus enabling the Faraday rotation technique to be effectively employed. Millman et al. [1964] noted that at 400 MHz the signal strength of the two orthogonal polarizations differs by no more than 6 to 7 dB, and they attributed the result to apparent depolarization due to what amounts to Faraday dispersion. (Were there no dispersion, the greatest difference between the transmit and orthogonal polarization channels would be defined by the interchannel cross talk level, and this should be ≥ 20 dB.) Their assessment is probably correct, since a rather large pulse length of $800 \mu s$ (or 120 km) was employed, and an appreciable amount of Faraday dispersion would be expected to occur within the scattering volume at the F2 maximum. In fact, dispersion ratios of 0.5 (ratio of Faraday minimum to maximum) have routinely been observed at Randle Cliff using 138.6 MHz and a pulse length $\tau = 50 \mu$ sec. Since the Faraday rotation angle Ω may be shown to be proportional to τ/f^2 , scaling to the radar frequency and pulse length of Millman et al. (425 MHz and 800μ sec) may be performed. Doing so, an anticipated dispersion ratio is $(138.6/425)^2(800/50)(0.5) = 0.85$. Obviously their unpolarized signals may be attributed to Faraday dispersion within the scattering volume. More will be said about dispersion in Chapter 5.

A rather detailed derivation of Faraday rotation is given in the appendix; the phenomenon will only be briefly reviewed at this point. The starting point for the discussion is the following equation for the two-way radar path:

$$\Omega(h) = 5.95 \times 10^{-2} f^{-2} \int_0^h H \cos \theta \sec \chi N(h') dh', \quad (3.1)$$

where Ω is the rotation angle (radians), f is the radar frequency (Hz), H is the magnetic field intensity (ampere-turns/meter), θ is the angle between the ray path and the field vector \mathbf{H} , and χ is the ray zenith angle. The geometrical function $\Psi = H \cos \theta \sec \chi$ has been studied by Yeh and Gonzalez [1960] over Illinois and by the author over Randle Cliff [1965]. Figure 3.1 illustrates the variation of Ψ with azimuth and elevation at Randle Cliff assuming an altitude of 300 kilometers. Figure 3.2 shows that in general Ψ (sometimes called the M factor) decreases with increasing altitude, this being a manifestation of the approximate inverse cube decrease in H with geocentric distance. Variation in this tendency is a reflection of the role played by the $\cos \theta \sec \chi$ factor. Upon examination of Figs. 3.1 and 3.2, it is seen that Ψ is largest toward the south (180°) and smallest toward the north (0°). This is, of course, because θ is close to 90° toward the north. Indeed it is even possible to view perpendicular to magnetic field lines at E-region height

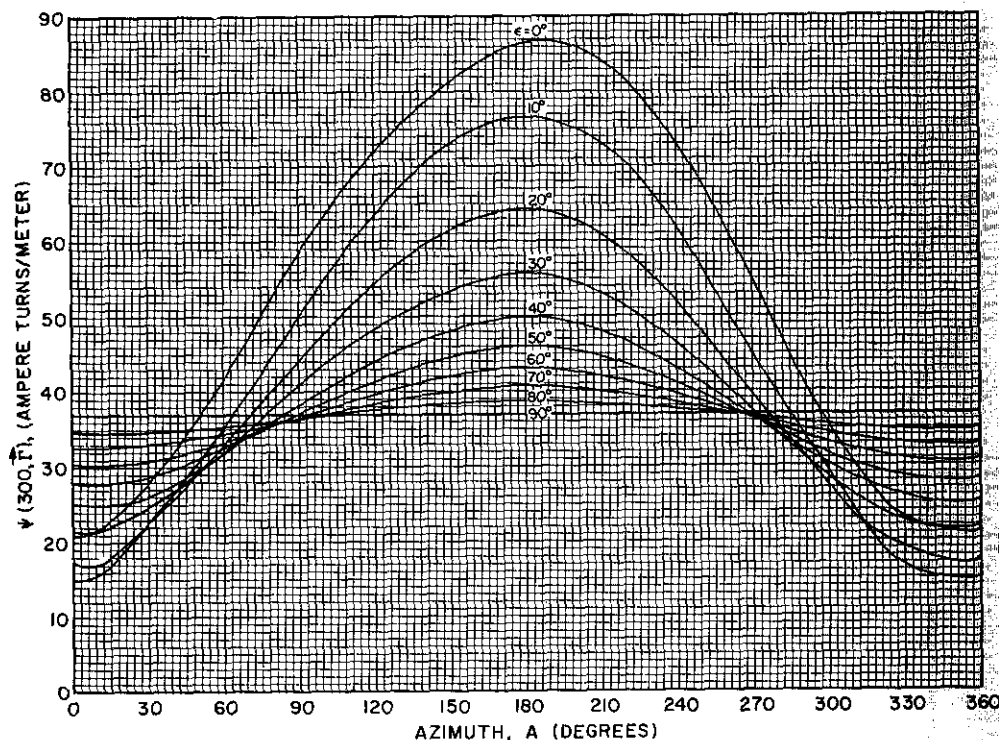


Fig. 3.1 - Magnetic field parameter for Randle Cliff as a function of azimuth, assuming a height of 300 km

(≈100 km). It will turn out desirable that this region be avoided in order to render our Faraday studies less cumbersome. This fact is probably obvious and has recently been reemphasized by Kelso [1970].

For a fixed azimuth A and elevation E, $\Psi(A, E, h)$ is a continuous function of h. Furthermore, since N(h) is everywhere positive, the theorem of the mean can be invoked and Eq. (3.1) can be written as

$$\Omega(h) = 5.95 \times 10^{-2} f^{-2} \bar{\Psi} \int_0^h N(h') dh', \tag{3.2}$$

where the azimuthal and elevation dependence of Ψ is suppressed and N is assumed to exhibit only altitudinal dependence in this argument. Clearly the mean value of Ψ (denoted by $\bar{\Psi}$) is defined by the expression

$$\bar{\Psi} = \frac{\int_0^h \Psi N(h') dh'}{\int_0^h N(h') dh'} \tag{3.3}$$

It has been shown (Goodman [1965]) that if $\Psi(h)$ is a reasonably linear function, then $\bar{\Psi}$ is simply $\Psi(\bar{h})$, where \bar{h} is the so-called ionospheric mean height which may be obtained by

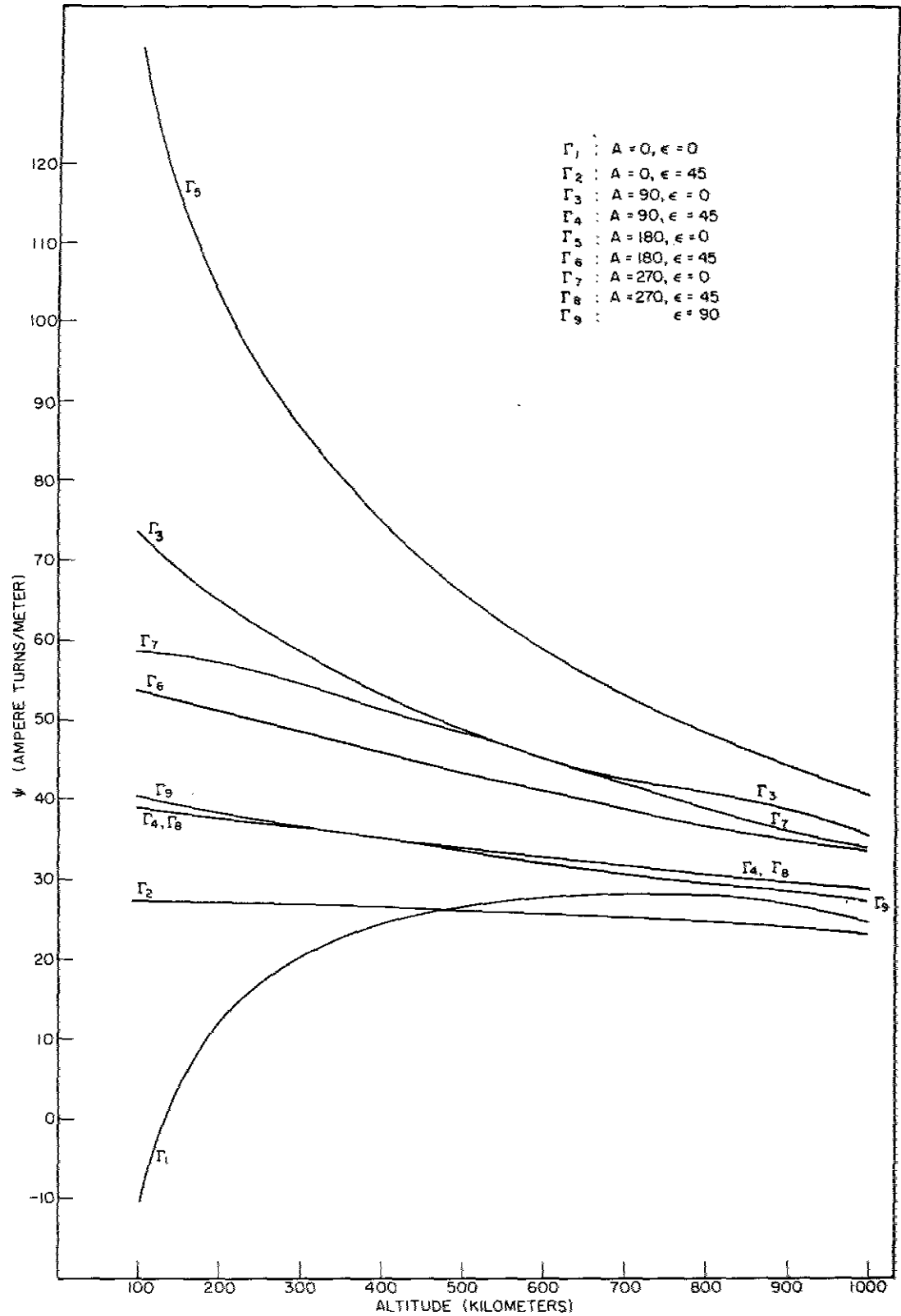


Fig. 3.2 - Magnetic field parameter for Randle Cliff as a function of height for a number of ray paths

assuming some appropriate electron density distribution. As a useful mathematical model of the F region, an α -Chapman profile is typically used (Mittra [1947]). It may be written as

$$N(h) = N_{F2} \exp \left\{ \frac{1 - (\delta h/H_s) - \exp(-\delta h/H_s)}{2} \right\}, \quad (3.4)$$

where $\delta h = h - h_{F2}$ is the distance from the F2 maximum, N_{F2} is the peak electron density, and H_s is the scale height of the distribution. The scale height here refers to the neutrals, and explicitly $H_s = kT/mg$ where k is Boltzmann's constant, g is the acceleration of gravity, and T and m are the temperature and mean molecular mass respectively. Figure 3.3 illustrates the Chapman profile for values of H_s between 50 and 120 kilometers. If one were making total content measurements using Eq. (3.2) (provided that any polarization ambiguities are removed), one would find that the appropriate value of \bar{h} associated with $\bar{\Psi}$ is approximately 400, assuming $H_s = 100$ km and $h_{F2} = 300$ km. Recall that if \bar{h} is known through some a priori calculation, the burden of carrying out the integration embodied in Eq. (3.3) no longer exists. Fortunately $\Psi(h)$ is rather slowly varying, and it is not too important to specify \bar{h} very accurately. In fact an error of 100 km in the selection of \bar{h} will affect Ψ only a few percent. Hence, by the process of assuming sort (e. g., Chapman profile) of rough distribution, in principle, it is possible to deduce the integral of the true distribution with some fidelity. The total content measurements however are only marginally significant in the context of this report. Nevertheless, they are important historically and may be accomplished by means of the process just described and through use of Eq. (3.2).

From Eq. (3.2) it is apparent that only the integrated distribution or electron content may be obtained if a single value of $\Omega(h)$ is measured, h being the ionospheric upper limit considered. This is the case in radar lunar investigations as well as satellite studies, active or passive. Numerous studies of this type have been conducted at Randle Cliff and elsewhere. It is also obvious that $\Omega(h)$ is actually a continuous function of h ,

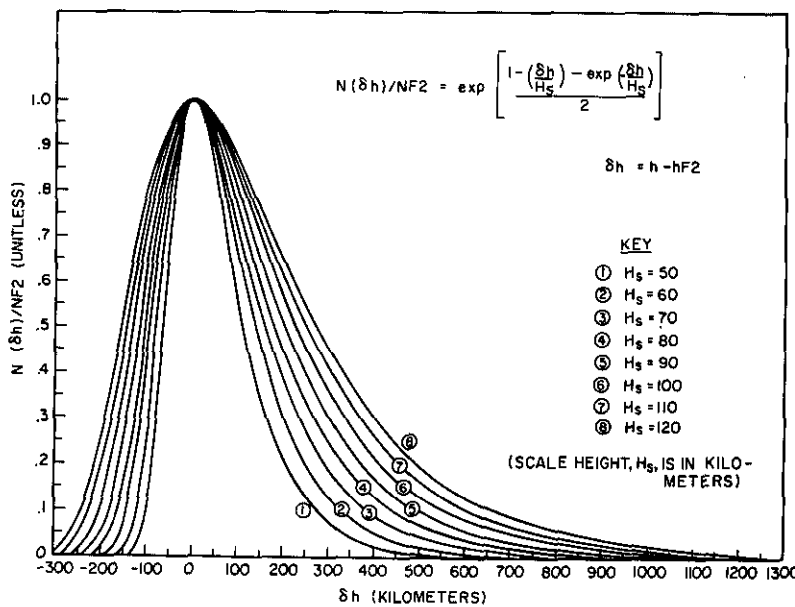


Fig. 3.3 - Chapman distributions

and it is the mechanism of Thomson scatter which enables one to ascertain this very function. In other words, it is found that h in Eq. (3.2) is fixed in total content studies and assumes its full range in Thomson scatter studies. This distinction is quite important, and for the case of Thomson scatter it becomes meaningful to differentiate Eq. (3.2) at all heights as follows:

$$\frac{d\Omega(h)}{dh} = 5.95 \times 10^{-2} f^{-2} \frac{d}{dh} \int_0^h N(h') \Psi(h') dh', \quad (3.5)$$

whereupon

$$\frac{d\Omega(h)}{dh} = 5.95 \times 10^{-2} f^{-2} \Psi(h) N(h) \quad (3.6)$$

or, rearranging,

$$N(h) = \frac{16.8 f^2}{\Psi(h)} \frac{d\Omega(h)}{dh}. \quad (3.7)$$

Therefore, by measuring the derivative of $\Omega(h)$ with respect to height and having $\Psi(h)$ given, $N(h)$ may be found.

At Randle Cliff $\Omega(h)$ is extracted from the Thomson scatter data by very precise bookkeeping of the height-dependent Faraday extrema exhibited by the linearly polarized backscattered signals. The derivative $d\Omega/dh$ is then estimated by the obvious procedure of finding the height difference between adjacent extrema (i. e., $d\Omega/dh = (\pi/2)/\Delta h$.) This feature of the data processing suggests that the altitude resolution associated with these studies is determined by the condition of the ionosphere itself. That is to say, the greater the electron population or content of the ionosphere, the greater will be the corresponding number of estimates of $d\Omega/dh$ and hence N . For this reason the Faraday rotation/Thomson scatter technique is rendered considerably less sensitive during nocturnal hours than during the daytime. Consequently, the main thrust of this study is centered about the behavior of the daytime ionosphere.

It is of interest to determine the approximate number of estimates of $N(h)$ which arise from Faraday rotation/Thomson scatter measurements at Randle Cliff. First, it may be remarked that

$$\int N dh = 1.24 \times 10^{10} (f_0 F_2)^2 \tau(H_s), \quad (3.8)$$

where $\tau(H_s)$ is the ratio of $\int N dh$ to the F2 maximum electron density represented by the term $1.24 \times 10^{10} (f_0 F_2)^2$, and $f_0 F_2$ is the ordinary-ray critical frequency of the F2 maximum (in MHz). For a Chapman distribution τ is directly related to H_s , and, assuming a value for H_s of 100 km (Seddon [1963]), the conclusion may be made that $\tau \approx 400$ km (Goodman [1965]) if the electron content in Eq. (3.8) refers to the entire ionosphere below ≈ 800 km. Some earlier work of the author [1968], among others, suggests a seasonal dependence for τ (see for example Fig. 3.4). It is found that on the average, however, most measurements of τ over middle latitudes corroborate 400 km as a reasonable working value during the daytime. It is not true in the neighborhood of the sunrise and sunset periods. These periods are characterized by massive distortions in layer shape arising from rapid expansion or contraction as well as from rapid changes in ionospheric composition. It is also untrue during and immediately following periods of strong magnetic activity. Taking $\tau = 400$ km, $\Psi = 40$ ampere-turns/m, and $f = 138.6$ MHz, and

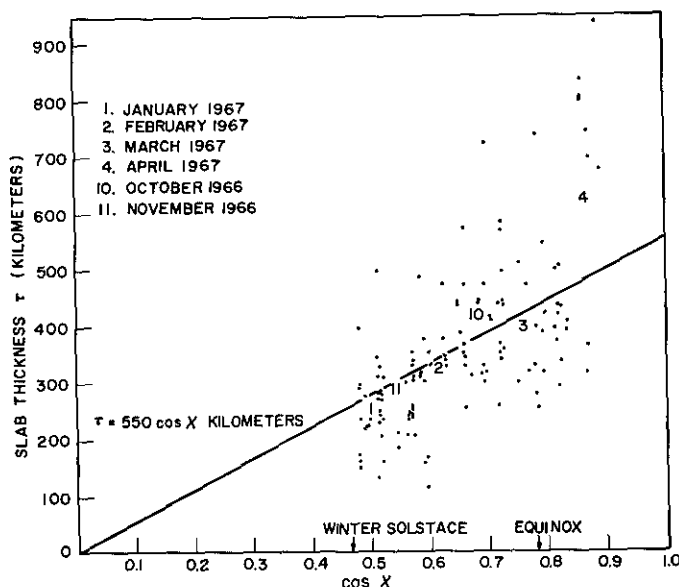


Fig. 3.4 - Slab thickness over Randle Cliff

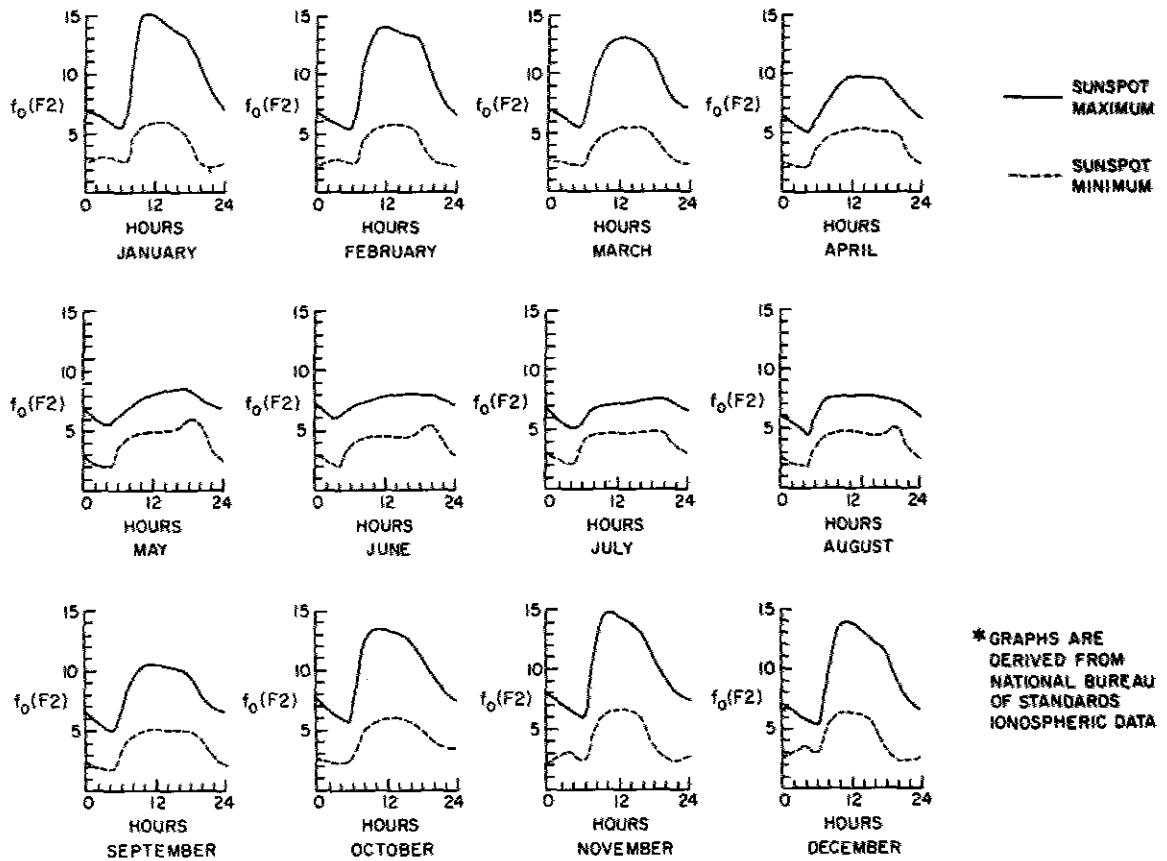
combining Eqs. (3.2) and (3.8), the following expression for the total Faraday rotation angle may be deduced:

$$\Omega = 0.614 (f_0 F_2)^2. \quad (3.9)$$

Since Ω is now expressed in terms of the F2 maximum critical frequency, it is a simple matter to estimate its daytime behavior. Figure 3.5, for example, shows that $f_0 F_2$ is usually above 7 MHz at sunspot maximum after 0800 EST, and this holds true until about midnight. At solar minimum $f_0 F_2$ is usually above 3 MHz between 0800 and 2400 EST. Thus, by selecting a range of 3 MHz to 15 MHz for $f_0 F_2$, Eq. (3.9) predicts an Ω variation between ≈ 5.5 and ≈ 138 radians. Furthermore, since one estimate may be generated per $\pi/2$ radians, these figures suggest that the number of electron density estimates range between ≈ 3.5 at night and ≈ 88 on days of high electron density. Most of these estimates are, of course, centered about the F2 maximum within a scale height (i. e., between 200 and 400 km in altitude).

The single, most important aspect of the Faraday method of conducting Thomson scatter measurements which makes it more satisfactory than other methods is that electron densities may be measured without distortion arising from fluctuations in T_e/T_i . In making measurements of traveling disturbances in the ionospheres, for example, great care must be taken to separate density and temperature fluctuations if the power-profile method is employed. By using the Faraday method, it is obviously not necessary to equivocate. The only fluctuations which can be measured are due to irregularities in electron density.

The principal drawback associated with the Faraday technique is that one is limited to studies below about 700 km due to the rapid reduction in the product of electron density and magnetic field strength with altitude. In this study the interest is not in the altitude regime above 700 km anyway, but if desired it would be possible to extend the Faraday profile to greater heights by matching an appropriate power profile at the Faraday profile termination height, while carefully considering effects of T_e/T_i . This procedure is followed at Jicamarca, where T_e/T_i is clearly unity above the F2 maximum.

PREDICTED TEMPORAL VARIATIONS OF f_oF_2 FOR WASHINGTON, D.C.*Fig. 3.5 - Predicted temporal variations of f_oF_2 for Washington, D. C.

At Randle Cliff the argument for $T_e/T_i \approx 1$ at great heights is somewhat more tenuous. In fact Evans [1967c] and Carru et al. [1967] find that T_e/T_i is significantly greater than unity at Millstone and St. Santin respectively. Nevertheless, it might be possible to assume that T_e/T_i is fixed (which is all that is necessary) between 700 and 1000 km.

Another drawback of the Faraday technique is Faraday dispersion, and this will be discussed in some detail in Chapter 5. It turns out that this is potentially quite troublesome at Jicamarca but is not too serious at Randle Cliff. Moreover, it will be shown that dispersion may become, under certain circumstances, an advantageous feature of the Randle Cliff operation.

CHAPTER 4

RANDLE CLIFF RADAR FACILITY

The Randle Cliff Radar Facility (RCR) is located at $38^{\circ}39'37.1''N$ latitude and $76^{\circ}32'9.4''W$ longitude on the premises of the Naval Research Laboratory's Chesapeake Bay Division (CBD). It is only 28 statute miles from Washington, D. C. --home of the main laboratory--and is roughly 83 statute miles from the nearest NASA ionosonde station at Wallops Island, Va. Fig. 4.1 shows the relative positions of Wallops Island, the RCR, and Washington, D. C., as well as Fredericksburg--location of the nearest magnetograph station.

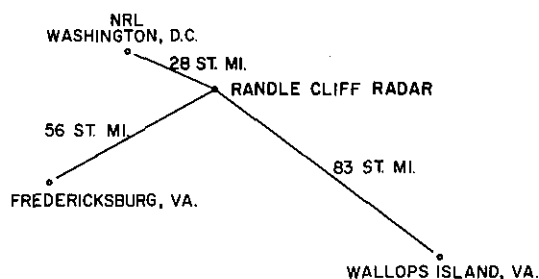


Fig. 4.1 - Relative locations of RCR, Fredericksburg, Wallops Island, and Washington, D. C.

The RCR was conceived in the period 1958-1960 as an outgrowth of a classified interest in missile detection. The instrumentation was developed specifically for that purpose, and early technical studies naturally emphasized the investigation of missile radar cross sections. Although the hardware associated with the RCR was exceedingly ad hoc, it was soon found that measurements of the cislunar electron content could be obtained using the phenomenon of Faraday rotation in conjunction with a moon-bounce experiment. Subsequently, a number of investigations of the earth's ionosphere were conducted using both radar and radio techniques in the radio-frequency neighborhood of 140 MHz. Between 1964 and 1969 the principal areas of investigation included measurements of the total electron content of the ionosphere and of its diurnal, seasonal, and sunspot-epochal variations. Also studied were the radio aurora, meteor trails, ionospherically induced amplitude scintillation, and effects of magnetic storms.

Due to the massive antenna of the RCR with its associated 34-dB gain at 140 MHz, the aforementioned experiments required only modest radar and/or radio receiving equipment. However, with the inclusion of Thomson scatter into the overall research program, it was clear that a high-power radar transmitter was needed as well as a low-noise receiver front end. Both features have been incorporated into the current version.

of the RCR, and, presently, Thomson scatter would have to be considered the central activity of the facility.

The main features of the RCR have been documented in an NRL report by Blake [1962], though certain sections of the report are quite naturally outdated by virtue of research-program changes which have necessitated equipment modifications and sundry acquisitions. A quick rundown of the present system is shown in the following list:

Randle Cliff Radar (RCR) Characteristics

Affiliation:	Naval Research Laboratory
Latitude:	38° 39' 37.1" N
Longitude:	76° 32' 9.4" W
Magnetic latitude:	≈ 50°
Frequency:	138.6 MHz
Antenna:	150-ft-diameter dish (≈ 46 m)
System noise temperature:	1590° K
Beamwidth:	3.6°
Antenna gain:	34.6 dB
Receiver bandwidth:	23 kHz
Peak power:	≈ 5 MW
Average power:	≈ 50 kW
Duty cycle:	1%
Pulse repetition frequency:	Variable
Pulse length:	Variable

Of special note is the 5-MW-transmitter peak power. The transmitter system, the heart of the RCR Thomson scatter facility, was obtained from Continental Electronics in 1968. It becomes operational during the spring of 1969, and the first Thomson scatter profiles were obtained during the summer of that year. Fig. 4.2 shows the final amplifier, which is capable of developing an average power of ≈ 50 kW, assuming a 1% duty cycle. This duty cycle limitation specifically means that the pulse length τ , times the pulse repetition frequency (PRF), equals 1% at most. A duty cycle of less than 1% may of course be selected. The transmitter pulse length may be varied between 5 μ sec and 1 msec, and the PRF may range between 10 and 2000 Hz subject to the 1%-duty-cycle limitation at fixed τ . In the Faraday measurements undertaken and discussed in this report, the pulse length was usually 50 μ sec for reasons of achieving good height resolution and elimination of problems related to Faraday dispersion. This suggests that the transmitter could be operated at a PRF of 200 Hz. However, it will be seen that certain features of the receiver/processing system limit the effective PRF in most cases. The entire transmitter system is in a separate building adjacent to the antenna. Due to size and weight considerations it could not be in the antenna house (shown in Fig. 1.1),

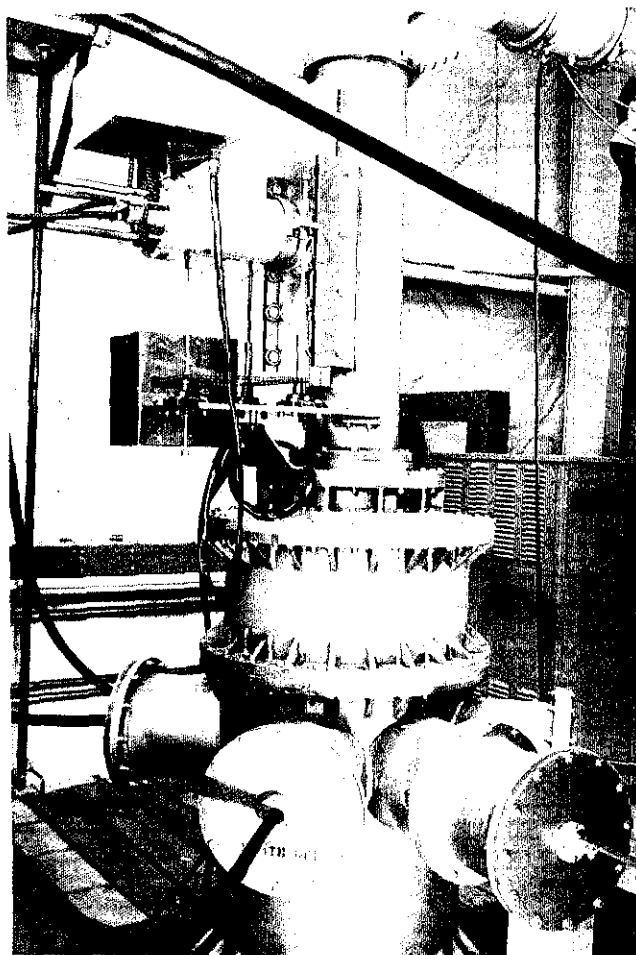


Fig. 4.2 - Transmitter final amplifier

as was the previous, modest transmitter system. Nevertheless, certain controls are available in the antenna house for convenience. These include the controls for PRF and pulse length selection.

The output of the final amplifier is fed over coaxial cable to the antenna building where it is connected to a solid-state duplexer system. The function of the duplexer is to direct the transmitter power to the antenna and to protect the radar receiver from this power level during the transmit phase. The duplexer system is shown in Fig. 4.3.

After passing through the duplexer system, the radar pulse energy is transmitted along coaxial line to the feed assembly (Fig. 4.4) located at the focus of the paraboloidal antenna surface. The VHF dipole separation is 44-1/2 inches, and a UHF horn (covered by a protective plate in the figure) which lies between the four dipoles has a square cross section with 33-1/4-inch sides. Depending upon the selection made on the receiver console, one may transmit either right-hand circular polarization (RHC) or linear polarization. This is accomplished either by feeding adjacent dipole elements out of phase by 90°, or by feeding them in phase respectively. If RHC is selected, then both RHC and left-hand circular polarization signals (LHC) are received. On the other hand, if the linear mode is chosen, then the transmitted linear polarization and a linearly polarized component orthogonal to it are received. In the RCR Thomson scatter

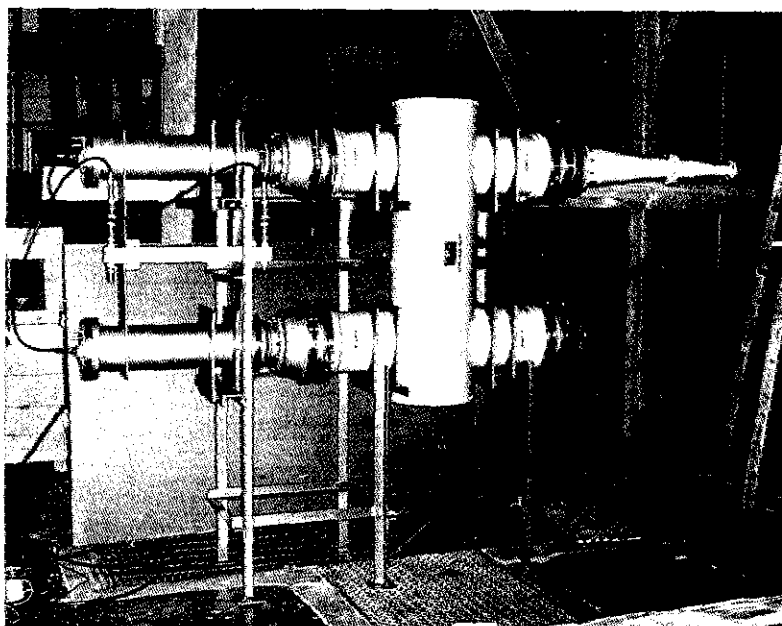


Fig. 4.3 - Duplexer system

investigations using Faraday rotation the linear mode is selected, of course, since circular polarization obviates the measurement of Faraday rotation unless radiowave phase is preserved and phase measurements are undertaken. As has been mentioned previously, the Faraday phase method is employed at Jicamarca sometimes in conjunction with a double-pulse correlation scheme. This requires a great deal of system sophistication and also demands a measurement of both RHC and LHC components. At Randle Cliff it is generally only necessary to measure a single linear component, and most often the crosspolarized channel is selected to reduce clutter effects.

The antenna configuration is such that transmitted and received signals are afforded a gain of 34.6 dB (an increase factor of 2512) in comparison with an isotropic antenna. The backscattered signals, having been focused at the feed assembly, are next carried from the feed through the duplexer system. This allows receiver operation, provided the transmitter is not active. Without a duplexer system, sensitive radar receivers clearly would be rendered inoperable by the insertion of tremendous transmitter pulse energy. (In fact, the ratio of transmitted pulse energy to typical Thomson scatter signals is about 10^{22} .) The duplexer system provides ≈ 80 dB protection during transmission and ≤ 1 dB loss during the reception phase. The recovery time of the duplexer is less than 20 μ sec for all pulse lengths.

A block diagram of the receiver/processing system is displayed in Fig. 4.5. It is seen that the antenna output is connected to a Telonic filter with a bandpass of 12 MHz prior to preamplification. The output of the Avantek preamplifier is heterodyned down to 10.9 MHz (first IF) by mixing it with a local oscillator frequency of 149.5 MHz (first LO). This is then mixed with 12.4 MHz (second LO) to obtain 1.5 MHz (second IF) which has an intrinsic bandwidth of 23 kHz. This is actually the overall receiver bandwidth as noted in the previous list. The basic 1.5 MHz is next amplified and passed through a linear-law envelope detector which rectifies the signal and removes the carrier frequency. It is at this stage that the phase information is destroyed, and amplitude information is retained for future processing.

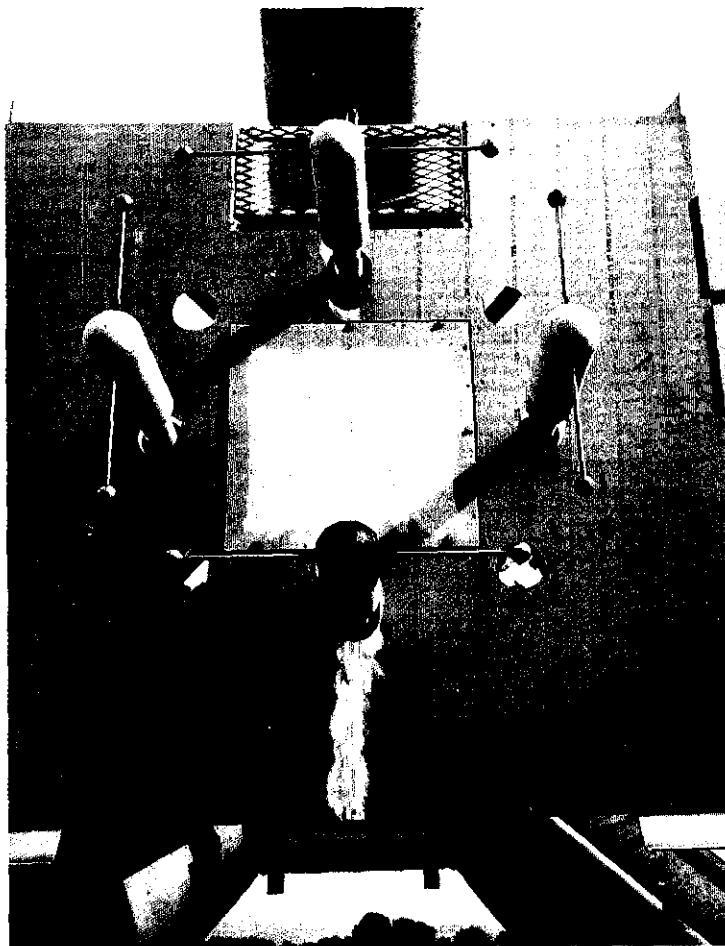


Fig. 4.4 - Antenna feed assembly

To "see" Thomson scatter profiles it is necessary to integrate the output of the linear detector for a number of sweeps*. The (S/N) associated with the Thomson scatter signals depends (from Eq. (2.6)) on the electron density $N(h)$ and on the range or height of the scatterers. At Randle Cliff the (S/N) is of the order of unity at F region heights for typical daytime conditions. Under these conditions the amplitude error associated with a single pulse is about 100%. If it is assumed that the Thomson scatter signal is buried in gaussian noise, integration of the detected signal envelope yields for the average rms error the following:

$$\langle E \rangle = E_0 (N)^{-1/2}, \quad (4.1)$$

where the corner brackets denote the resultant error, N is the number of sweep integrations, and E_0 is the initial rms error. Therefore, about 10^4 sweep integrations are required to reduce the uncertainty of the signal amplitude determinations to 1%. The

*A sweep is radar jargon for one trace of an A scope. An A scope presentation is an oscilloscope display of signal amplitude versus signal range (signal distance), and a single receiver trace is obtained during the off-time between adjacent transmitter pulses.

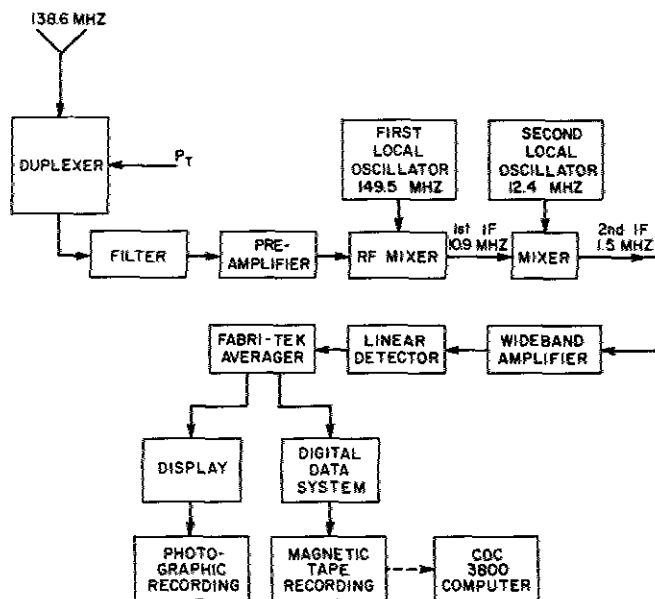


Fig. 4.5 - Receiver processing system

procedure tried initially at Randle Cliff (prior to the acquisition of the high-power transmitter) necessitated the recording of each sweep on magnetic tape at specified range gate settings. The sweeps were subsequently integrated off-line on the NRL/CDC-3800 computer. This process was wasteful of tape and was costly as far as the computer was concerned. An additional disadvantage was that only a small number of range gate selections could be made at a time, and, in practice, only a single range gate setting was recorded. This meant that several hours would be required to deduce a single electron density profile at the expense of numerous magnetic tapes (more than ten). Obviously such a procedure would not only be costly but foolish, since temporal fluctuations in ionospheric electron content and sundry wave motions would be completely washed out or distorted severely. Needless to say, this preliminary procedure was never employed on a routine basis.

To achieve an adequate (S/N) as well as save off-line computer cost, a Fabri-tek signal averager was obtained. Its function in the analysis is important enough to warrant a few remarks as to its operation.

The system obtained for NRL may be used in several modes, each with its inherent advantages and disadvantages. There are 1024 storage locations available in the unit, and the "dwell time" selection determines the range extent which may be covered. Thus, if a small "dwell time" is selected for purposes of obtaining a more refined altitudinal sample, then one cannot operate on the entire radar sweep. This fact is in most cases relatively unimportant, since the ionosphere "disappears" at very great heights anyway (i. e., the interpulse period (1/PRF) is often large, and a great portion of it may be irrelevant).

Two options concerning the digitization speed are available. They are called high and low speed for short. To switch from one to another, plug-in units are simply exchanged. For the slow-speed option, dwell times of 50, 100, 200, and 500 μ sec, and 1, 2, 5, and 10 msec may be selected. In the present application a dwell time of 50 μ sec is barely acceptable so the slow speed option is of marginal usefulness. It has the

advantage, however, of offering essentially no duty cycle limitation. That is, the averager is not PRF limited if the slow-speed option is used.

For the high-speed option, dwell times of 4, 8, 16, 40, 80, 160, and 320 μsec are available. Hence, this system is of most use in Thomson scatter studies using Faraday rotation. The disadvantage in this mode of operation is that 1/2 of the 1024 storage locations are used as a buffer. In addition, there arises an effective upper limit to the radar PRF - 18Hz - due to internal processing time. This is potentially quite troublesome, especially during periods when the noise environment is enhanced or when wave motions are pronounced. In fact, since the normal pulse length is 50 μsec one could operate at 200 Hz without exceeding the 1% transmitter duty cycle restriction. This suggests that at least a threefold increase in the average rms error is induced through use of the high speed digitizer. However, it is emphasized that the high-speed digitizer enables one to obtain altitude resolution more appropriate for Faraday rotation studies at 138.6 MHz. In addition, it enables one to extract more altitude samples per Faraday fade and, as was discussed in the previous chapter, reduce the uncertainty associated with the electron density determination.

Another feature of the averager is that two channels, designated as A and B, may be operated on simultaneously. In the measurements conducted at Randle Cliff, the A and B channels are either cross linear polarized or right and left circularly polarized components. (In either case only one channel is transmitted.) The use of this option is advantageous in Faraday studies, especially whenever it is not clear whether certain fluctuations are due to Faraday rotation, clutter, or simply noise. The $\pi/2$ phase difference between the two linearly polarized channels is readily visible.

The averager also has a number of other features including a low-pass filter for high-frequency noise rejection, autostop capability, and a limited data reduction capability. It is augmented by a Hewlett-Packard display and by a high-speed printer.

The central features of the data processing console are shown in Fig. 4.6. In general the sweep trigger which is fed into the Fabri-tek averager is delayed so as to eliminate clutter regions which render the radar signals useless for Thomson scatter purposes. In addition it is often desirable to reset the averager system before its internal sweep period is completed. These two functions are accomplished by means of

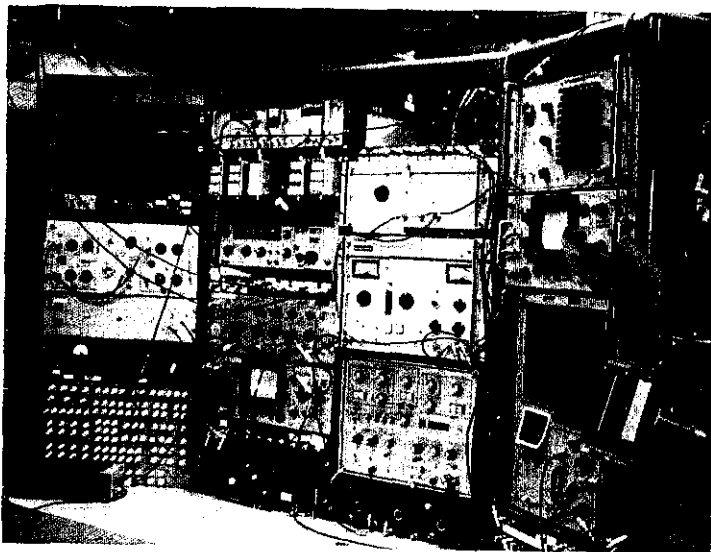


Fig. 4.6 - Data processing console

delayed pulse generators. From Fig. 4.5 it can be noted that the output of the averager can be displayed on a screen, photographed, printed out, or recorded on magnetic tape. The tape recording is made through use of the digital data system shown in Fig. 4.7. The tape recording includes other pertinent data such as time, transmitter power, pulse length, PRF, antenna azimuth and elevation, and various gain settings, as well as the averager data-address location and address contents. The tape uses standard IBM 7090 format and has a packing density of 200 bits/inch. It is compatible with the NRL/CDC-3800 computer, on which all programs are currently run.

The exact receiver/processing setup depends on the nature of the experiment being conducted. However, the above description is generally accurate as to the general flow of data and the processing involved in orthodox experiments.

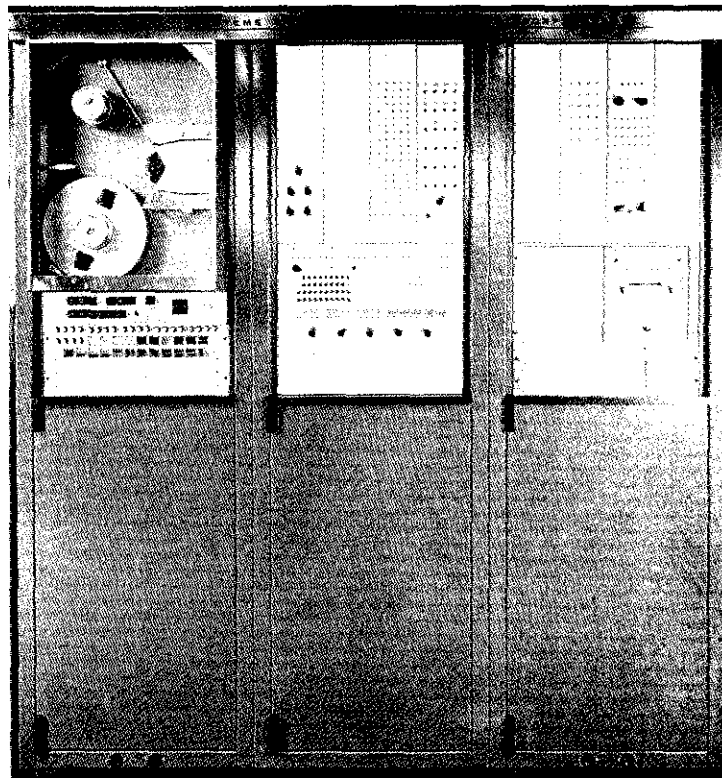


Fig. 4.7 - Digital data recording system

CHAPTER 5

CONSTRAINTS UPON THOMSON SCATTER MEASUREMENTS USING FARADAY ROTATION

It is obvious, since $\Omega(h) \propto (\bar{\Psi}/f^2) \int_0^h N dh$, that measurements of N using Faraday rotation depend critically on the geometric parameter $\Psi = H \cos \theta \sec \chi$ as well as the radar frequency f . It has been suggested that the pulse length τ also has great importance, and in fact if τ is too large, then $d\Omega/dh$ (and hence N) is indeterminate.

RAY PATH ORIENTATION

Recall from Fig. 3.1 that the parameter $\Psi = H \cos \theta \sec \chi$ depends quite strongly on the orientation of the ray path. For the reference height of 300 kilometers shown, Ψ ranges between roughly 15 and 88 ampere-turns/meter. Taking all altitudes into account (and in particular E-region heights), Ψ is found to range between -10 and +135 ampere-turns/meter. Since $d\Omega/dh \propto \Psi N$, significant differences in the character of the Faraday rotation profiles may be obtained for different antenna pointing angles.

To illustrate the pointing angle dependence of Ω , an azimuthal scan was conducted at an elevation of 60° . The results of the scan (Fig. 5.1) show that to good accuracy the maximum value of Ω , suitably normalized, agrees with the normalized value of Ψ . Any disagreement must result from either temporal or spatial variations in the total

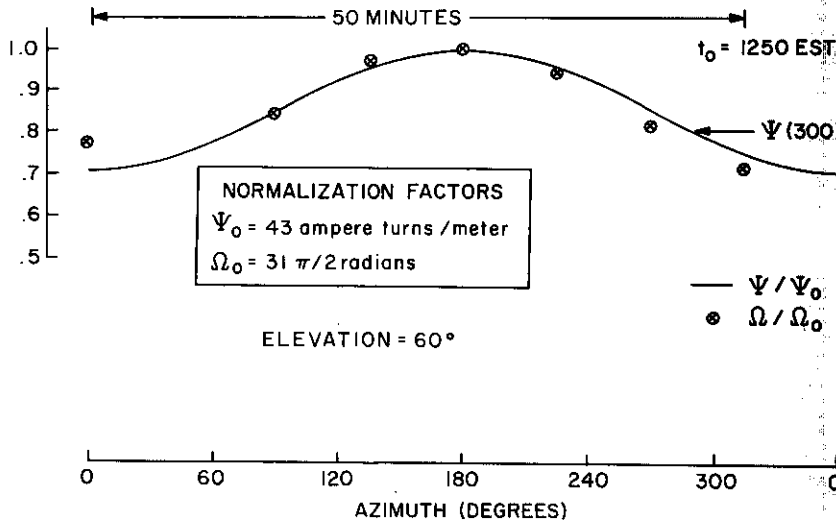


Fig. 5.1 - Variation in Faraday rotation with azimuth. Comparison of $\Psi = H \cos \theta \sec \chi$ at 300 km with Ω to 530 km (RCR: 3/9/70.)

electron content below 530 kilometers. Note also that it is presumably preferable to examine the ionosphere toward the south rather than toward the north in order to obtain the greatest number of Faraday fades, and as a consequence of this, there is an increase in the number of electron density estimates per profile. From Fig. 3.1, one might expect to see at an elevation of 0° a variation in Ω of 800% between azimuths of 0° and 180° .

It is rather well known that the majority of the ionospheric electrons lie within several scale heights of the F2 maximum. Assuming a Chapman distribution with a scale height H_s of 100 km, it is found that roughly 85% of the ionospheric electrons reside below 600 km. This may be seen from Fig. 5.2, which illustrates the altitudinal variation of the normalized total electron content with H_s as a parameter. From a practical standpoint the maximum height of the observable ionosphere is taken to be 600 kilometers for purposes of Faraday measurements. As a general rule of thumb, if one takes $\int_{100}^{600} N dh$ to be 5×10^{17} electrons/meter² (a substantial daytime value), one finds that Ω (in units of $\pi/2$ radians) is approximately equivalent to Ψ_{300} , as displayed in Fig. 3.1. Furthermore, under these conditions Ψ_{300} is approximately equal to the number of electron density estimates which may be obtained through the processing procedures currently being employed at Randle Cliff. Therefore, one may obtain as 85 or as few as 15 estimates of N between 100 km and 600 km, depending on the choice of azimuth and elevation.

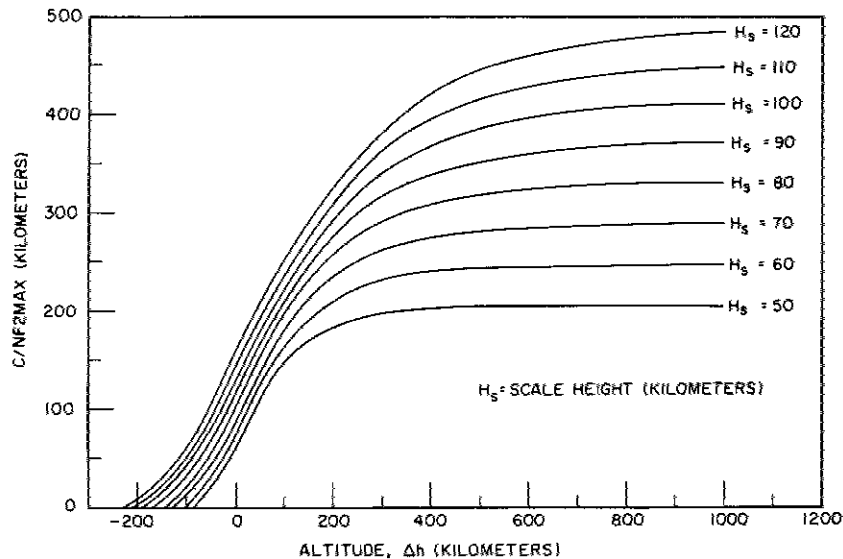


Fig. 5.2 - Ionospheric slab thickness versus altitude with scale height as a parameter

Although one now has some indication as to how the ray path orientation affects Ω , there is not yet a complete set of guidelines by which to choose the antenna "look" angles. Other considerations are often quite important in the ultimate selection. One obvious consideration is the experiment itself. For example, to compare RCR Thomson scatter results with those from the Wallops Island ionosonde, it is essential to point the antenna toward Wallops Island. The F2 maximum over Wallops Island is intersected by an RCR launched ray having an elevation of 70° and an azimuth of 134° . Also, to make comparisons of total electron content obtained from Thomson scatter with that which may be extracted from ATS-5-satellite VHF transmissions, one must direct the RCR antenna to an azimuth of $\approx 217^\circ$ and an elevation of $\approx 38^\circ$. (The ATS-5 satellite is in an approximately synchronous orbit which makes it roughly geostationary.)

If particular geometries associated with special experiments are disregarded, such as those mentioned in the previous paragraph, one finds that there are basically four factors which will control the ultimate selection of the "best" antenna look angles:

- (a) maximization of Ψ ,
- (b) maximization of (S/N) ,
- (c) specification of the ionospheric height domain to be covered, and
- (d) minimization of clutter effects.

With respect to (a), it has already been noted that to achieve the greatest amount of Faraday rotation, it is advisable to depress the antenna significantly and point in a generally southern direction. Depressing the antenna has the added advantage of reducing the effect of contaminating ground clutter in all cases, and it also reduces the effect of aircraft in some cases. This effect is due to the fact that the ionosphere is being "pushed away" from the radar site while the clutter targets remain essentially fixed in range.

To maximize (S/N) at a fixed ionospheric height as specified by (b), one naturally requires as high an elevation angle as possible, provided the ionosphere is spherically stratified (there exist no horizontal gradients). It is noteworthy that if the antenna elevation is made too low, then the (S/N) which is proportion to R^{-2} will drop appreciably at fixed ionospheric heights, rendering the upper ionosphere unobservable unless extensive integration times are employed. So, in general terms, lowering the antenna elevation puts the lower ionosphere under scrutiny but not the upper part, and raising the antenna enables observation of the upper ionosphere but not the lower portion. Thus, (a) and (b) are generally conflicting, and (b) has a tremendous bearing on (c).

Consideration of numerical values will show the extent to which (a) and (b) conflict and how one tries to arrive at an optimum choice for antenna azimuth and elevation as far as these two factors are concerned. First, assume that at 90° elevation one has a region of visibility between 200 and 600 km, the lower limit $h_<$ determined by clutter echoes appearing through antenna side lobes and the upper limit $h_>$ determined by the (S/N) and Faraday rotation considerations. If the antenna is depressed so that $\chi = 40^\circ$, one finds that the clutter targets which previously appeared at an ionospheric height of 200 km now reside at an ionospheric height of about 155 km, since $R = h \sec \chi$. So one gains 45-km coverage at the lower end of the ionosphere, and the question now is: how much coverage is lost at the upper end? Suppressing the parameter Ψ for a moment, one may write

$$(S/N \propto N(h)/R^2 = N(h)/(h^2 \sec^2 \chi), \quad (5.1)$$

where one ignores the factors such as $1/kTB$. Therefore, (S/N) at 600 km is reduced by about 40% if χ is taken to be 40° . Taking $N(h)$ to be fixed, $h_>$ would have to be reduced from 600 km to ≈ 460 km to recover the same (S/N) at the upper limit of the ionosphere. This suggests that ≈ 140 km of coverage is lost at the upper end of the ionosphere by depressing the antenna by 40° . But this is not the whole story. It appears that since the upper limit $h_>$ is above the F2 maximum, the reduction in $h_>$ will increase (S/N) on two accounts: (1) a decrease in $1/R^2$ spreading and (2) an increase in backscattered power due to an enhancement in N . Let $h_>^i$ refer to the initial upper limit and $h_>^f$ refer to the final upper limit. Then, require for $\chi = 40^\circ$ and $h_>^i = 600$ km that

$$\frac{(S/N)h_>^f}{(S/N)_{600 \text{ km}}} \approx 1.7. \quad (5.2)$$

For convenience, N will be in normalized units. From Fig. 3.3 one can conclude that $N(600) = 0.36$ if H_s is taken as 100 km and the height of the F2 maximum is taken to be 300 km. Rewriting Eq. (5.2), one has the following transcendental expression:

$$\left(h_{>}^f\right)^2 \approx \frac{(600)^2 N\left(h_{>}^f\right)}{(1.7)(0.36)}$$

or

$$\left(h_{>}^f\right)^2 \approx 5.9 \times 10^5 N\left(h_{>}^f\right), \quad (5.3)$$

where $h_{>}^f$ is expressed in kilometers. This may be solved graphically with the result that $h_{>}^f \approx 550$ km. Now one must find out how much Faraday rotation is lost by reducing $h_{>}$ from 600 to 550 km. With the usual assumptions regarding the ionospheric distribution of electrons it is found that $\int_{550}^{600} N \, dh \approx 2 \times 10^{16}$ electrons/m², which yields a rotational change $\Omega(600) - \Omega(550)$ of about 45°. Thus at a zenith angle of 40° one stands to lose only half of an N estimate by neglecting the altitude region between 500 and 600 km. But by means of the beam depression, nine estimates are gained in the region below 600 km by virtue of the change in Ψ (this is simply read from Fig. 3.1). Hence, one experiences a net gain of 8.5 estimates of N by lowering the antenna in the prescribed fashion (toward the south with a zenith angle of 40°). In addition, the range in heights covered is virtually the same--400 km.

To recapitulate, depressing the radar antenna from the vertical position reduces the (S/N) in the upper ionosphere, thus reducing the maximum height of observation. But it has also been found that this reduction is not as severe as expected since the electron density decreases with height above the F2 maximum. By depressing the antenna toward the south for the purpose of maximizing the parameter Ψ , one finds that the Faraday rotation is enhanced considerably, more than offsetting the minor reduction in the observable rotation in the upper ionosphere. Furthermore, antenna depression has the added advantage of reducing some clutter effects, specifically ground clutter, thus exposing a greater portion of the lower ionosphere.

As already mentioned concerning (d), clutter may be decreased by depressing the antenna. This is because ground clutter has a cutoff in range due to earth curvature, and this cutoff is more or less independent of antenna-beam depression angle. (For fixed ranges clutter echoes will become stronger as the beam is depressed, since more radio energy illuminates the targets. In fact, some of the echoes may appear quite strong as clutter targets become illuminated by strong side lobes. Nevertheless, the maximum range of the clutter region is not appreciably advanced by antenna depression.) It is important to note at this point that aircraft targets often appear above the horizon at great ranges, perhaps even at an apparent ionospheric height of 300 km. The azimuthal dependence of the aircraft targets is quite variable and depends on local flight patterns (Friendship airport at Baltimore, Dulles in Virginia, Andrews in Maryland, and National in Washington, plus local private airports) which are controlled by the weather. Therefore, the most clutter-free data is obtained during poor weather conditions. It is not possible to remark at present on any preferential azimuth and elevation as far as clutter is concerned, but it is currently under study.

PULSE LENGTH EFFECTS AND FARADAY DISPERSION

Fig. 5.3 is a representation of a portion of the crosspolarized* channel data obtained on January 30, 1970. Eleven runs for which the antenna was pointing toward zenith are depicted and were obtained over a time span of about 2 hours. Each run corresponds to roughly a 7-minute average and exhibits quasi-periodic fading with respect to height as a result of Faraday rotation. On these data approximately 11 fades (the number of "bumps") are visible below 450 km, which suggests that ≈ 22 estimates of N may be obtained. Since the lower limit in height is 150 km, this implies an average height separation for the estimates of ≈ 14 km, although it is slightly better in the neighborhood of the F2 maximum and slightly worse away from this region. One of several noteworthy features is the clutter region which distorts the initial segment of each run even though the starting point for each curve is 150 km. Clearly clutter effects extend to at least 180 km consistently. A second feature is that the (S/N) is beginning to deteriorate rapidly by 450 km, which is approximately the terminal point of the display. The third feature is that the baseline upon which the Faraday data rides is distorted. In fact,

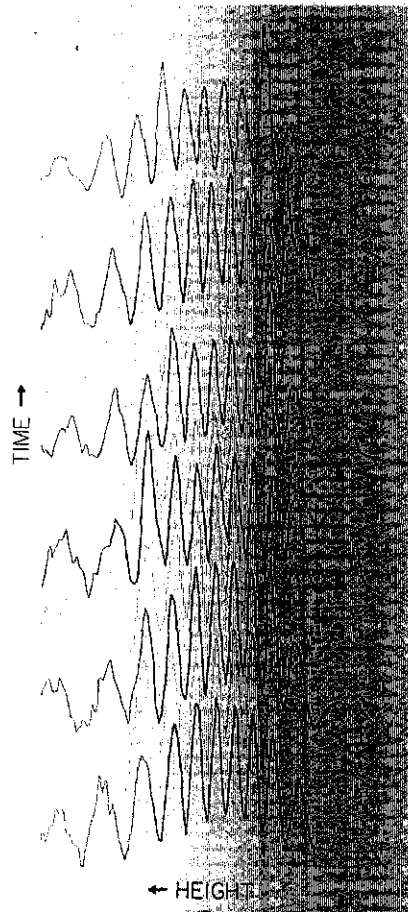


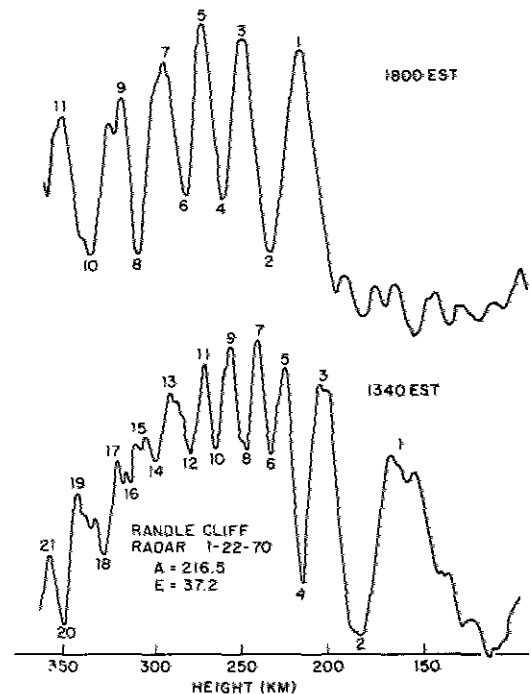
Fig. 5.3 - Some consecutive Faraday rotation profiles obtained on January 30, 1970

*In these runs the transmitted signals were linearly polarized in the horizontal plane with a fixed electric vector orientation of 0° . On receive, two signals are obtained--one corresponding to 0° and another (crosspolarized) corresponding to $0 + 90$ degrees. For clutter limitation, the crosspolarized channel is most often used for purposes of analysis.

the baseline level is raised to its maximum value near the F2 maximum. This will be shown to be primarily the result of so-called Faraday dispersion within the radar pulse. In these particular data a pulse length of $50 \mu\text{sec}$ was employed, and this corresponds to an effective length of $c\tau/2 = 7.5 \text{ km}$. Evidently a nonnegligible amount of Faraday rotation occurs over a height interval of 7.5 km in the F region.

Another example of Faraday dispersion is given in Fig. 5.4. In this case data is being obtained at a rather low elevation angle, and a $50\text{-}\mu\text{sec}$ pulse is used. Note that the Faraday fade rate is greatest in the region where the baseline is most distorted. This indicates that the dispersion is proportional to electron density, as it would be expected to be.

Fig. 5.4 - Two widely spaced Faraday rotation profiles obtained on January 22, 1970



It is quite important at this point in the discussion to mention a possible alternative reason for the baseline distortion. Since the Faraday fading is quasi-periodic, it represents an RF perturbation to the receiver. From Fig. 5.4 one estimates that the shortest time for a complete fade is about $100 \mu\text{sec}$, and this corresponds to a frequency of 10 kHz . If the receiver bandwidth were of this order or smaller, say 5 kHz , the signal to be severely reduced. So for small bandwidths, a baseline distortion similar to that exhibited in Fig. 5.4 might be observed. However, the RCR receiver bandwidth is 23 kHz (i. e., matched to a $50\text{-}\mu\text{sec}$ pulse), and the response over this bandwidth is reasonably flat. Hence, the baseline distortion is not merely a bandwidth effect.

Note also that the amount of Faraday fading is less in the late afternoon than it is at 1340 EST , and the baseline distortion is also less severe. These features of the Faraday rotation profiles are highly suggestive of an alternative procedure for deducing the electron density of the ionosphere. This procedure will soon be explored, but first an attempt will be made to develop a simple theory to describe the dispersion phenomenon.

Assume that the radar antenna is directed toward zenith, that the radar beamwidth $\theta_{1/2}$ is sufficiently small (recall that $\theta_{1/2} = 1/2\text{-power beamwidth} = 3.6^\circ$ at Randle Cliff),

and that a fixed time delay corresponds not only to a definite range but also to a definite height h . Also assume that one is sampling a single linear component of the E vector associated with the downcoming Thomson scatter signal. Recall that the Faraday rotation angle corresponding to a signal scattered from a height h is given by

$$\Omega(h) = 5.95 \times 10^{-2} f^{-2} \int_0^h N(h') \Psi(h') dh' \quad (5.4)$$

Since the radar beam is finite and not infinitesimal, the crosspolarized component of the E vector is actually related to a certain distribution of E vectors combined with appropriate weight factors. These factors are governed by the character of the antenna beam pattern (its symmetries, side lobes, etc.). Now let ϕ stand for a particular direction contained within the beam solid angle denoted by ϕ , and let $d\phi$ be a differential element of solid angle. Then the Faraday angle is the following composite:

$$\langle \Omega(h) \rangle = 5.95 \times 10^{-2} f^{-2} \int_{\phi \in \Phi} g(\phi) d\phi \int_0^h N(h') \Psi(h') dh', \quad (5.5)$$

where the corner brackets indicate that we have averaged over the beam at fixed h .

The integral $\int_0^h N(h') \Psi(h') dh'$ actually depends on ϕ as well as h . However, one can simplify the dependence by assuming N to be locally invariant. This is safe, since for a beamwidth of 3.6° the corresponding horizontal distance at an altitude of 30 km is ≈ 19 km, significantly smaller than most large-scale irregularities. Now how does Ψ depend on ϕ ? Fig. 5.5 shows the variation of Ψ in both the north-south (N-S) and east-west (E-W) planes. In the E-W plane, Ψ is almost constant, which suggests that Ω is almost constant, resulting in no dispersion. In the N-S plane, Ψ varies quite drastically, and a large variation in Ω would be expected. Nevertheless, since Ψ varies approximately linearly in this plane and the antenna beam is assumed to be symmetrical, then the extensive dispersion in Ω about the zenithal value would be expected to be negated by vectorial cancellation. Thus within the framework of assumptions which have been made (the important ones being localized density invariance and a symmetrical antenna beam), one may neglect any dispersion which might be associated with a finite beamwidth at least insofar as the determination of the the E -vector orientation is concerned. Clearly, however, the N-S dispersion will affect the (S/N), since a certain fraction of the back-scattered E field is canceled. As a consequence the locus of Faraday minima would be essentially unaffected, whereas the locus of Faraday maxima would be expected to be reduced to some extent. In addition, the reduction of (S/N) due to

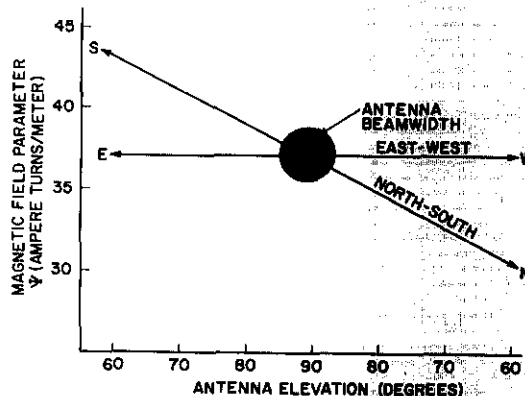


Fig. 5.5 - Variations of Ψ in the north-south and east-west planes

dispersion in the N-S plane is a cumulative effect, increasing with radar range. Thus, the baseline distortion, which is exhibited in Fig. 5.4 and which is roughly defined by the locus of Faraday minima, cannot be ascribed to beamwidth dispersion. On the other hand the Faraday maxima might be affected to some extent.

Having for the most part discarded beamwidth dispersion, one can now consider pulse dispersion and can develop an expression by which the electron density may be obtained through a measurement of this dispersion. Letting τ represent the pulse length, one has for the pulse average of the Faraday rotation angle

$$\langle \Omega(h) \rangle = 5.95 \times 10^{-2} f^{-2} \int_{t \in \tau} h(t) d\tau \int_0^h N(h') \Psi(h') dh', \quad (5.6)$$

where $h(t)$ is the pulse-shape weighting factor. In actuality $h(t)$ is proportional to the convolution of the pulse shape with the receiver gate function $\alpha(t)$. However, if the gate function is small in comparison with the pulse length, $h(t) * \alpha(t) \approx h(t)$. This follows from the sifting property of the delta function and the definition of the convolution integral. The analysis can be further simplified by assuming $h(t)$ to be constant over the pulse length τ , and for convenience it is taken to be unity. Hence, the amount of Faraday dispersion within a pulse of length τ is given by

$$\delta\Omega = 5.95 \times 10^{-2} f^{-2} \int_{[h_0 - c\tau/4]}^{[h_0 + c\tau/4]} N(h') \Psi(h') dh', \quad (5.7)$$

where c is the speed of light, $c\tau/2$ is the pulse length in units of distance rather than time, and h_0 is the height corresponding to the midpoint of the pulse. Assuming $N(h)$ and $\Psi(h)$ are fixed within τ , one concludes that

$$\delta\Omega(h_0) = 5.95 \times 10^{-2} f^{-2} (c\tau/2) N(h_0) \Psi(h_0). \quad (5.8)$$

Since $\Psi(h_0)$, f , and τ are presumably known, then a measure of the dispersion $\delta\Omega$ within τ leads to an estimate of the electron density N . One next defines a dispersion parameter \tilde{R} to be the ratio of the minimum signal to the average of its adjacent maxima. Under the conditions which have been stated (constant N and Ψ within the pulse), it is trivial to show that the dispersion parameter is quite simply related to the dispersion angle $\delta\Omega$. One finds that

$$\tilde{R} = \tan(\delta\Omega/4). \quad (5.9)$$

It is noted that for $\delta\Omega = 180^\circ$, (one fade within τ), $\tilde{R} = 1$; obviously $\delta\Omega$ must be less than 180° to make useful measurements of \tilde{R} .

Fig. 5.6 shows the effect on the maximum value of \tilde{R} -- call it \tilde{R}_{\max} -- if the radar pulse length is changed. Although the dispersion is large for all pulse lengths, it is most pronounced for the 200- μ sec pulse. One interesting feature is that the \tilde{R}_{\max} for the 25- μ sec pulse is no better than that for the 50- μ sec pulse. This appears inconsistent with the notion that $\delta\Omega$ (and therefore \tilde{R}) is proportional to τ (via Eq. (5.8)). Since the receiver bandwidth is 23 kHz and the bandwidth associated with a 25- μ sec pulse is 40 kHz, one is effectually throwing away signal energy. In other words, in view of the fact that $(S/N) \propto \tau/kTB$ for fixed N and h , (S/N) is reduced as τ is reduced with the bandwidth B held constant. For pulse lengths greater than 50- μ sec, one finds that (S/N) is actually increased if B is held fixed. In short, it is suggested that the reduced (S/N) associated with the 25- μ sec pulse renders the data somewhat more noisy, and as a consequence any

measurement of \bar{R} is of dubious value. It is rather obvious that the optimum situation is one in which the pulse length is made arbitrarily large and the system bandwidth is made arbitrarily small. In practice the best signal-to-noise ratios are obtained by matching the system bandwidth to the radar pulse length. Thus, for a 1-msec pulse one would require a bandwidth of roughly 1 kHz to recover most of the backscattered spectrum, if we neglect the intrinsic spectrum of the ionosphere.

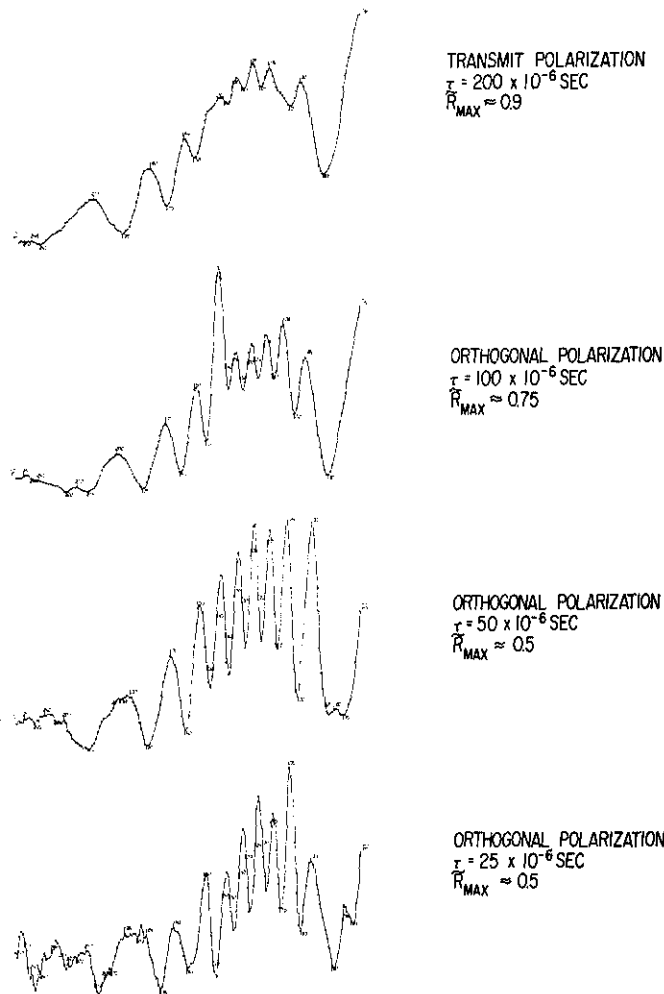


Fig. 5.6 - Dependence of dispersion ratio upon pulse length

Fig. 5.7 is a plot of \tilde{R} against the electron density N which was obtained by another method* for a number of runs obtained between 1330 and 1500 EST on November 20, 1969. In this experiment the antenna was depressed $\approx 20^\circ$ from zenith, but this fact should not seriously affect the analysis as long as N may still be taken to be approximately constant within the volumetric resolution cell. There is clearly a relation linking \tilde{R} with N , and it is suggested that this relation is obtained by combining Eqs. (5.8) and (5.9) as follows:

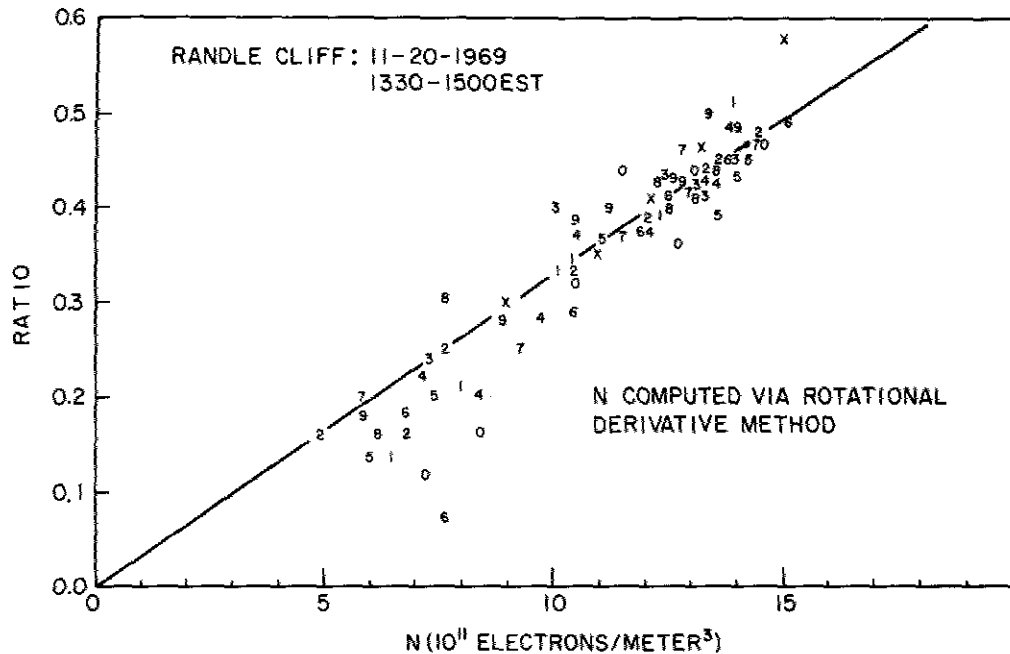


Fig. 5.7 - Ratio of extrema versus electron density

$$N(h_0) = \frac{67.2 f^2 \tan^{-1} \tilde{R}(h_0)}{(c\tau/2) \Psi(h_0)} \quad (5.10)$$

Fig. 5.8 depicts the average electron density profile corresponding to the data displayed in Fig. 5.7. Both the Faraday dispersion method (via Eq. (5.10)) and the standard rotational derivative method were employed. It is obvious that the dispersion method yields values which are in reasonably good agreement in the E region and the upper F region, but the values of N are about 25% greater in the neighborhood of the F2 maximum. Although beamwidth dispersion would be expected to lower the locus of Faraday maxima and thus increase \tilde{R} (and estimates of N), it should be an increasing function of radar range R ; consequently, the discrepancy near the F2 maximum is not a manifestation of unaccounted-for beam dispersion. The discrepancy is presently felt to be the result of another dispersion effect which has thus far not been mentioned -- temporal dispersion. Due to the relatively long integration times required in this experiment (about 6.5 minutes), electron content fluctuations become important and may give rise to shifting of the rotational extrema. It will be discovered later in this report that fluctuations in the isorotation contours of 1 km/min are not uncommon, and this amount would easily be sufficient to account for the observations.

*The standard method used in the Faraday studies at Randle Cliff embodies the determination of $d\Omega/dh$ and is called the rotational derivative method.

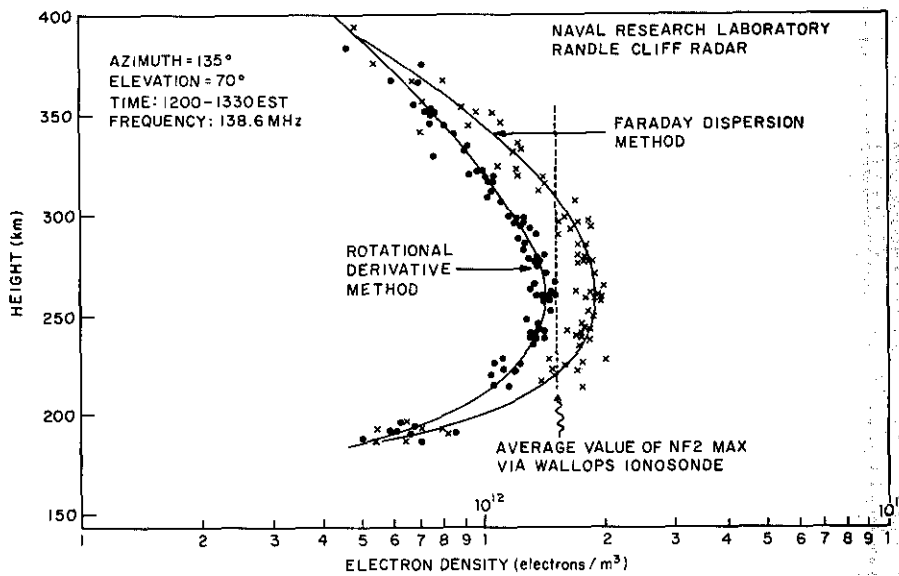


Fig. 5.8 - Comparison of electron densities obtained by the rotational derivative and Faraday dispersion techniques

Note Added in Proof: 4/1/71

Since the first draft of this report was submitted it has been pointed out to the author that the measured voltage at the output of the linear detector is actually proportional to the backscatter power provided the signal-to-noise ratio is $\ll 1$. This fact has been discussed by Evans* [1969]. At Randle Cliff such a proviso is likely to be valid even during daytime operations. Thus the dispersion parameter \bar{R} should be replaced by $\bar{R}^{1/2}$ in this section. Whereas the values of N deduced from a dispersion analysis were $\sim 25\%$ too high before, we find that they are substantially higher now if we assume $(S/N) < 1$.

Factors which must be considered to give rise to measureable overestimation in electron density include: (a) sampling rate (error $\sim 13\%$), (b) temporal dispersion (error $\sim 20\%$), and (c) system bandwidth (error $\sim 10\%$).

In sum, we find that the dispersion method yields overestimates of the electron density. Although a substantial fraction of that overestimate may be accounted for, there are certain troublesome features that warrant further investigation before the technique will be completely useful.

*Evans, J. V., "Millstone Hill Thomson Scatter Results", Lincoln Laboratory Technical Report 474, 8 December 1969.

CHAPTER 6

SPATIAL AND TEMPORAL DEPENDENCE OF THE ELECTRON DENSITY OVER RANDLE CLIFF

COMPARISON OF RANDLE CLIFF DATA WITH WALLOPS ISLAND IONOSONDE

To assess the degree of confidence which might be placed upon the electron density estimates which are obtained at Randle Cliff via the Faraday rotation technique, the F2 peak values are compared with those deduced from vertical-incidence ionosonde at Wallops Island, Virginia. As shown in Fig. 4.1, Wallops Island is about 70 nautical miles from Randle Cliff; so, apart from certain irregularities which "periodically" arise, one would hope that the general behavior of the electron densities extracted from the two facilities would be in substantially good agreement. The basic principles of the ionosonde will now be briefly reviewed.

In the analysis of free plasma oscillations there emerges to so-called plasma frequency f_p , which is directly proportional to the square root of the electron density N . Specifically,

$$f_p = \sqrt{N e^2 / (4\pi^2 m \epsilon_0)},$$

where ϵ_0 is the free-space permittivity, and f_p is in MHz.

With the assumptions of no collisions and no magnetic field, it is shown in Appendix A that the index of refraction n associated with a radiowave of frequency f is given by

$$n = \sqrt{1 - X},$$

where $X = (f_p/f)^2$. The boundary condition for reflection at normal incidence from an ionized layer is simply

$$n = (1 - X)^{1/2} = 0,$$

since $n = 0$ implies an infinite phase velocity c/n and a vanishing group velocity c/n' (the so-called group refractive index n' may be shown to be $1/n$. For details refer to Budden [1961] or Davies [1965]). Thus, below a frequency of f_p , the plasma will no longer support propagation and the radio wave will be reflected. The electron density profiles of the lower ionosphere which are obtained by ionosonde are based on this principle.

The typical ionosonde is a radar system in which the frequency of transmission is swept so that the entire domain of possible plasma frequencies is covered. For typical ionospheric profiles having a single peak, one would find that a plot of echo delay (or virtual height h') versus frequency would be a monotonically increasing single-valued function. It is also true that dh'/df is usually an increasing function, and the frequency at which dh'/df is approximately infinite corresponds to the critical frequency, which is the maximum plasma frequency of the layer. Of course, if the ionosphere is composed of several layers, then a number of functions $h'(f)$ are obtained. An additional complication arises if one considers the effect of the magnetic field, for in that case the radiowave is split into two parts: an ordinary mode and an extraordinary mode. These two modes travel with slightly different group velocities and thus exhibit distinct traces. In addition

the boundary conditions for reflection of the ordinary (x) and extraordinary (o) modes are different. Taking f_o and f_x to be the ordinary and extraordinary critical frequencies, Mitra [1947] notes that either

$$N = 1.24 \times 10^{10} (f_x^2 - f_x f_g)$$

or

$$N = 1.24 \times 10^{10} f_o^2$$

where f_g is the electron gyrofrequency and all frequencies are in MHz. In practice the second expression is used to deduce N , since no assumption need be made concerning the magnetic field. To convert $h'(f_o)$ curves to true height profiles $h(f_o)$, and these eventually to electron density profiles $N(h)$, it is necessary to incorporate the magnetic field in a rather involved computer routine.

The inaccuracy associated with the measurements of the ordinary ray critical frequency is stated by Grey* to be ± 0.01 MHz. Assuming this figure to be true, it suggests that ionosonde measurements are good to within about $\pm 0.2\%$ at $f_o F2 = 10$ MHz. However, Grey has indicated that the ± 0.01 MHz figure is an upper limit on accuracy, and for poorly defined traces the situation would be worse. On the basis of the least significant digit recorded on the standard 7-E forms used by ESSA (i. e., 0.1 MHz), one should take the uncertainty in $f_o (F2)$ to be ± 0.05 MHz. Assuming this uncertainty to be representative, one concludes that the ionosonde values of electron density are good to $\pm 1\%$ for $f_o F2 = 10$ MHz and $\pm 4\%$ for $f_o F2 = 5$ MHz. This is the probable range of F2 critical frequencies with which one shall be concerned. Hence, the best relative accuracy of ionosonde data is obtained at the F region peak during the daytime.

The Randle Cliff measurements of electron density are typically good to about $\pm 2.5\%$ provided adequate smoothing is employed. Single estimates of electron density are obtained every $\pi/2$ radians of rotation, and these values are good to about $\pm 10\%$ at worse if a 4- μ sec dwell time is employed but may be only good to $\pm 20\%$ if an 8- μ sec dwell time is selected. To compensate for this built-in error (arising from the finite receiver gate width) one simply computes the rotational derivatives over greater altitude spacings. Thus, the relative effect of the measurement error is reduced by smoothing the data. One typically employs either three-point triangular or five-point trapezoidal weighting functions which preserve some local effect yet reduce the endpoint error. This procedure becomes effectually an altitudinal smoothing of the order of 25 km in most cases, albeit somewhat greater when the electron density is low or when a higher value of dwell time is selected.

To compare Wallops Island derived values of N_{F2} with the Thomson scatter values, the Randle Cliff antenna was directed at an azimuth of $\approx 135^\circ$ and an elevation of $\approx 70^\circ$ so that the radar beam center approximately intersected the F2 region over Wallops Island at 300 km. Fig. 6.1 shows the rather good correlation between the N_{F2} (Wallops Island) and N_{F2} (RCR) for several trial experiments in 1969. Another illustration of the agreement of the two methods is given in Fig. 6.2. In this case we are comparing vertical incidence ionosonde data at Wallops Island with the RCR results also at vertical incidence. Each data point represents the mean hourly value of N_{F2} at both facilities, and the error bars are actually the range of values obtained during the hour. Six comparisons

* Environmental Science Services Administration (ESSA).

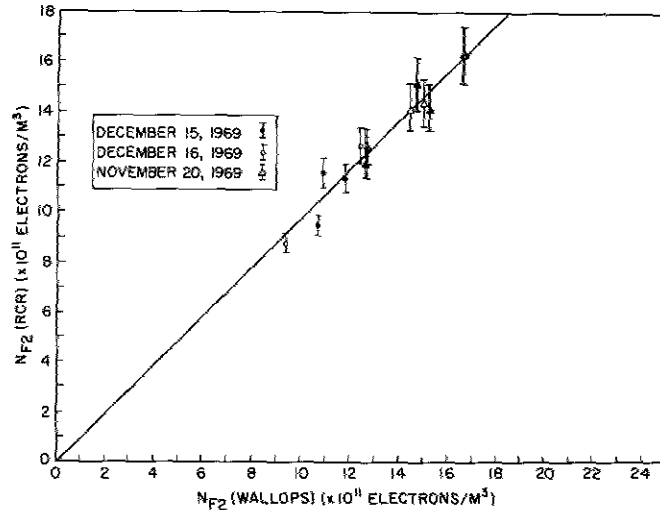


Fig. 6.1 - Comparison of Wallops Island ionosonde with RCR Thomson scatter

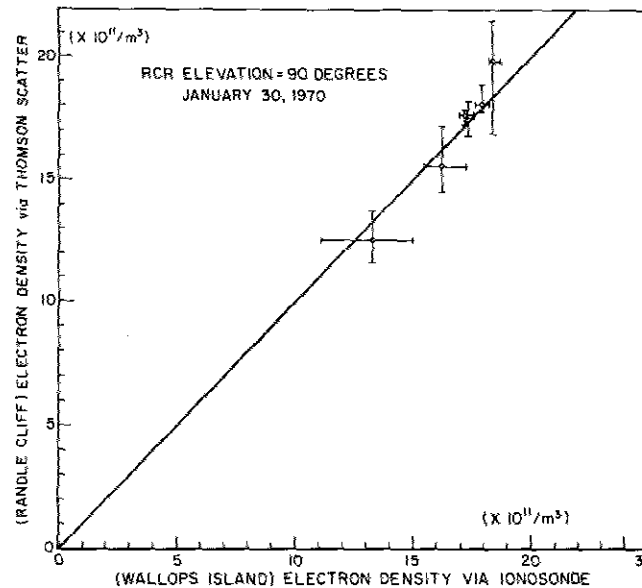


Fig. 6.2 - Comparison of Wallops Island ionosonde with RCR Thomson scatter data taken at 90° elevation

were made, and in all cases the 100% correlation curve (the 45° line) has intersection with the data range. This peculiar form of presentation was used to compensate for the fact that Randle Cliff Radar and Wallops Island ionosonde sample portions of the ionosphere which are physically separated by ≈ 93 km in latitude. We are, in a certain sense, allowing for spatial inhomogeneities which may be exhibiting a north-south drift. In view of the generally good agreement displayed between the Wallops Island and Randle Cliff data, one may proceed with some confidence in using the Faraday method for deducing F-region electron densities.

COMPARISON OF TOTAL CONTENT FLUCTUATIONS VIA ATS-5 WITH THOMSON SCATTER

In this section some findings are described regarding some measurements made on January 22 and May 5, 1970, in which ATS-5 satellite transmissions at 137.350 MHz were received with concurrent operation in a Thomson scatter mode. Fig. 6.3 gives the geometry of the experiment. The ATS video signals were displayed by pen recorder, and horizontal and vertical components of the RF were heterodyned down to 120 kHz and were fed into orthogonal amplifiers of an xy oscilloscope. Thus, the Faraday rotation of the elliptically polarized radiowave could be displayed and photographed. Fig. 6.4 is a photograph of a single frame of data from ATS-5. These displays may typically be read to an accuracy of ± 10 degrees which corresponds to better than $\pm 1\%$ in electron content.

Fig. 6.3 - Geometry of the geostationary satellite-Thomson scatter experiment

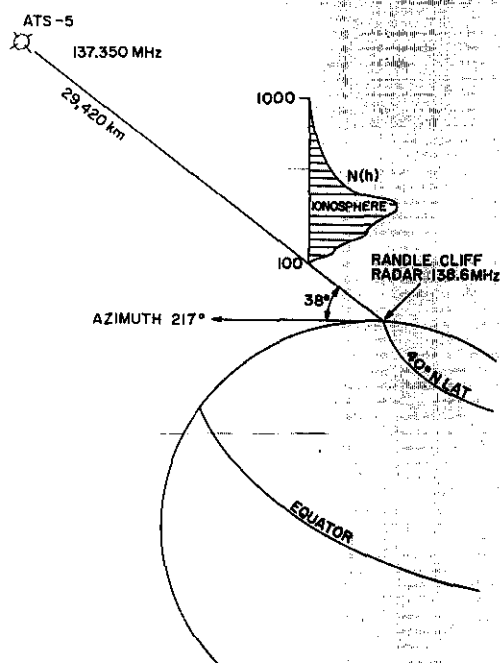


Fig. 6.4 - Representative data obtained from the ATS-5 satellite

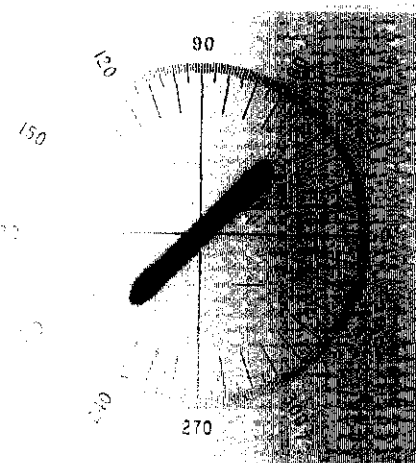


Fig. 5.4 depicts the Faraday rotation profiles obtained at 1340 and 1800 EST on January 22, 1970. At 1340 EST, one observes about $21 \pi/2$ radians of rotation below 350 km. One notes also that the rotation rate, indicated by the decreasing period of the amplitude fades, increases with height, in general, with its maximum value occurring at an altitude in the neighborhood of 280 km. At 1800 EST, only $11 \pi/2$ radians of rotation are observed to occur below 350 km. This decrease is of course a manifestation of the decrease in electron content between 1340 and 1800 EST. Finally, one sees that the baseline associated with the Faraday fades is raised above the background noise level, and this behavior is related to so-called Faraday dispersion within the radar pulse, which in this case has a length of $50 \mu\text{sec}$ (7.5 km). A height-dependent dispersion parameter may be defined which is related to the electron density, and this suggests an alternative way to deduce the density profiles. This was discussed in Chapter 5.

The Faraday rotation contours obtained during the experiment are shown in Fig. 6.5. Faraday dispersion was too severe at midday near the F2 maximum to make useful measurements, and interference was troublesome between 1100 and 1130 EST. Apart from these regions it was possible to construct isopleths of constant rotation which exhibit some rather interesting features. Since the rotation is an integrated effect, it follows that a height fluctuation associated with a particular isopleth is related to the presence of an integrated irregularity, i. e., an inhomogeneity in the electron content to the height in question. A negative or downwardly directed fluctuation represents an enhancement in content, and a positive or upwardly directed fluctuation represents a depletion in content. Furthermore, a Faraday rotational irregularity in the lower ionosphere must in a sense be propagated upwardly unless of course it is canceled by a fluctuation of opposite sign above it. If a rotational irregularity is propagated upwardly without extensive amplification, this implies that it resulted from a real density fluctuation but that the density fluctuation is localized. If the rotational irregularity is greatly amplified as it propagates upward, then the density fluctuation is extended in height. A further, useful editing feature is that if an irregularity is not propagated, then it is either spurious or exactly canceled.

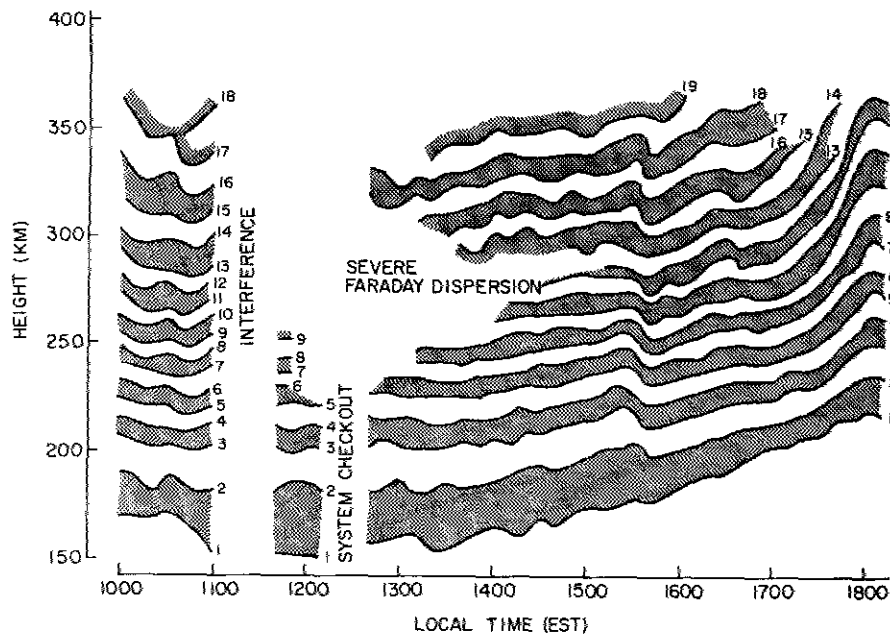


Fig. 6.5 - Faraday rotation contours obtained on January 22, 1970

Several irregularities in the isopleths are evident in Fig. 6.5. There is a positive fluctuation, implying depletion, at 1030 EST, and there is also an interesting region between 1500 and 1800 EST. Fig. 6.6 compares the ATS-5 satellite data with the Faraday rotation observed via Thomson scatter to 200, 250, 300, and 350 km respectively. Since the Thomson scatter values correspond to a two-way path, they are appropriately halved. It is seen that the general lower ionospheric irregularity structure is not distorted violently due to irregularities above 350 km. That is, undulations in total content (which is proportional to the Faraday rotation angle) are generally one-to-one with undulations in the Thomson scatter rotational isopleths. Judgements as to where in height the density fluctuations occurred may be made on the basis of the Thomson scatter data. In general, of course, the comparison may not be good if large irregularities occur above the height in which Thomson scatter facilities are limited due to lack of sensitivity.

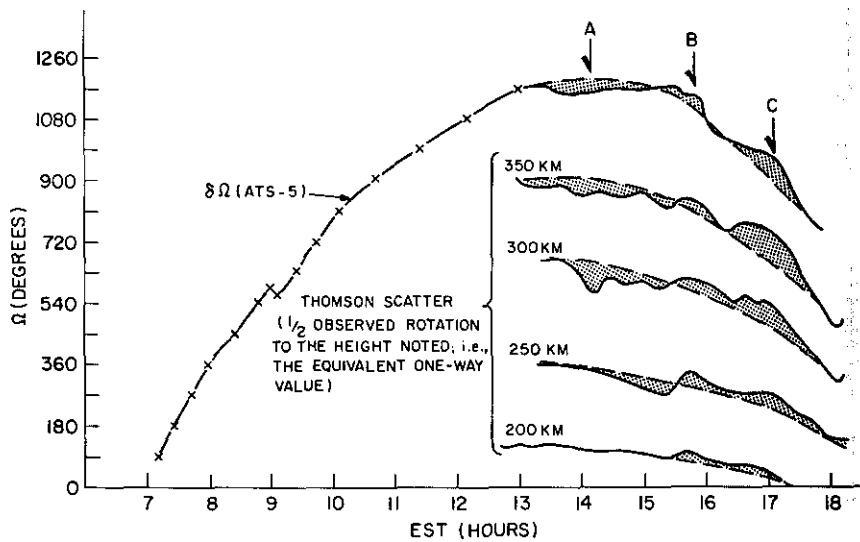


Fig. 6.6 - Comparison of Faraday rotational fluctuations associated with ATS-5 VHF transmissions and RCR Thomson scatter data. The zero level for Ω is arbitrary.

Fig. 6.7 shows the Faraday rotation isopleths obtained on May 5, 1970, and also the negative of the ATS-5 rotation (ambiguous). A comparison of this type is not inappropriate, since fluctuations in both the altitude of rotational isopleths (Δh) and in the rotation angle ($\Delta\Omega$) are proportional to the content fluctuations (ΔC)*. In the latter case,

$$\Delta\Omega(h) \approx 2.97 \times 10^{-2} f^{-2} \bar{\Psi}(h) \Delta C(h) \tag{6.1}$$

for the one-way path, where $\bar{\Psi}(h)$ is the weighted mean value of $H \cos \theta \sec \chi$ taken between the base of the ionosphere and the height h . In the former case,

* A change in electron content $\Delta C(h) = \Delta \int_0^h N dh$ may be produced by either a change in the "thickness" parameter $\tau(h)$ or in some reference electron density $N(h)$. Regarding the shape of the ionosphere as fixed, one takes $\tau(h)$ to be a constant. Thus one has $\Delta C(h) \approx \tau(h) \Delta N(h)$. On the other hand, upon examination of the altitudinal fluctuations of rotational isopleths it is found that $\Delta C(h) = N(h) \Delta h(h)$ where $N(h)$ is assumed fixed over Δh . These two relations suggest that $\Delta N(h)/N(h) \approx \Delta h(h)/\tau(h)$. Furthermore, since $\Delta C(h) \propto \Delta\Omega(h)$, it follows that $\Delta h(h) \propto \Delta\Omega(h)$.

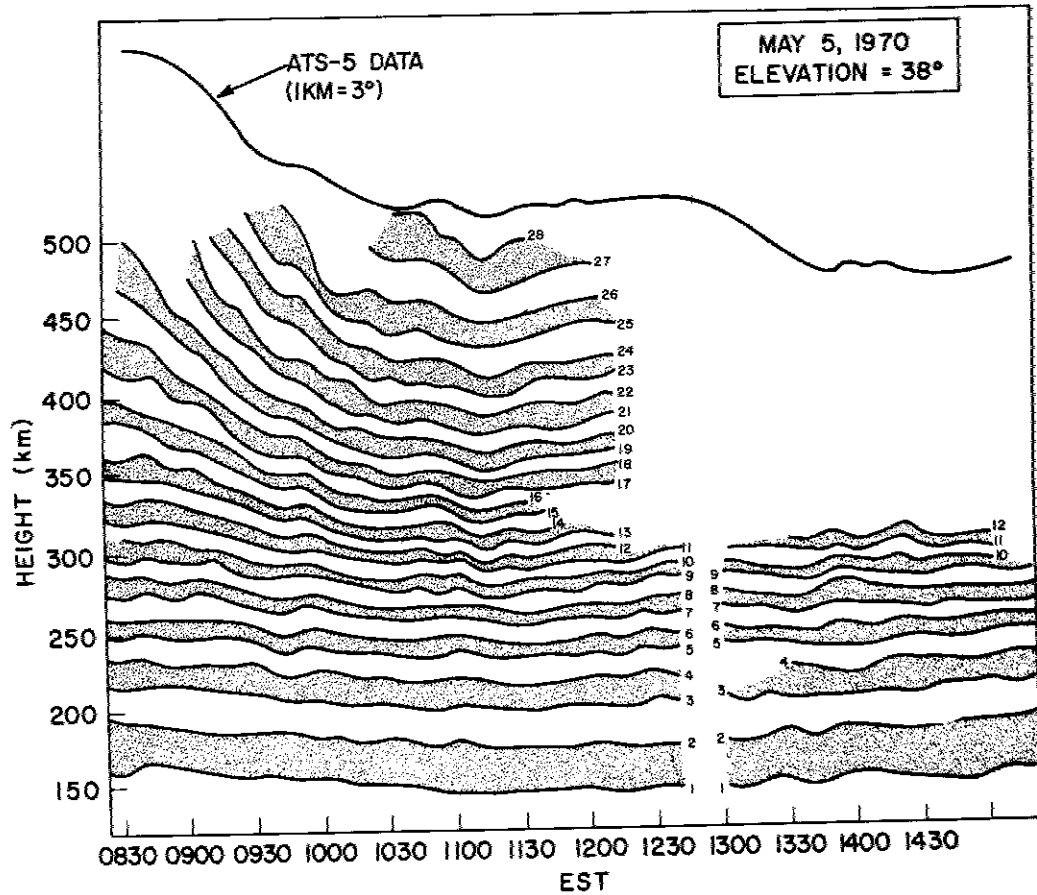


Fig. 6.7 - Faraday rotation contours obtained on May 5, 1970

$$\Delta h(h) \approx -\frac{1}{N(h)} \Delta C(h), \quad (6.2)$$

where $N(h)$ is the electron density in the neighborhood of the particular isopleth being examined. Thus, one finds that the altitudinal excursion Δh strongly depends on the local value of $N(h)$. An irregularity in the lower ionosphere will yield isopleth distortions which, generally speaking, will decay in the direction of the F2 maximum. If the irregularity ΔC is completely localized, Δh will never quite vanish at h_{F2} , since $N(h_{F2})$ is noninfinite. Above the F2 maximum the isopleth distortion associated with ΔC will grow in accordance with Eq. (6.2). This particular situation is illustrated in case A of Fig. 6.8. In addition two other cases are shown: (B) a localized irregularity at the F2 maximum and (C) a simple redistribution below the F2 maximum. Ignoring the slight altitudinal variations in the magnetic field, one finds that the condition for the exact cancellation of a rotational isopleth fluctuation between height h_1 and h_2 is

$$\Delta C(h_1) = -\frac{N(h_1)}{N(h_2)} \Delta C(h_1, h_2), \quad (6.3)$$

where $h_1 < h_2$ and $\Delta C(h_1, h_2)$ represents the content excursion between h_1 and h_2 . Therefore, if redistribution ($-\Delta C(h_1) = \Delta C(h_1, h_2)$) gives rise to a significant difference in the local electron concentrations at heights h_1 and h_2 , one would anticipate a nonvanishing Δh situation. For case C illustrated in Fig. 6.8, it is suggested that low-lying ionization

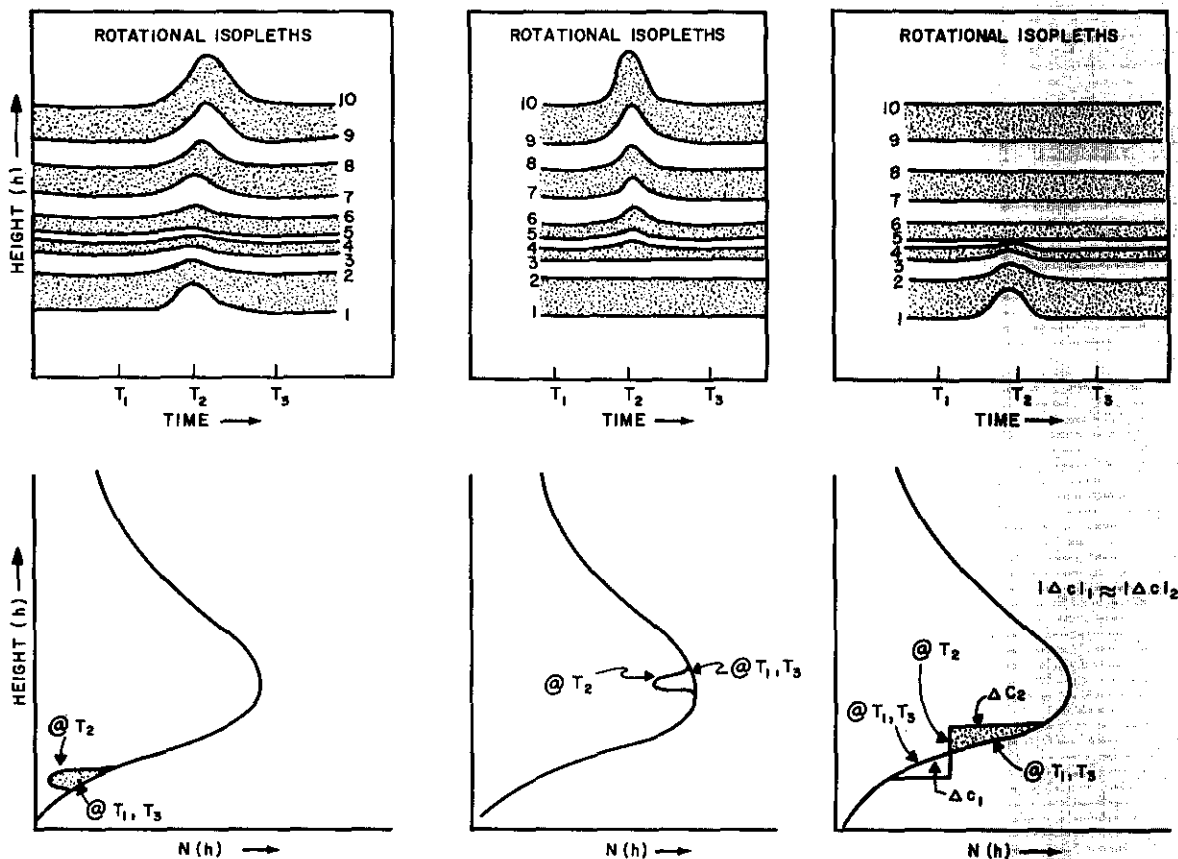


Fig. 6.8 - Effect of electron density fluctuations on rotational isopleths

is being enhanced (positive ΔC at h_1) by a downdrift from above (negative ΔC at h_2). For this hypothetical situation one would expect no isopleth distortion to exist in the region above h_2 . Had the situation be reversed (the signs of the ΔC 's reversed), there would be no cancellation. If one wishes to compare directly the rotational contour fluctuations with the change in $\Delta\Omega$, one simply equates the expressions for ΔC in Eq. (6.1) and Eq. (6.2). Doing this one obtains

$$\Delta h(h) = \frac{-\Delta\Omega(h)}{2.97 \times 10^{-2} f^{-2} \bar{\Psi}(h) N(h)} \tag{6.4}$$

Taking $\bar{\Psi} \approx 45$ ampere-turns/meter (it varies only a few percent along the ray path) and $N \approx 7.2 \times 10^{11}$ electrons/m³ for convenience, it is found that $\Delta h \approx 20 \Delta\Omega$ km, where $\Delta\Omega$ is in radians. Under these conditions, a height excursion of 10 km is equivalent to a rotational change of roughly 30 degrees. On the basis of this simple argument, Fig. 6.7 was scaled so that 1 km = 3 degrees.

One interesting feature of the comparison in Fig. 6.7 is that the maximum content on the basis of ATS-5 and Thomson scatter data are in rather good agreement—occurring at about 1115 EST.

Perhaps the most interesting facet of the comparison is a large afternoon excursion in Ω . The approximate simultaneity of the dispersion trouble and the afternoon content enhancement is clearly not just accidental. The late afternoon buildup in content is

thought to result because: (a) the temperature of the electron-ion plasma drops due to the rapidly increasing solar zenith angle, thus reducing the scale height above the F2 maximum and forcing a gradual collapse of the distribution of electrons, (b) the increase in ionization at lower levels is multiplied by a greater magnetic field strength so as to increase its efficiency in producing Faraday rotation, and (c) the greater recombination at lower heights evidently does not proceed rapidly enough to reduce the total content of the ionosphere appreciably. Thus, one concludes that Faraday-rotation total-content studies (as given by synchronous satellite studies such as those using ATS-5) misrepresent the afternoon anomaly and that the ionosonde parameter $f_o(F2)$ will have limited usefulness as an indicator of total content. One does find that $f_o(F2)$ will increase (as will usually the content below some moderate altitude, e. g. 500 km), but the total content $\int_0^\infty Ndh$ will decrease unless there exists some additional source of ionization. An alternative mechanism to account for the afternoon anomaly involves the work of $\mathbf{E} \times \mathbf{B}$ forces driving ionization to greater altitudes where electron loss proceeds less rapidly. There does not appear to be a need to invoke electrodynamic drifts in this case however. The obvious way to settle the matter is to measure the total content of the ionosphere by means of dispersive doppler for which there are no magnetic field considerations.

QUASI-PERIODICITIES OBSERVED AT RANDLE CLIFF

For a number of years traveling ionospheric disturbances (TID) have been studied by various workers using different techniques. Munro [1950], Heisler and Whitehead [1961], Becker et al. [1965], Klostermeyer [1969], and others have used ionosondes to detect oscillatory vertical movements of ionization. Total-content measurements by Taylor [1965] and Davis and Da Rosa [1969] have also shown the presence of the TID. Other manifestations of TID include scintillation effects (Elkins and Slack [1969]) and fluctuations in the vertical drift velocity (Evans, et al. [1970]). The first study of TID which embodied the entire ionosphere was by Thome [1964] using the Arecibo UHF Thomson scatter facility; subsequently Sterling [1967] has investigated TID over Jicarcarca.

It is now generally accepted that TID owe their existence to a certain class of neutral-gas wave motions in the atmosphere known as internal gravity waves (Hines [1960]). These waves have a limiting horizontal speed approaching ≈ 0.9 times the speed of sound and have a low-period cutoff of several minutes. In principle these waves may have an isotropic pattern, but it is generally found that TID in the F region travel in the N-S plane. This peculiar feature is a result of the action of the magnetic field on plasma motion, which freely allows motion along the field but constrains it in a direction orthogonal to the field. Perhaps the first direct evidence linking neutral-gas gravity waves in the thermosphere with TID in the ionosphere was provided by Dyson et al. [1970]. They conducted in situ measurements of both the electron and neutral particle densities using Explorer 32, and found that although the phase relationship between the neutral and electron density waves was often ambiguous, the wave patterns were similar.

The first Thomson scatter measurements of midlatitude TID using Faraday rotation were conducted at Randle Cliff during the Fall of 1969. It is important to note that the Faraday rotation method should in principle present a more refined picture of the electron density waves associated with TID, since the effect of T_e/T_i on the measurement is not as important as in the power profile method. This remark is made in light of the fact that direct measurements of N and T_e suggest that the two may be out of phase (Dyson et al. [1970]). Since the ionic cooling rate due to collisions would be expected to be slower than the electronic cooling rate, and since the electronic cooling is proportional

to N , this implies that T_e/T_i may be out of phase with the electron density N . If this is true, the power profile method will generate an overestimation of the electron-density wave amplitude. (To see this one need only consider the relation $(S/N) \propto N(h) / [1 + T_e/T_i R^2]$.)

Table 6.1 gives the pertinent data relating to all Thomson scatter experiments which have been conducted at Randle Cliff since November 20, 1969, and which extend over time periods of at least 4 hours. Included in the listing is the daily-sum magnetic index from Fredericksburg ($\sum K_{Fr}$) and the most significant wave period P (if any) associated with each experiment. The period P , which is basically the average time separation between isorotation maxima (or minima), was extracted by inspection of the Faraday rotation contours.

Table 6.1. Data Associated with Faraday Rotation Experiments

Exp. No.	Date	T_0 (EST)	T_f	Elevation Angle Degrees	Daily Sum Magnetic Index at Fredericksburg, Virginia, $\sum K_{Fr}$			Wave Period (Minutes)
					Day Before	Exp. Day	Day After	
1	11/20/69	0930	1600	70	11	6	2	52.5
2	12/15/69	0920	1600	70	4	9	15	47.5
3	12/16/69	0930	1500	70	9	15	3	30.0
4	12/17/69	0850	1500	90	15	3	2	38.0
5	1/22/70	1000	1815	38	11	5	9	20.0
6	1/30/70	0930	1515	90	14	20	10	70.0
7	2/10/70	1040	1510	90	4	9	6	32.5
8	2/11/70	0910	1530	90	9	6	6	34.0
9	3/7/70	1000	1730	63	26	33	51	67.5
10	3/9/70	0930	1700	63	51	32	9	23.0
11	4/28/70	0850	1520	80	13	7	11	49.0
12	5/4/70	0800	1443	70	16	15	18	25.0
13	5/5/70	0825	1520	38	15	18	10	50.0

The Faraday rotation contours for all experiments listed in Table 6.1 are presented in this report. The ATS-5 correlation experiments were already discussed in the beginning of this chapter; thus the Faraday contours for experiments 5 and 13 are not repeated. Furthermore, the contour associated with the solar eclipse experiment (9) will be discussed separately in Chapter 7. The remainder of the contours are displayed here as Figs. 6.9 through 6.18.

It is interesting that irregularities are exhibited by the Faraday rotation contours in all experiments and that within the sampling period limitation they can be described as quasi-periodic. Upon inspection of Table 6.1 it is noted that the average wave periods range between 23 minutes and 70 minutes and the overall, average period is 41.5 minutes.

Fig. 6.19 (top left-hand corner) is the periodicity distribution associated with the experiments. Each bin is 10 minutes wide and centered about the time noted. In constructing the histogram, values of the wave period which occurred at the partition point of two bins were assigned the number 1/2 and placed in both bins. The resulting distribution of wave periods decreases gradually toward long periods (low frequencies) but terminates rather abruptly at the low period (high frequency) end. This rapid termination

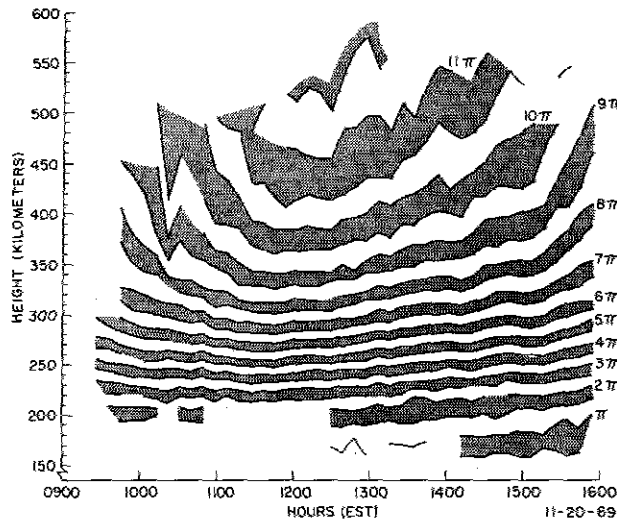


Fig. 6.9 - Faraday rotation contours obtained on November 20, 1969

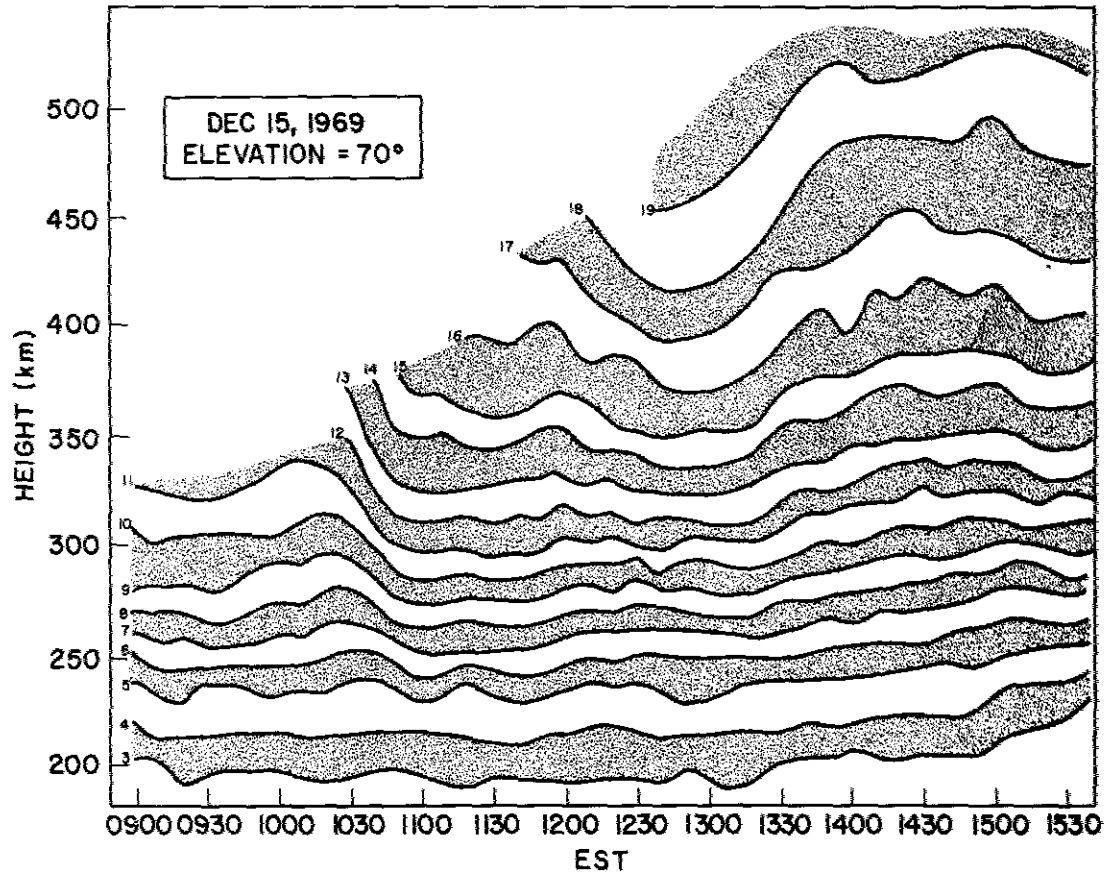


Fig. 6.10 - Faraday rotation contours obtained on December 15, 1969

would have to occur, since a sampling period of 10 minutes was normally employed, and the sampling theorem states that one may not resolve waves having periods less than 20 minutes. However, the Vaisala-Brunt period (which is the lower limiting period for internal gravity waves) is about 15 minutes. As a consequence, if the disturbances,

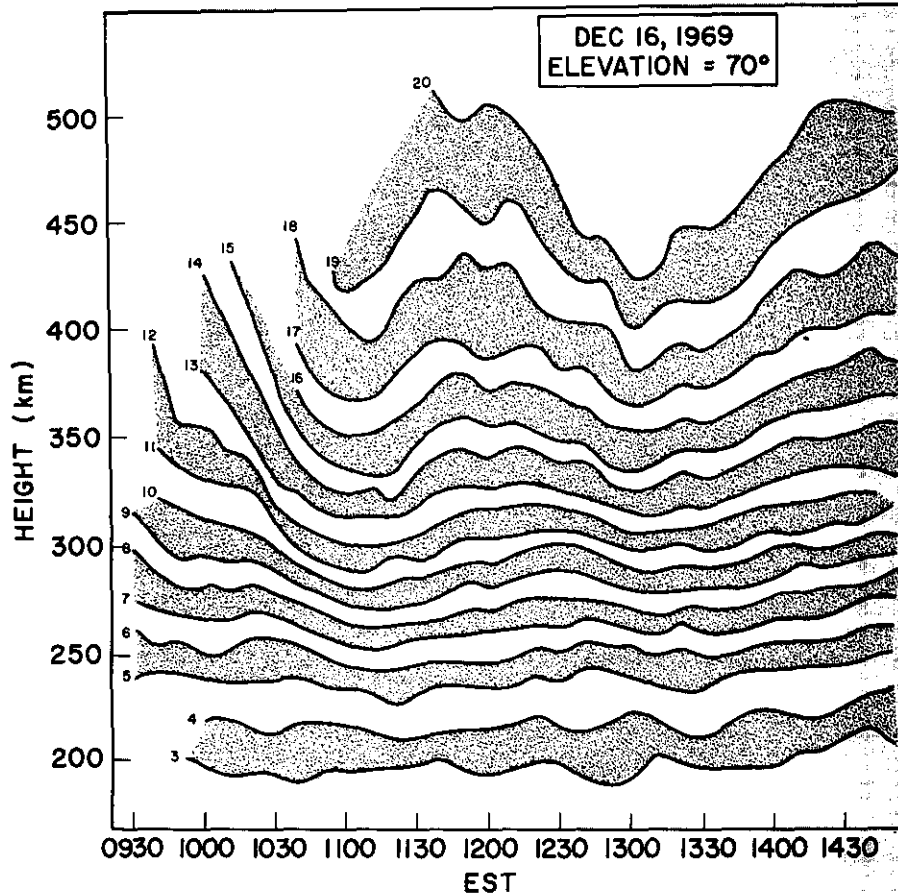


Fig. 6.11 - Faraday rotation contours obtained on December 16, 1969

assumed to be traveling, are a result of internal gravity waves, it is likely that few wave patterns are lost by choosing a 10-minute sampling period.

Fig. 6.19 suggests that there is only a weak relationship between wave period and magnetic activity. Nevertheless, both of the experiments having wave periods in excess of 55 minutes were conducted on moderately disturbed days. This is in agreement with Thome [1968], who measured large-scale traveling ionospheric disturbances having wave periods between about 1 and 3 hours and concluded that they resulted from southward moving waves generated during magnetic storms. Recently, Davis and da Rosa [1969] have shown by means of synchronous satellite studies that large-scale TID wave amplitudes are proportional to magnetic activity. Fig. 6.19 shows that if one considers only the low-period disturbances over Randle Cliff, one finds no relationship whatsoever between the wave period P and the magnetic index K_{F_r} . Even considering all recorded disturbances, the relationship between the two was weak at best. Perhaps this should be expected, since the average wave period during the present study was only 41.5 minutes, whereas the disturbances reported by Thome and Davis and da Rosa had a much greater duration. Possibly another source of internal gravity waves operates in the low-wave-period domain.

Fig. 6.20 is a scatter plot of the wave amplitude Δh (in kilometers) in the neighborhood of 250 km as a function of wave period P . Each data point corresponds to the total isopleth fluctuation associated with a single wavelet. Only temporally nonoverlapping

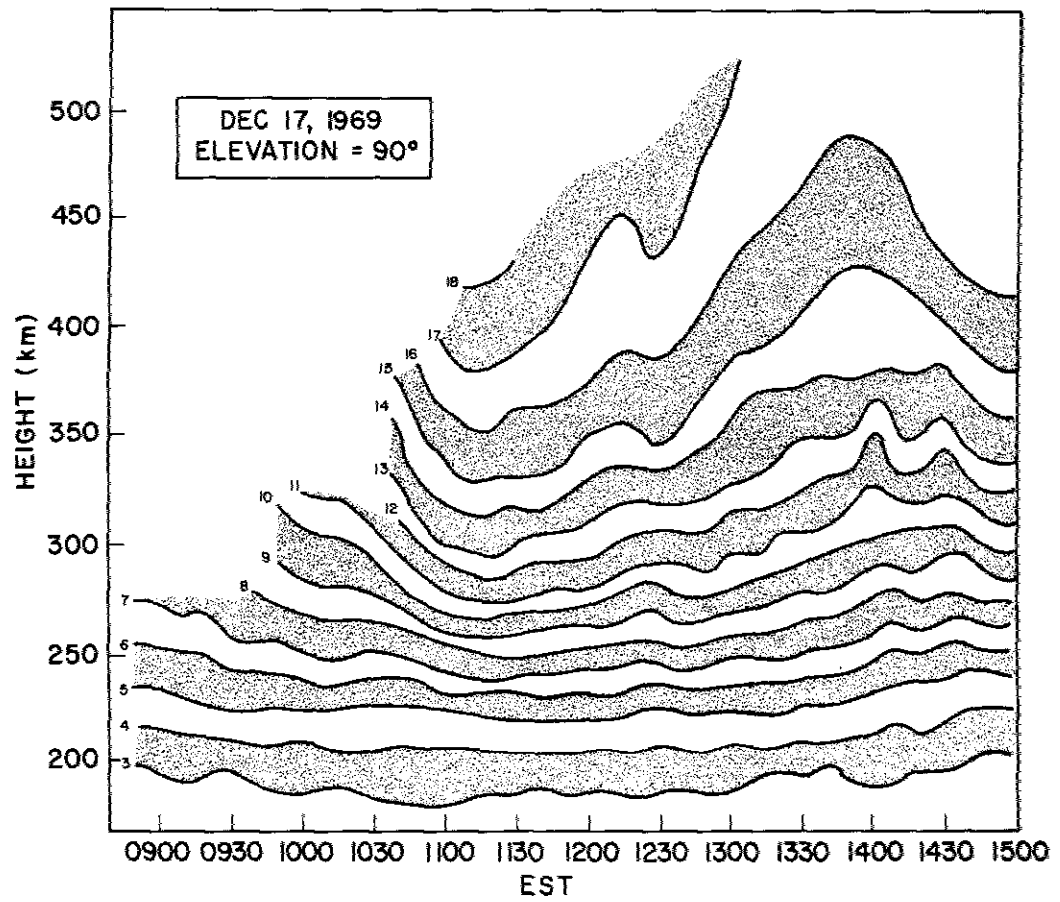


Fig. 6.12 - Faraday rotation contours obtained on December 17, 1969

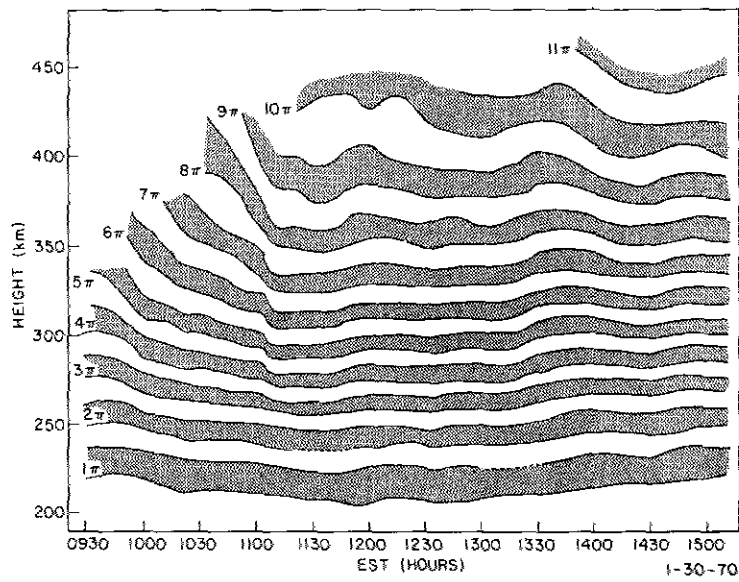
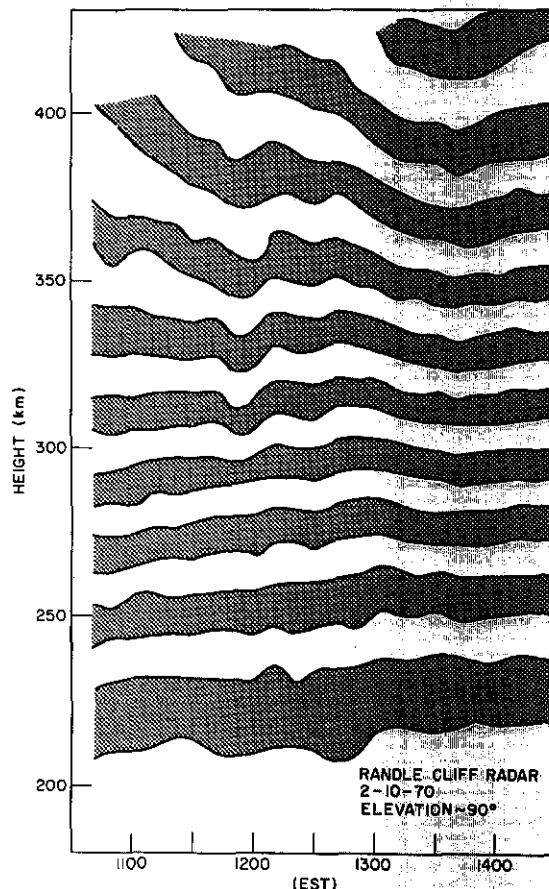


Fig. 6.13 - Faraday rotation contours obtained on January 30, 1970

Fig. 6.14 - Faraday rotation contours
obtained on February 10, 1970



wavelets were considered, and the significance of each wavelet was established by requiring both adjacent isopleths to have similar structure. The height of 250 km as reference is again a compromise between two factors: first, a desire to observe as low in the ionosphere as possible to reduce isopleth distortion arising from the integration effect and, second, the necessity to restrict analysis to altitudes above about 200 km to eliminate clutter distortion. It is happily a good choice, since the F2 maximum height is roughly 250 km during the daytime over Randle Cliff. The choice of the F2 maximum as reference will turn out to be convenient in the interpretation of the data also. One sees from Fig. 6.20 that Δh is roughly proportional to the wave period--the wave amplitude increasing about 1 km per 10 minutes.

Using Eq. (6.2) and the fact that a content fluctuation $\Delta C(250\text{km})$ may, to first order, be considered to be the product of electron density fluctuations $\Delta N(250)$ and the slab thickness $\tau(250)$, one obtains the order-of-magnitude relation:

$$\frac{\Delta h(250)}{\tau(250)} \approx - \frac{\Delta N(250)}{N(250)},$$

which is valid at the F2 maximum (taken to be at 250 km). Consequently, it is proper to use $\Delta h/\tau$ as an indication of relative density fluctuation. Henceforth, $\tau(250\text{ km}) = 100$ km will be regarded as the canonical distance for normalization purposes. Except under unusual circumstances, τ should range between roughly 75 and 125 km during the daytime; consequently, 100 km is a reasonable as well as appealing choice, since its use implies that the values of Δh in Fig. 6.20 may readily be scaled in terms of percentage

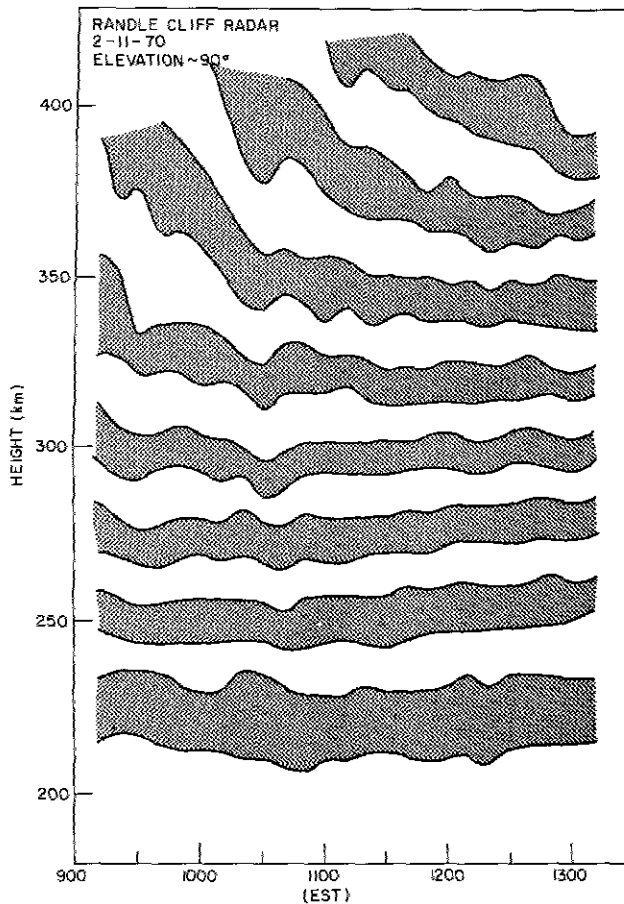


Fig. 6.15 - Faraday rotation contours obtained on February 11, 1970

excursion. Since the average wave period was found to be 41.5 minutes, one concludes that the average wave amplitude is about 4.2 km and that the ratios $\Delta h/\tau$ and $\Delta N/N$ are $\approx 4.2\%$. The maximum value of $\Delta N/N$ was observed to be $\approx 12\%$ within the framework of the assumptions which have been made. The average value of ΣK_{F_r} was ≈ 13.7 during the course of the experiments, which suggests that the average 3-hourly K index was roughly 1.7. Referring again to the paper on large-scale TID by Davis and da Rosa [1969], one finds that their total-content data imply a relative amplitude fluctuation of about 1% in the total content if $K_p \approx 1.7$. This appears inconsistent with the Randle Cliff value of $\approx 4\%$. However, if one assumes that TID are largely lower ionospheric perturbations, it is not surprising that the total content fluctuations are less pronounced, since the ratio of total content to the subpeak content is roughly 3.1, assuming a Chapman distribution. In addition, it is well known that measurable increases in the general level of magnetic activity will have a tendency to increase this ratio even more. Hence, it is felt with ample justification that the Randle Cliff percentages are actually in accord with the results of Davis and da Rosa, provided the data are interpreted with care. In this connection it is remarked that the Arecibo fluctuations are at least 10% and even greater during severe magnetic disturbances (Thome [1964, 1968]). Satellite studies also indicate that fluctuations of $\pm 10\%$ are not uncommon (Dyson et al. [1970]). It is noteworthy that TID-related fluctuations over the magnetic equator are considerably smaller than those observed at high latitudes, being only a few percent (Sterling [1967]). This is presumed to be related to the strong magnetic control of plasma motion.

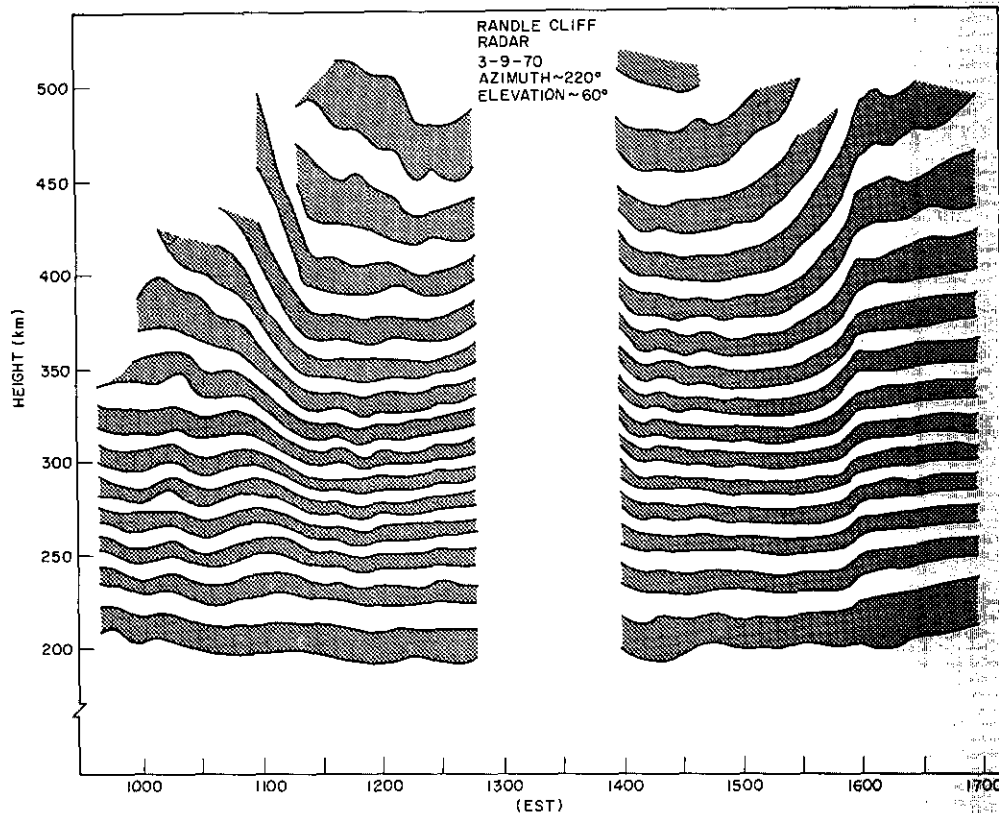


Fig. 6.16 - Faraday rotation contours obtained on March 9, 1970

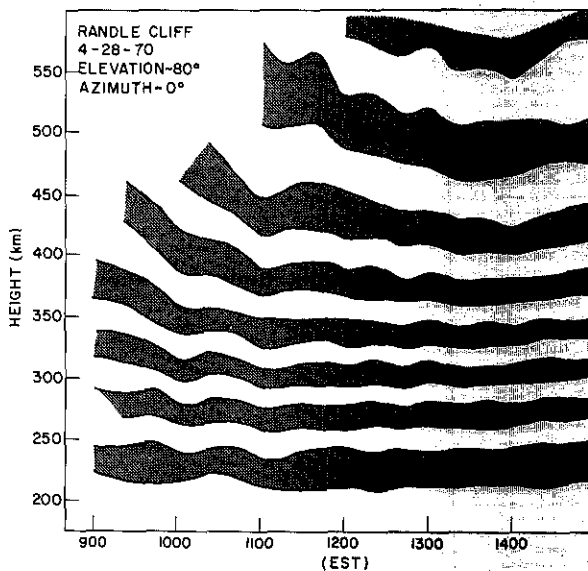


Fig. 6.17 - Faraday rotation contours obtained on April 28, 1970

Recall from Fig. 6.20 that wave amplitude is roughly proportional to wave period. To show that this would be expected on the basis of simple theory, one can reformulate an expression which relates the TID perturbation $\Delta N/N_0$, the wave velocity U , and the period P of the disturbances for the Randle Cliff latitude.

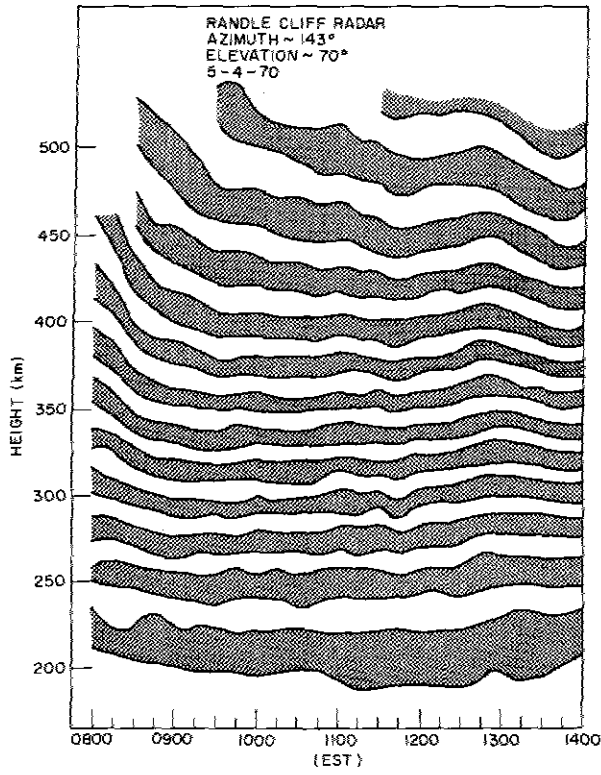


Fig. 6.18 - Faraday rotation contours obtained on May 4, 1970

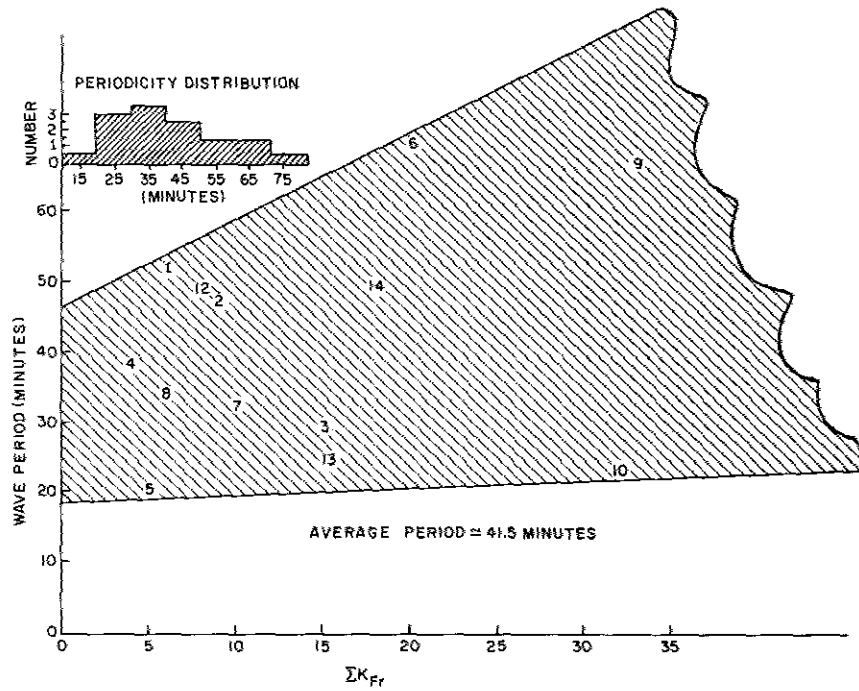


Fig. 6.19 - Irregularity wave period versus magnetic activity index

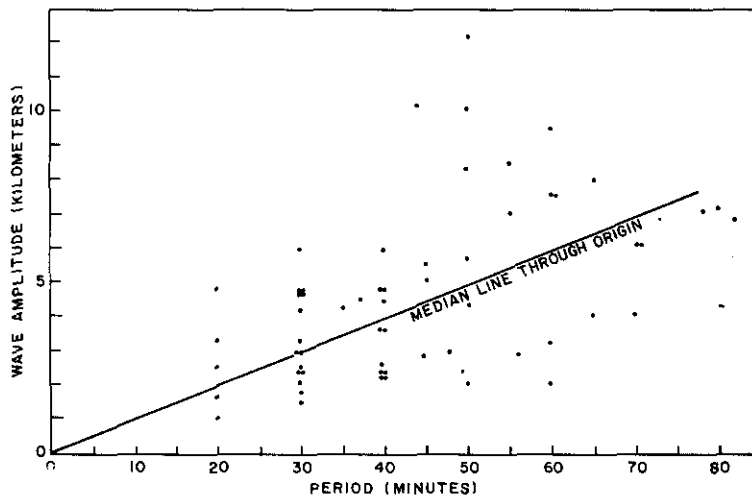


Fig. 6.20 - Scatter plot of wave amplitude at 250 km versus wave period

Recall the continuity equation:

$$\partial N / \partial t - \alpha N^2 - \beta N + q + \text{div}(N \mathbf{v}) = 0, \quad (6.5)$$

where the loss terms αN^2 and βN represent recombination and attachment processes, q is a production term, and $\text{div}(N \mathbf{v})$ is a movement term. For examining the first-order effect of neutral-gas wave motion on the plasma, it is legitimate to assume that the unperturbed electron density N_0 is constant; i. e., $\partial N_0 / \partial t \approx 0$. This condition is most likely to be valid during the daytime hours and especially near local noon. Additionally, one can suppose that a small perturbation ΔN in the electron density arising from a perturbation in the movement term alone does not affect either electron production or loss processes. This matter has been studied by Hooke [1968], who concludes that this is an acceptable view at or above the F2 maximum. Assuming that the perturbation has a harmonic time dependence, one finds that the relevant equation for the perturbed electron density is

$$i\omega \Delta N = -\text{div}(N_0 \Delta \mathbf{v}). \quad (6.6)$$

Thus, one sees immediately that the perturbation must be proportional to the wave period $P = 2\pi/\omega$. But there are additional things one can learn. Hooke [1968] has shown that in the vicinity of the F2 maximum and above, the divergence term is given by

$$\text{div}(N_0 \Delta \mathbf{v}) = [(\mathbf{u} \cdot \mathbf{e}_B) (\nabla N \cdot \mathbf{e}_B)] + [N_0 \nabla \cdot (\mathbf{u} \cdot \mathbf{e}_B) \mathbf{e}_B], \quad (6.7)$$

where $(\mathbf{u} \cdot \mathbf{e}_B)$ is the component of the neutral wind velocity \mathbf{u} along the magnetic field (denoted by the unit vector \mathbf{e}_B), $\nabla N \cdot \mathbf{e}_B$ is the field directed gradient of the electron density, and $\nabla \cdot (\mathbf{u} \cdot \mathbf{e}_B) \mathbf{e}_B$ is the divergence of the field directed wind velocity. The first bracketed term in Eq. (6.7) represents the effect upon the perturbation of a gradient in the electron density. To first order, it is permissible to neglect horizontal gradients except during the periods of sunrise and sunset; consequently, one may replace the first bracketed term by $[U_B (\partial N / \partial z) \sin I]$, where I is the magnetic inclination or dip angle and U_B is the field-directed value of the neutral wind (i. e., $U_B = \mathbf{u} \cdot \mathbf{e}_B$). The second bracketed term in Eq. (6.7) represents an expansion or contraction of the gas due to field-line convergence or divergence. It is now convenient to assume a solution for the neutral-gas motion of the form

$$U \propto \exp(-ik \cdot r + i\omega t). \quad (6.8)$$

It will further be assumed that ω is real and unique and that the form of the wave vector $k = (k_x, k_y, k_z)$ allows for amplification in the z direction. It can be shown (e. g. Hines, [1960]), that this amplification is exactly the amount required to compensate for decreasing gas density in the vertical direction. That is, k_x and k_y are real and k_z is complex. Thus

$$U \propto \exp i(\omega t - k_x x - k_y y - k_{zr} z) e^{k_{zi} z}, \quad (6.9)$$

and the second bracketed term in Eq. (6.7) can be written

$$N_0 \nabla \cdot (U \cdot e_B) e_B = i N_0 U_B (k_x \cos I + k_{zr} \sin I + ik_{zi} \sin I), \quad (6.10)$$

provided we select a coordinate system such that $k_y = 0$.

Using Eq. (6.10) and knowledge that the first bracketed term is $[U_B (\partial N / \partial z) \sin I]$, one may reconstruct Eq. (6.6) using the fact that $\partial N / \partial z \approx 0$ near the F2 maximum. Therefore,

$$\Delta N / N_0 \approx (i U_B / \omega) \left[\left(\frac{2\pi \sin I}{\lambda_{zi}} \right) - i \left(\frac{2\pi \cos I}{\lambda_x} + \frac{2\pi \sin I}{\lambda_{zr}} \right) \right] \quad (6.11)$$

where the wave numbers have been replaced by wavelengths. Thus, two terms are 90 degrees out of phase. Shortly it will be seen that the longer period disturbances may not exhibit significant vertical phase propagation. (This type of disturbance would likely be generated at a great distance from the observer. The auroral zone is a potential candidate for the source.) Consequently, one can assume $k_{zr} = 0$, thus allowing only surface-type waves. As a result,

$$\frac{\Delta N}{N_0} = \frac{2\pi U_B}{\omega} i \left(\frac{\sin I}{\lambda_{zi}} - i \frac{\cos I}{\lambda_x} \right) \quad (6.12)$$

The "wavelength" λ_{zi} plays a role in the amplification of the perturbation. Indeed, Eq. (6.9) suggests that the perturbation must grow with increasing altitude. Consequently, the present treatment (only small perturbation allowed) may be invalid in the upper F region unless other circumstances control the growth. In fact, the exponential amplification would be expected to be checked eventually by viscous forces (Hines [1960]). In any case, Eq. (6.12) has been formulated for conditions at or near the F2 maximum, where the linear treatment should be valid. For unducted modes λ_{zi} is roughly $4\pi H(250)$, where $H(250)$ is the neutral scale height at 250 kilometers. However, for ducted or partially ducted modes which resemble surface waves, the relation is not so clear. The assumption of at least two layers (having distinct scale heights) is necessary for a ducted mode calculation. Nevertheless, λ_{zi} characterizes the neutral gas in some sense. Since $\Delta N / N_0 \approx -\Delta h / \tau$ we have

$$\frac{\Delta h}{\tau} \approx -\frac{2\pi U_B}{\omega} i \left(\frac{\sin I}{\lambda_{zi}} - i \frac{\cos I}{\lambda_x} \right) \quad (6.13)$$

Recall that the neutral gas velocity is presumed to be strictly horizontal. Thus

$$\mathbf{u} = (U_x, 0, 0). \quad (6.14)$$

Hence, the plasma velocity is

$$\begin{aligned} \mathbf{v} &= (U_B \cos I, 0, U_B \sin I) \\ &= (U_x \cos^2 I, 0, U_x \cos I \sin I). \end{aligned} \quad (6.15)$$

As a result, for the Randle Cliff side, where $I \approx 70^\circ$; one finds

$$\mathbf{v} \approx U_x (0.117, 0, 0.322). \quad (6.16)$$

Hence, the electronic displacement vector is

$$i\omega \mathbf{D} = (X, Y, Z) = U_x (0.117, 0, 0.322). \quad (6.17)$$

As a consequence the vertical displacement is roughly three times as important as the horizontal displacement, even though the neutral driving motion is purely horizontal. Returning to Eq. (6.13) and realizing that $U_B \sin I = i\omega Z$ and $U_B \cos I = i\omega X$ one sees that

$$\frac{\Delta h}{\tau} \approx 2\pi \left(\frac{Z}{\lambda_{zi}} - i \frac{X}{\lambda_x} \right), \quad (6.18)$$

where $Z/X \approx 2.75$. For long-period waves ($P \geq 1$ hour) which travel at speeds close to the speed of sound, one suspects that λ_x may be several thousand kilometers. On the other hand, λ_{zi} is fixed by the character of the neutral atmosphere and may be close to 1000 km. If this is true, then $Z/\lambda_{zi} \gg X/\lambda_x$ to first order. Thus, for the long-period disturbances, one obtains the following very useful order-of-magnitude relation:

$$\frac{\Delta h}{\tau} \approx \frac{2\pi Z}{\lambda_{zi}} \quad (6.19)$$

So one finds that the isopleth fluctuations will be in phase with the vertical displacement, whereas the corresponding electron density fluctuations will be 180° out of phase. The exact phase relationship would not be expected to be clear for the majority of fluctuations in the disturbances encountered in the present study. However, if the horizontal wavelength is greater than or equal to roughly $1/3$ the vertical "wavelength" λ_{zi} , it turns out that Δh will lag Z by less than 45° . So for a wide band of horizontal wavelengths and especially for those associated with large-scale TID, there would be expected to be reasonably close agreement between layer-height fluctuation Z and Δh (or $-\Delta N$). In particular for the January 30, 1970, experiment, for which the average period was ≈ 70 minutes, one might anticipate that

$$[\Delta h(250)/\tau(250)] \propto Z. \quad (6.20)$$

Assuming $\lambda_{zi} = 1000$ km, the proportionality factor would be 6.28×10^{-3} , and a jump $\Delta h/\tau$ of 5% would raise the layer about 8 km according to this relation. To exhibit this effect explicitly, the January 30 data were analyzed to find the F2-layer peak, and the smoothed results were then compared with the smoothed density fluctuations. One notes from Fig. 6.21 that ΔN is indeed generally out of phase with Z . This appears to be true for both the long-term and short-term variations, although the long-term variations are not thought to be manifestations of TID.

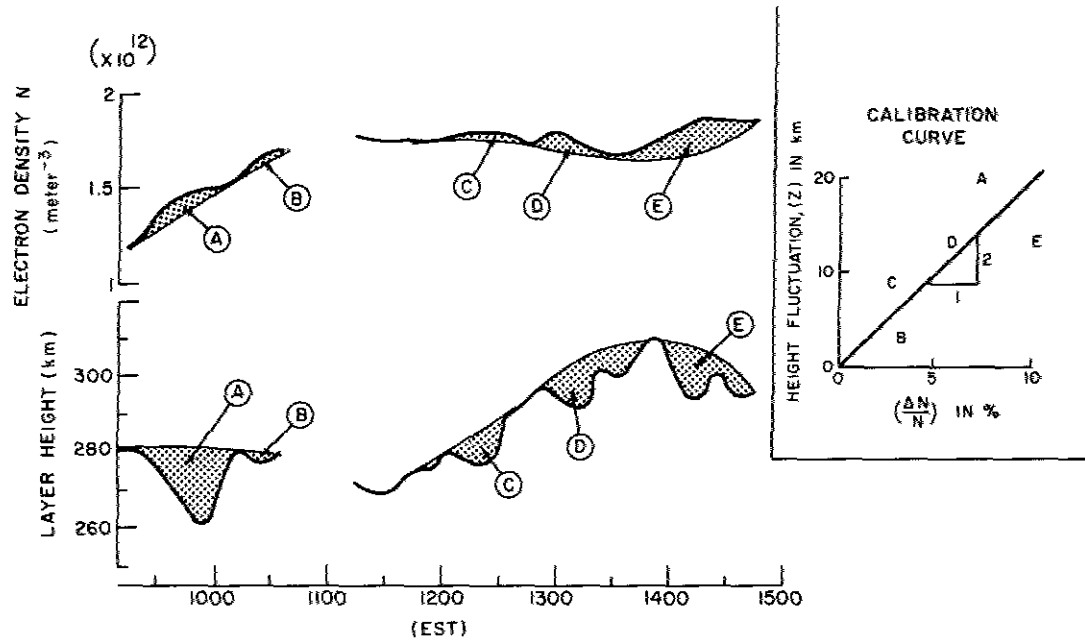


Fig. 6.21 - Comparison to electron density and layer height fluctuations for January 30, 1970

It is possible that the long-term fluctuation may be related to neutral wind patterns over Randle Cliff. If one assumes that the neutral wind (which has its largest field-aligned component near midday) drives ionization down field lines (Kohl and King [1967]), one would expect the layer height to descend, and this was observed to first order. Since the peak density fluctuation appears to be out of phase with this motion, it is suggested that the electron loss processes may not be as important as the term $\text{div}(N \mathbf{v})$ in affecting a change in the peak density (even for the long-term fluctuations). This, however, is a heuristic deduction and not rigorously reasoned.

As noted in Fig. 6.21, five regions (designated A, B, C, D, and E) have been marked for obtaining a calibration curve from which the average relationship between Z and $\Delta N/N$ may be obtained. One finds that a layer height fluctuation of 10 km gives rise to an electron density fluctuation of 5% on the average. Assuming these fluctuations to be properly described by Eq. (6.19), one concludes that $\lambda_{zi} \approx 1256$ km. However, Hines [1960] assertion that $\lambda_{zi} = 4\pi H$ pertains only to the unducted mode. As a consequence it is not possible to obtain a measure of the neutral scale height directly. Assuming a two-layer model, Thome [1968] has suggested that the following relation may be valid in the upper ionosphere:

$$k_{zi} = \frac{1}{H_2} \left(\frac{\gamma - 1}{\gamma} + \frac{\gamma - 1}{\gamma^2} \frac{H_1}{H_2} \right) \quad (6.21)$$

where H_1 is the scale height for the lower layer and H_2 is the scale height for the ionospheric region of interest in the present discussion. Taking $\gamma = 1.4$ and $H_1 \approx 10$ km below the mesopause (Johnson [1961]) one finds after a short calculation that the present results lead to a value for H of 63 km. This is in almost exact agreement with the anticipated value for H at 250 km (the working height) under sunspot-maximum conditions (Johnson [1961]). It may be possible therefore to formulate experiments of the present type for the express purpose of deducing neutral-gas temperature.

It is possible that increased magnetic activity may amplify TID, and consequently there might arise a correlation between the wave period P and the Fredericksburg index of magnetic activity K_{Fr} . Following magnetic storms the neutral scale height is enhanced, based on both satellite-drag data and total electron content experiments, and Jacchia [1964] has found that the neutral scale height is essentially proportional to the magnetic index a_p^* . Dessler [1959] has suggested that the electron-ion plasma will be heated by interaction with magnetohydrodynamic waves emanating from the sun following flares. Ultimately, this energy finds its expression in terms of an enhancement in the neutral scale height (since $H = kT/mg$, where T is the neutral temperature). This causes the lower atmosphere to heave upward, increasing the gravitational potential energy. Since the ionic component of the perturbed solar wind (which presumably carries the MHD waves) is largely deflected toward the magnetic poles due to presence of the magnetic field, the enhanced gravitational energy is more concentrated in the auroral zones. Subsequently the perturbation is relaxed by the generation of gravity-wave modes which travel southward. The electrons (which is all that can be sensed in Thomson scatter studies) act as tracers of the neutral motion, and since variations in electron density are peculiarly periodic and usually enhanced during magnetic disturbances, observations generally support this particular mechanism for the production of gravity waves. Assuming that this mechanism is operating, one would, first, expect the wave period P will be roughly proportional to the wave amplitude $\Delta h/\tau (\propto \Delta N/N_0)$ and, second, suspect that both P and $\Delta h/\tau$ will be increasing functions of the magnetic index K_{Fr} . Fig. 6.20 illustrates that $\Delta h/\tau$ is indeed proportional to P . However, for the periodicity domain under consideration here, there is little apparent connection between P and the index K_{Fr} or between $\Delta h/\tau$ and K_{Fr} . On the basis of these experiments and to a certain extent the work of others, one must conclude that magnetic activity does not strongly control either the occurrence or magnitude of TID for wave periods less than 1 hour. The exact mechanism responsible for the low-period TID observed at Randle Cliff is not presently known. The statistics are not good enough to determine if the effect has any seasonal dependence, but this matter is being pursued.

Figs. 6.22 and 6.23 are the electron density contours which were obtained upon differentiation of the Faraday rotation contours shown in Figs. 6.9 and 6.13. The curves of constant N (the values being given as the log of N to the base 10) clearly reveal the irregularities in both the November and January experiments.

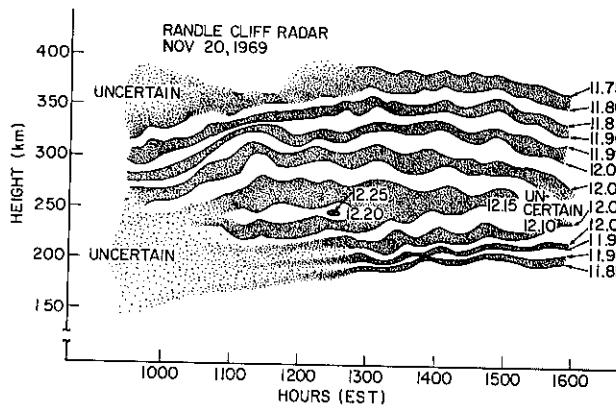


Fig. 6.22 - Electron density contours
for November 20, 1969

*The index K is proportional to the logarithm of the index a . The subscripts p and Fr refer to planetary and Fredericksburg respectively.

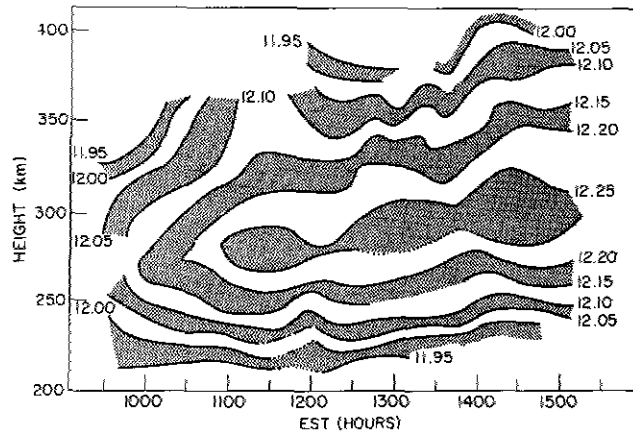


Fig. 6.23 - Electron density contours
for January 30, 1970

In conclusion, wave motion of the ionospheric plasma over Randle Cliff is probably always present in the daytime. Also, as others have concluded, TID may be related to increased magnetic activity, although the magnetic control in the present series of observations was far from overwhelming. To make direct use of the Faraday rotation contours, a relation was derived between the rotational altitude fluctuation Δh , the slab thickness τ , the wave period P , the wave phase velocity U_x , and the vertical "wavelength" λ_{zi} , which roughly characterizes the scale height of the medium. By means of an example, it is suggested that the wave motion characterized by the long period disturbances is probably either a ducted or partially ducted type, since the rotational isopleth fluctuations are in phase with the layer height fluctuations. This conclusion was previously reached by Thome [1968] to explain his observations of large-scale TID. Employing Thome's two-layer model, a value was extracted for the neutral scale height at the F2 maximum, and good agreement was found with a model atmosphere due to Johnson [1961]. This suggests that regular measurements of TID may be useful in the determination of upper atmospheric constitution or temperature. It was also found that the perturbation amplitude is an increasing function of wave period, as required by theory

It is emphasized that a distinct advantage of using Faraday rotation for studying TID is that the wave motions which are detected are truly indicative of plasma motion. This is not necessarily true if fluctuations of T_e/T_i are pronounced and the power profile method used. Thus the present observations, representing the first midlatitude study of TID using the combination of Faraday rotation and Thomson scatter, are unique. With additional refinement of the RCR instrumentation, it will be possible to identify the shape of the irregularities more clearly, and it is planned that measurements of T_e/T_i and electron density will be made simultaneously. To date such measurements have been made.

THE MIDDAY BITEOUT OVER RANDLE CLIFF

In addition to the traveling ionospheric disturbances evident in the Faraday rotation contours, one of the more interesting features is probably related to the so-called "midday biteout," which is an anomalous decay of F-region electron density at approximately local noon. In the present data the effect manifests itself as a rise in the Faraday rotation isopleths at midday implying a decrease in the electron content. Although it occurs on a number of days, it was perhaps most pronounced on December 16, 1969, as illustrated in Fig. 6.11. It was also present to some degree on adjacent days—December 15 and 17.

Midday biteout has been noticed in some daily records of $f_0 F_2$ for more than a decade. In fact, even for the averaged data appearing in Fig. 3.5, there is a hint of midday depletion over Washington, D. C. Although the effect is largely concentrated at the F2 peak, it has been observed to occur at all altitudes. Total content studies (Goodman [1966]) employing the synchronous satellite Early Bird (1965-28A) also indicate that the entire electron population is often affected in the temporal neighborhood of local noon over Randle Cliff.

The biteout effect is usually mentioned in conjunction with the late afternoon anomaly, which is the rapid buildup of electron content in the temporal neighborhood of sunset. (The late afternoon anomaly was mentioned in the second section of this chapter.) Due to the "sluggishness" of the F region, one would expect its maximum density to occur at least an hour following local noon. If one superposes the afternoon anomaly one would obtain a midafternoon biteout due to presence of peaks in electron density at 1300 hours and 1800 hours, say.

An alternative mechanism for producing the midday biteout has been observed by Kohl and King [1967] and Kohl et al. [1968]. Basically it suggests that the global neutral wind system drives ionization downward to where electron losses are greater, thus producing a content decay. The field-directed component of the neutral wind at 300 km appears to be maximum over Randle Cliff between 1400 and 1500 EST if the peak density is taken to be $\approx 10^6$ electrons/cm³. For the lower summertime densities the time of the maximum field-directed component is closer to local noon, and the magnitude is also greater, since ion drag is less pronounced. Recently Vasseur [1970] has shown that the summertime midday biteout in peak density over St. Santin-Nancay is accompanied by a downward movement in the layer maximum, which he attributes to the neutral wind mechanism. A wintertime day was also analyzed, but no midday biteout was observed.

Fig. 6.24 is a plot of the F2 peak density obtained via the Randle Cliff Radar facility on December 15, 16, and 17 in 1969. On all these days the times of the density peaks between which the biteout region occurs fall in the neighborhood of 1100 hours and 1300 hours EST, and the average time of the biteout minimum is at ≈ 1215 hours EST. It is noteworthy that a rather substantial biteout occurs in the midafternoon on both December 15 and 17 between 1300 hours and 1500 hours EST; this feature, rather than the former, might be more readily explained as a manifestation of the neutral wind theory. The electron-content biteouts such as those observed in this study, however, have not been

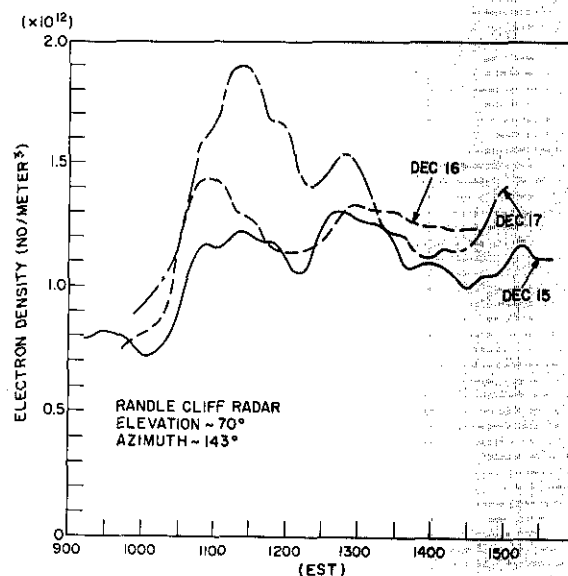


Fig. 6.24 - F-region peak densities obtained on December 15, 16, and 17, 1969 at Randle Cliff

observed as frequently during winter, which has led some observers to consider the effect to be primarily a summer phenomenon.

Fig. 6.25 gives the electron density profiles at five appropriate times on December 16; 0950, 1100, 1210, 1300, and 1400 EST. It is found that the total content to 400 km ($\int_0^{400} N dh$) increased 12% between 1210 and 1300 EST and finally decreased 10% between 1300 and 1400 EST. Since the F2 peak density decreased by $\approx 37\%$ between 1100 and 1210 EST and the content depletion is only 4%, one concludes that the midday biteout effect on December 16 is largely localized at the F2 maximum.

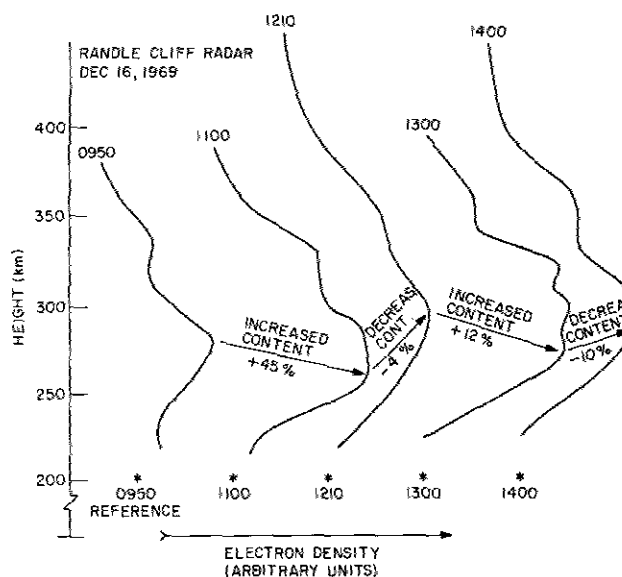


Fig. 6.25 - Electron density profiles for December 16, 1969

Although the exact placement of the arrows may be subject to question, Fig. 6.25 suggests that the altitude of the lower boundary of the F2 maximum exhibits fluctuations which are out of phase with the corresponding content fluctuations. This would run counter to the argument that the ionization is descending along field lines, and it would go a long way toward invalidating the neutral wind mechanism as far as producing the December 16 biteout is concerned. However, due to the irregularity of the profiles (the noticeable double peak), the exact location of the peak is made difficult, and any hard conclusions based on its apparent variation are probably unjustified. Although one would not wish to summarily discard the neutral wind mechanism as a factor in the noontime biteout, there is probably little hope for it since the predicted biteout is not favored in the wintertime and would not be expected to be centered so nearly about local noon.

Due to the relatively minor midday biteouts on December 15 and 17 as well as their shorter durations, one probably cannot rule out that they are merely moderately amplified TID troughs if they are considered independently. On December 16, however, the magnitude and duration of the effect obviates the TID hypothesis. Furthermore, the similar positioning of the biteout regions on the three consecutive days implies that the phenomenon is more than fortuitous and is highly suggestive of a similar causal mechanism.

This section has obviously raised some additional questions regarding the occurrence and the causal mechanism(s) for the midday biteout. It is clearly necessary to

measure both the electron density distribution and the drift velocities associated with the biteout event, if they indeed do exist. Currently the drift velocity may only be inferred, and such an inference would be expected to be grossly inaccurate owing to the altitude dependence of electron production and loss processes. In this regard a long-term bistatic experiment is being considered for measuring drift velocities and would use the Randle Cliff Radar and a large antenna in West Virginia. By comparing the drift velocity and electron density data, it is hoped that much needed light will be shed on the effect disclosed in this section. A byproduct of the drift measurement will be a determination of T_e and T_i , and thus the importance of redistribution (presumed to be governed by the plasma scale height $H_{ei} = kT/mg$, where $T = (T_e + T_i)/2$) can be analyzed.

Note added in Proof: 4/1/71

From the determination of λ_{zi} using equation 6.19 and the results from the January 30, 1970 experiment we found that a surface wave approach suggested a neutral scale height of ~ 63 km at the F2 maximum. This was seen to be in close agreement with a model due to Johnson [1961]. A comparison with the U.S. Standard Atmosphere* [1966] which takes solar activity and magnetic activity more completely into account is not so favorable. In order to improve the accuracy associated with "reading" the calibration curve given in Fig. 6.1, it was subsequently decided to include the data points extracted from the November 20, 1969 experiment on the same graph. In this manner more confidence will be placed in the final result. (This is justified by the fact that the U.S. Standard Atmosphere predicts comparable values of $H = 45$ km and 49 km for the conditions existing on November 20, 1969 and January 30, 1970 respectively.) As a result of this revised analysis a composite thermosphere for both days was found to have a neutral scale height which varied between 45 and 55 km using the surface wave approach. The standard deviation of the determination is 10%. On the basis of free wave theory the same data suggests a value for H of 67 km. It is thus tentatively concluded that the long period waves described in this report are of the surface variety. These remarks are discussed in a paper to be presented at the 52nd Annual AGU Meeting[†] in Washington, D. C.

*U.S. Standard Atmosphere, "U.S. Govt. Printing Office, 1966.

[†]"Traveling Ionospheric Disturbances Observed Near Washington, D. C. Using the Thomson Scatter Technique," 52nd Annual Meeting American Geophysical Union, Washington, D. C., J.M. Goodman, April 12, 1971.

CHAPTER 7

RESPONSE OF THE IONOSPHERE TO A SOLAR ECLIPSE

INTRODUCTION

The great affect of a solar eclipse on the constitution of the upper atmosphere has fascinated aeronomists, and eclipse-induced perturbations of the ionospheric electron density distribution have been studied often. Since 1903 over 200 papers have been written concerning the relationship between ionospheric perturbations and the solar eclipse. Most of these papers relied on early rudimentary radio techniques (e. g. , wireless telegraphy: Eccles [1912], Schledermann [1912], Kiebitz [1912], and many others) or used the ionosonde method as a basis (e. g. , Ilias and Anastassiadis [1964], Minnis [1958], and Becker [1956] to name a few). These techniques naturally yielded little information about the upper ionosphere and provided no explicit information about temperature effects. With the advent of Thomson scatter radars a whole new dimension of eclipse effects was uncovered. The equatorial eclipse, which is entirely different from the mid-latitude variety, has been observed at Jicamarca by Petterson et al. [1967] using Thomson scatter, and Evans [1965] has examined the upper midlatitude F region during a solar eclipse using the Millstone Thomson scatter radar. Although there is seemingly a plethora of information already available, Thomson scatter studies of the ionospheric response to a solar eclipse at near-maximum solar activity have not been reported in the literature. In addition, the occurrence of an eclipse near the time of the vernal equinox adds to the interest. On March 7, 1970, the path of a solar eclipse passed near the Randle Cliff Radar facility, with near totality occurring at about 1338 EST. This chapter is devoted to an analysis of the ionospheric response.

GEOMETRY OF THE ECLIPSE

Fig. 7. 1 shows a segment of the path of the March 7 eclipse. The Randle Cliff Radar facility is seen to be about 75 statute miles from the region of totality and roughly 120 miles from the centerline. Under these conditions the fraction of the sun to be eclipsed is close to 95% at maximum phase for ground observers at Randle Cliff. However, it was found that at 1338 EST, the approximate maximum phase time, the sun was at an elevation angle of 43° and an azimuth angle of 207° as viewed from Randle Cliff. Astronomically, one finds that the centerline of the eclipse is displaced from that depicted in Fig. 7. 1 if one considers altitudes of interest in the ionosphere. During the observation period, the radar path was fixed at an aximuth of 225° and an elevation of 63° . * On the basis of data supplied by the Nautical Almanac staff at the Naval Observatory, it was found that the maximum fractional obscuration of the sun occurs at E-region heights. Nevertheless, the times of maximum phase are virtually the same for all ionospheric

*The eclipse experiment conducted at Randle Cliff on March 7, 1970, consisted of two parts. The first part, for which the author had primary responsibility, consisted of obtaining monostatic Faraday rotation profiles from which electron densities could be obtained. The second part, under the direction of Drs. J. B. Mead and L. S. Wagner, colleagues at NRL, was a bistatic experiment necessitating an oblique antenna orientation. From this part of the experiment it is hoped that some measure of the movement (divergence) term in the continuity equation will be obtained. This aspect of the experiment will not be discussed in this manuscript, it involves the determination of the Thomson scatter spectrum from which drift vectors may be obtained.

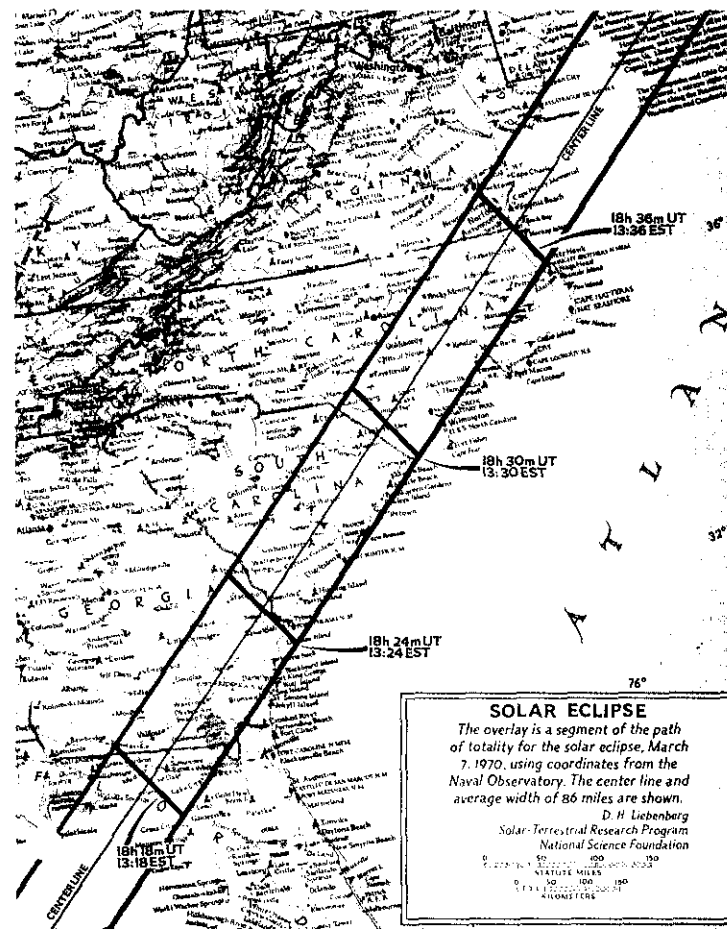


Fig. 7.1 - Path of the March 7, 1970 solar eclipse

heights of interest. Table 7.1 gives the time of maximum phase along the radar path at altitudes of 100, 200, 300, 400, 500, and 600 km in addition to the percentage obscuration. Fig. 7.2 depicts the fractional obscuration functions from which the data in Table 3

Table 7.1. Eclipse Characteristics at Ionospheric Heights

Height (km)	Time of Maximum Phase (EST)	Obscuration (%)
100	1338:00	95.5
200	1338:30	94.3
300	1339:30	93.1
400	1340:00	91.9
500	1341:00	90.7
600	1341:30	89.7

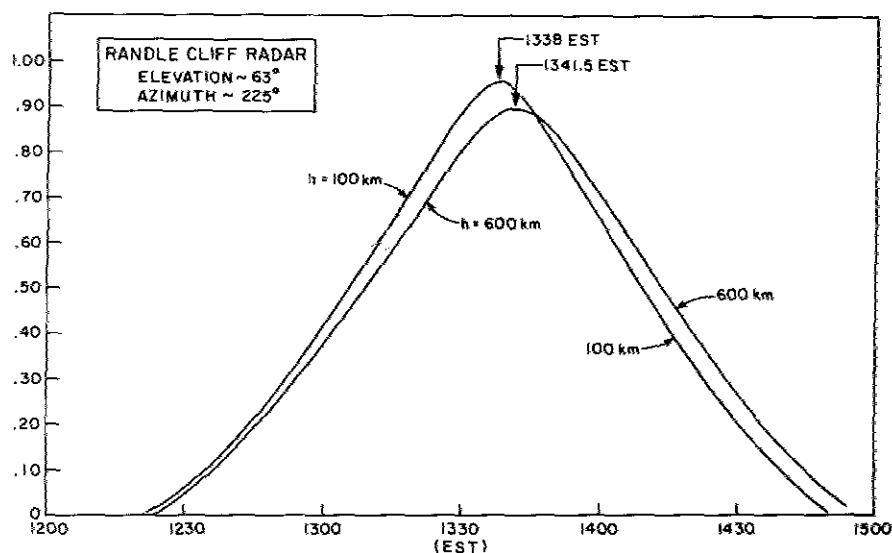


Fig. 7.2 - Eclipse obscuration functions at 100 km and 600 km

were derived. The semiduration of the eclipse at all altitudes was about 75 minutes with nominal terminal points at 1220 and 1450 EST respectively.

MEASUREMENTS

Table 7.2 gives the times and characteristics of the 29 Faraday rotation runs obtained during the course of the eclipse experiment. Each run lasted about 4 minutes (except as noted), and the Faraday profiles extended to about 420 km prior to 1000 EST and to ≈ 530 km after that time. Wallops Island Ionosonde data were used to get some indication of the consistency of the Faraday rotation results, and values of the parameters f_0E and f_0F2 between 0800 and 1800 EST are presented in Table 7.3.

Fig. 7.3 shows three Faraday profiles: one before, one during, and one following the eclipse. One finds in noting the difference in the character of the profiles, that the first Faraday extremum, exhibited by the $\pi/2$ point, is significantly higher during the eclipse than before or after, indicating a decay in the lower ionospheric electron content.

Faraday rotation profiles have been shown to be useful themselves, since they readily yield Faraday rotation isopleths. Chapter 6 established that an upward excursion of the contours suggests a depletion of the electron content, and a downward excursion implies an enhancement of the same. The tremendous effect of the eclipse phenomenon is illustrated by the rotation contours of Fig. 7.4. It is seen that the 26th $\pi/2$ contour, for example, varies by at least 100 kilometers as the electron content diminishes and subsequently recovers to its approximate equilibrium level. Some incipient wave motion occurs prior to the eclipse, and these waves appear to be in phase with some wavelike disturbances after the eclipse. The wave period is approximately 65 minutes. This matter was discussed in Chapter 6.

ELECTRON DENSITY DISTRIBUTION

Fig. 7.5, in which the isopleths of constant logarithm of electron density have been plotted in 1/2-dB steps, shows how the electron density distributions varied as a function

Table 7.2. Faraday Rotation and Total Electron Content

Run* No.	Start/Time (EST)	Duration (Min.)	Maximum/Faraday/Angle/ Observed/ $(\pi/2$ radians)	Approximate/Total/Content (10^7 electron/m ²)
1	0821	4.00	12.4	1.61
2	0827	6.00	12.4	1.61
3	0846	4.00	14.0	1.82
4	0911	4.00	16.0	2.08
5	0936	4.00	18.0	2.34
6	1008	12.00	24.8	3.22
7	1026	4.00	25.0	3.25
8	1051 ³⁰	4.50	25.0	3.25
9	1116	4.00	28.2	3.67
10	1148	4.00	29.5	3.83
11	1208	4.00	32.2	4.18
12	1233	4.00	34.8	4.52 (Pre-eclipse maximum)
13	1258	4.00	33.8	4.40
14	1323	4.00	29.0	3.77
15	1328	4.00	28.0	3.64
16	1333	4.00	27.2	3.54
17	1337 ⁴⁵	2.25	25.8	3.36
18	1357	5.00	25.7	3.34 (Eclipse minimum)
19	1422 ³⁰	4.50	26.2	3.40
20	1447 ³⁰	4.50	29.8	3.98
21	1513	6.00	31.2	4.06
22	1540	4.00	31.5	4.10 (Post-eclipse maximum)
23	1545	4.00	31.2	4.05
24	1550	4.00	31.0	4.03
25	1555	4.00	29.8	3.88
26	1603	4.00	29.8	3.88
27	1628	4.00	30.0	3.90
28	1653	4.00	28.0	3.64
29	1718	4.00	27.0	3.51

*The first five runs are based upon a maximum observable height of 420 km; the remainder of the runs are based upon a maximum observable height of 530 km.

of time. Several features are worth noting. First, one sees that the maximum eclipse effect is roughly centered at a time which is midway between maximum phase (maximum obscuration) and last contact. It may be inferred that the eclipse biteout, as indicated by the content depletion also shown in Fig. 7.5, is largely due to the rapid lower ionospheric response, which is presumably governed by the attachment process. (Also, it is interesting that the layer height fluctuations are generally out of phase with the total content fluctuations, which as stated earlier is a characteristic of long-period TID and may also occur during midday biteout.) As was expected, the layer peak, indicated by the dotted line in the figure, rises rapidly during the eclipse reaching about 350 km before last contact. It subsequently drifts downward, reaching its more or less unperturbed level at roughly an hour following last contact. By this time the content curve has started its descent due to the increased solar zenith angle, and the layer height once again rises. Recent theoretical results due to Stubbe [1970] suggest a similar height fluctuation pattern but over a shorter time frame. Stubbe predicts that $h_{max} F2$ will rise following first contact, achieving a maximum in the neighborhood of maximum phase. It is then supposed to descend, reaching its minimum near last contact. It is worth emphasizing that the fluctuations in F-layer height do not necessarily reflect ionospheric motions.

Table 7.3. Ionosonde Data and Projected Electron Content

Time/(EST)	$f_0(E)$ /(MHz)	$f_0(F2)$ /(MHz)	Projected/Total/Content*/ (10^{17} electrons/ m^2)
0800	2.90	10.00	3.10
0815	3.00	9.60	2.86
0830	3.05	10.00	3.10
0845	3.10	9.50	2.79
0900	3.15	9.90	3.04
0915	3.30	9.80	2.98
0930	3.40	10.20	3.19
0945	3.40	10.70	3.52
1000	3.35	10.90	3.63
1015	3.40	11.30	3.75
1030	3.40	11.30	4.03
1045	3.50	11.50	4.10
1100	3.55	11.30	3.96
1115	3.65	11.40	4.03
1130	3.70	11.40	4.03
1145	3.70	11.30	3.96
1200	3.70	11.80	4.32
1215	3.70 [†]	12.30	4.69
1230	3.68	12.30	4.69
1245	3.58	12.70	5.00
1300	3.38	12.00	4.46
1315	3.20	11.80	4.32
1330	2.50	11.30	3.96
1345	2.30	10.55	3.45
1400	2.61	10.45	3.38
1415	2.82	10.25	3.25
1430	2.98	11.00	3.72
1445	3.25	11.00	3.78
1500	3.35	11.10	3.82
1515	3.30	11.90	4.39
1530	-	-	-
1545	3.10	12.00	4.46
1600	3.00	11.80	5.32
1615	2.90	11.90	4.39
1630	2.75	11.90	4.39
1645	2.60	11.70	4.24
1700	2.49 [†]	11.70	4.24
1715	2.39 [†]	11.65	4.21
1730	2.20	11.45	4.06
1745	1.92	11.30	3.96
1800	1.80	11.40	4.03

*The projected total content is based on the relation $\int N dh \approx 1.24 \times 10^{10} f_0^2(F_2) \tau_s$, where the integral is in mks units, f_0F_2 is in MHz, and τ_s is the slab thickness in meters.

[†] Value uncertain, because two values of f_0E were tabulated, --perhaps due to multiple echoes. This is the most reasonable value (according to the author).

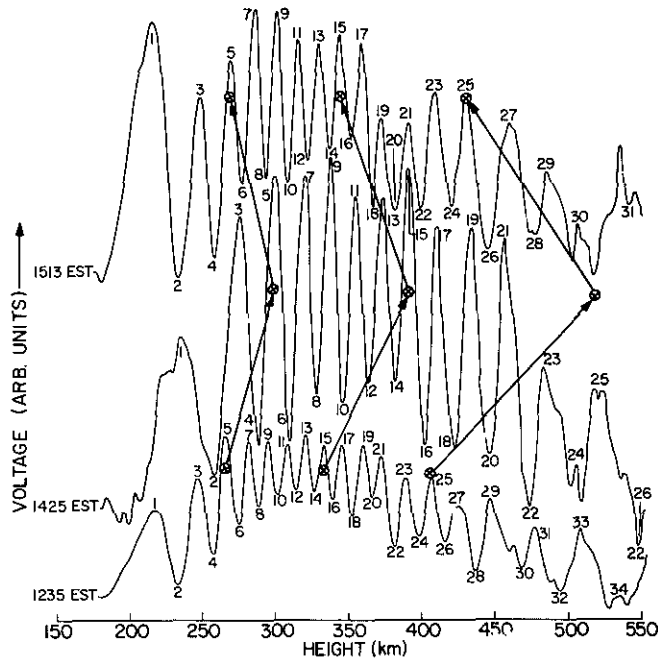


Fig. 7.3 - Faraday rotation profiles obtained before, during and following the eclipse biteout

The total content has been replotted in Fig. 7.6 and is compared with the estimated content based upon Wallops Island ionosonde data given in Table 7.3. The estimated values were obtained by assuming that the F2 peak-density controls the content and that the ionosphere is characterized by a constant slab thickness of $\tau_s = 250$ km. The agreement is quite good in the eclipse biteout region but is not as good elsewhere. The excessive values of the projected content on either side of the biteout region imply that τ_s increases during the eclipse as a result of a disproportionate decrease in N_{F2} compared with the total content. This is reasonable, since the upper ionosphere is roughly static in terms of electron concentration, whereas diminution is the rule in the middle ionosphere, and decay is thought to be detectably less severe in the E region due to the presence of a residual chromospheric ionization source (Piddington [1951]) which is incompletely obscured even at totality. (The existence of a chromospheric source has been given additional credence by the discovery of coronal x-rays during totality (Friedman [1960].))

Although the density contours in the topside ionosphere terminate in the vicinity of 450 km, there is some suggestion of a downdrift of ionization from above, since the density is decreasing at ≈ 425 km where attachmentlike losses are negligible. This feature was first discussed by Evans [1965] in his study of an eclipse over Millstone Hill in July, 1963, with maximum phase occurring at about 1700 EST. In addition the 1963 eclipse produced an anomalous enhancement in N_{F2} during the biteout region, and Evans claims that this was a consequence of the rapidity with which the ion distribution collapses, overriding electron removal processes. An electronic downdrift has also been predicted by Stubbe [1970] but with no accompanying enhancement in N_{F2} . In the present case there is clearly no evidence of an increase in N_{F2} during the eclipse period, even though high-altitude ionization is presumably descending. A recent paper by Klobuchar and Malik [1970] describes the effect of the March 7 eclipse over Hamilton, Massachusetts, on the basis of a Faraday rotation analysis of VHF transmission from Early Bird, ATS-3, and ATS-5 satellites. These authors found τ_s to be about 275 km,

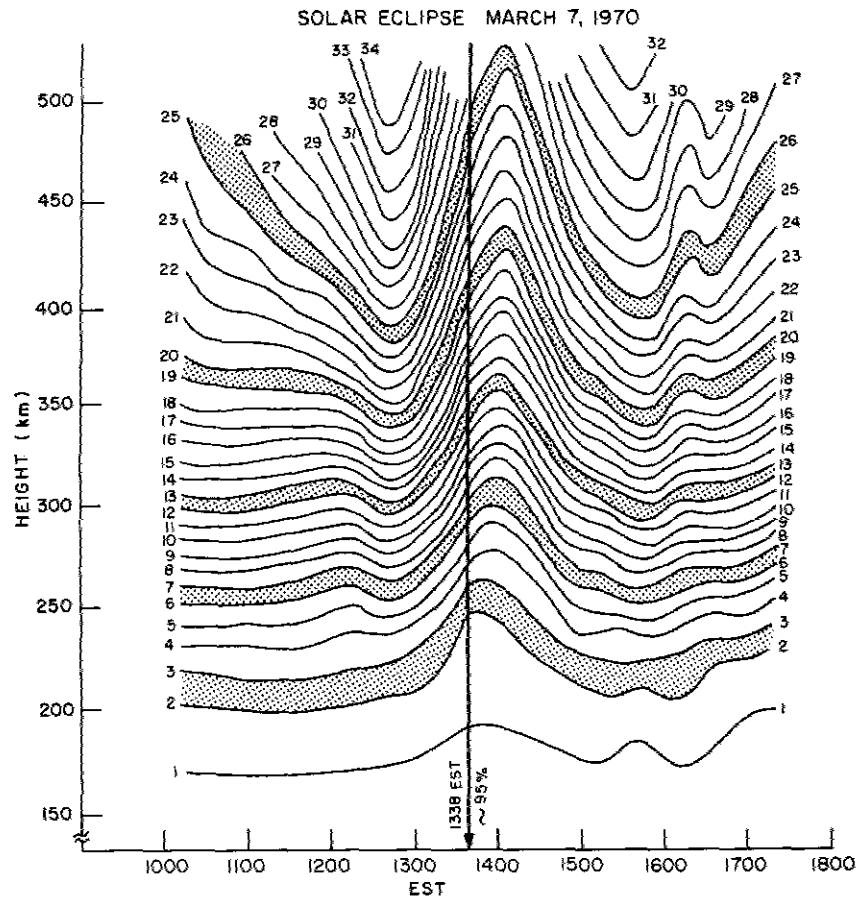


Fig. 7.4 - Faraday rotation contours obtained at Randle Cliff on March 7, 1970

judging from Fig. 3 in their paper, but more importantly found that the eclipse produced no striking changes in this parameter. Thus at their location, the downdrift of ionization was almost exactly canceled by increased electron loss, resulting in a preservation of the layer shape. On the other hand, Almeida and Da Rosa [1970], using a phase path-length method with a synchronous satellite, show significant τ_s variations. Although the changes observed by Almeida and Da Rosa were not regular, there was a definite tendency toward larger values during the biteout region, in agreement with the Randle Cliff Radar results mentioned in this section. Thus the data currently available concerning the March 7, 1970 eclipse would appear to refute the notion that ionization is piling up at the F2 maximum, a phenomenon which evidently did occur during the 1963 eclipse reported by Evans [1965]. It is probably important to remark, however, that Evans' results were extracted from a late afternoon eclipse during Summer at sunspot minimum, whereas the present results were obtained in the early afternoon at nearly equinox and at solar maximum. These various factors combine to render the mean electron densities associated with the present experiment at least four times larger than during the 1963 eclipse. This fact alone may give rise to a more rapid loss rate at the F2 peak in the present case, thus negating the effect of additional electrons supplied from above.

Additional measurements of the March 7 eclipse from nearby Norfolk, Virginia (36.56°N, 72.24°W) using VHF transmission from the ATS-3 satellite (Flaherty et al., [1970]) and for which the 350-km ionospheric point was 33.87°N and 77.07°W, indicate

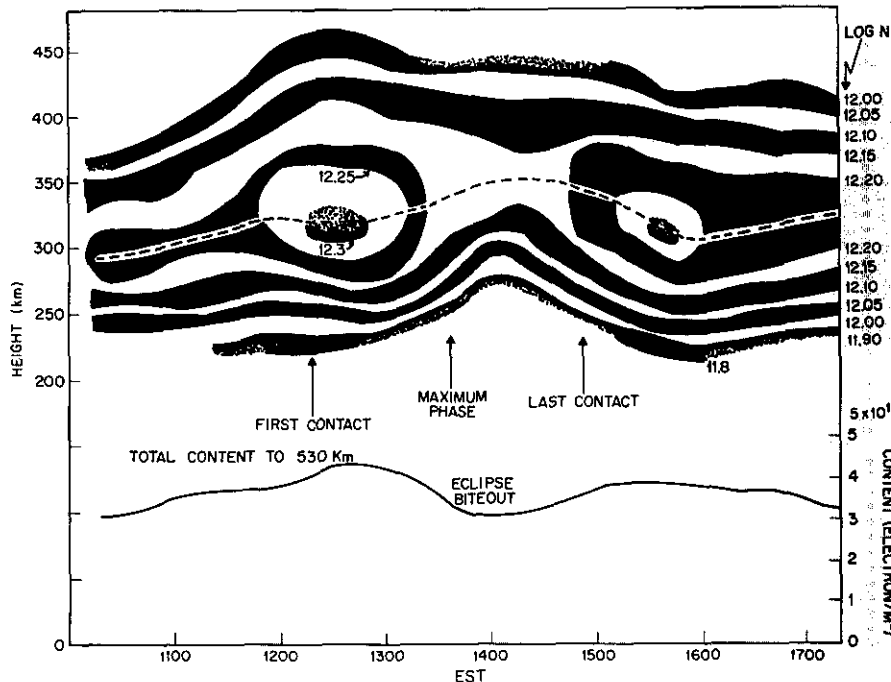


Fig. 7.5 - Electron density contours for the solar eclipse

that the total content $\int_0^{\infty} N \, dh$ prior to the eclipse was about 5.5×10^{17} electrons/m². Since $\int_0^{530} N \, dh = 4.5 \times 10^{17}$ electrons/m² at Randle Cliff, which had a 350-km ionospheric point of 37.5°N and 77.7°W, one concludes that $\approx 10^{17}$ electrons/m² or roughly 18% of the total content resides above 530 km if one accepts the figures of Flaherty et al. These authors also note that $\int_0^{\infty} N \, dh$ decreases by 12.8×10^{16} electrons/m² between the first maximum and the biteout minimum and increases by 8.5×10^{16} electrons/m² between the biteout minimum and the final maximum. At Randle Cliff the respective changes (From Table 7.2) are -11.8×10^{16} and 7.6×10^{16} electrons/m², although they refer to the content below 530 km. Thus $\approx 10\%$ of the ionization above 350 km is depleted during the eclipse biteout. Since the time constant for attachmentlike loss is estimated by Ratcliffe et al. [1956] to be about 20 hours even at 400 km, it is quite unlikely that the 10% loss above 530 km is produced by effects other than div Nv. It is tacitly assumed that the relevant electronic movement is directed downward along magnetic field lines and that this movement will feed the lower ionosphere. However, as the content above 530 km is but 22% of that below 530 km and since $\int_{530}^{\infty} N \, dh$ decreases only 10% during the eclipse, one finds that the content biteout (due to all causes) associated with $\int_0^{550} N \, dh$ is unaffected by downdrift from above, at least to within an order of magnitude. It is emphasized, however, that due to the separation of the two ionospheric paths which have been compared (the Randle Cliff data and the data of Flaherty et al.), the exact percentages of content depletion which have been derived here are indicative of only a general trend. If one considers the difference in the amount of solar obscuration between the two paths ($\approx 93\%$ for Randle Cliff data and $\approx 100\%$ for the data of Flaherty et al.), one can conclude that the eclipse depletion is almost *entirely* the result of attachment below 530 km. This consideration surely strengthens the previous conclusion that downdrift is relatively unimportant.

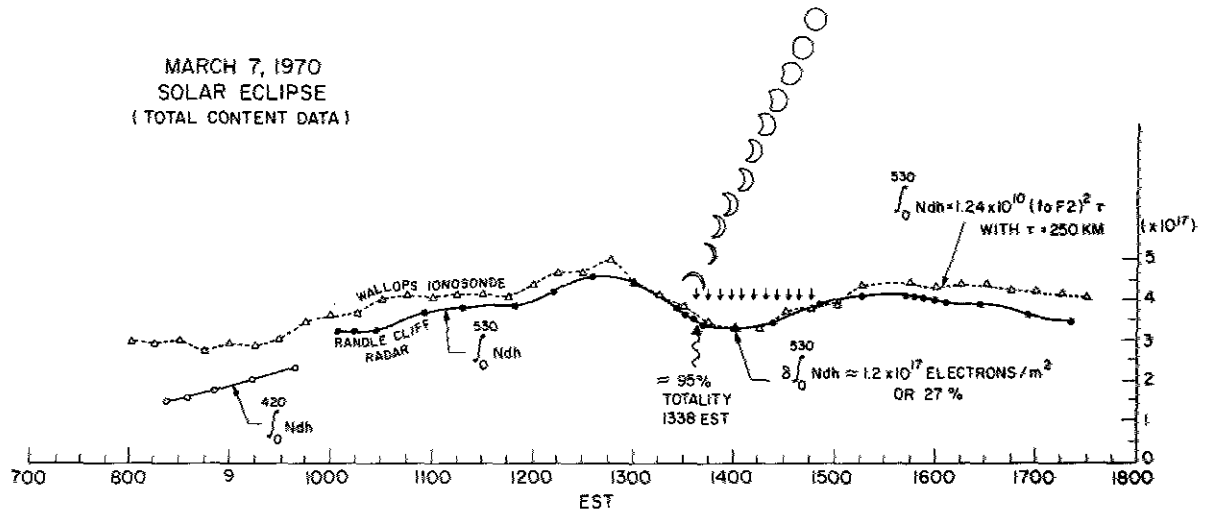
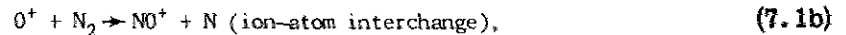
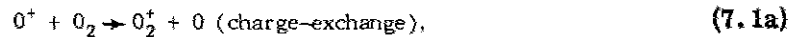


Fig. 7.6 - Total electron content below 530 km on March 7, 1970

ESTIMATION OF THE ELECTRON LOSS COEFFICIENT

A number of investigators have been deduced values for the effective recombination coefficient α for the lower ionosphere by measuring the decay of electron density following a solar eclipse. For example, a recombination function has been reported by Ilias and Anastassiadis [1964] for an eclipse over Athens in 1961. However, in the ionosphere above the F2 maximum, the dominant processes for electron loss are given by the following reactions (Belrose [1965]):



Thus the charge exchange and ion-atom interchange between the atomic and molecular species (Eqs. (7.1a) and (7.1b)) enables dissociative recombination (Eqs. (7.1c) and (7.1d)) to occur. This sequence of events is necessary because atomic ions are dominant at great heights, and charge exchange is required to produce molecular ions. Direct recombination with atomic ions is radiative and thus has a very low cross section; it normally is neglected. Although both charge exchange and recombination with molecular ions are involved (with the first being proportional to the number of electrons N , assuming charge neutrality, and the second being proportional to N^2), the net electronic loss rate is controlled by the slower process (charge-exchange), and the process is attachmentlike.

In accordance with the preceding notions the altitude-dependent attachment coefficient has been extracted from eclipse observations over the magnetic equator using Thomson scatter (Peterson et al. [1967]). A detailed consideration of the distribution of electrons in the F region has led Ratcliffe et al. [1956] to suggest the following midlatitude model for the loss coefficient:

$$\beta = 10^{-4} e^{(300-h)/50} \text{ sec}^{-1}, \quad (7.2)$$

where h is in kilometers. This model implies that the time constants associated with attachmentlike loss at 250, 300, 350, and 400 km are 1, 3, 7.5, and 20 hours respectively. If this model is accepted during solar eclipse, one may surely neglect the loss term βN in the continuity equation for the upper F region, since the eclipse semiduration is about 75 minutes. For this reason an explanation of F-region eclipse phenomena, at least in the upper F region, is usually sought in terms of electronic movement through the term $\text{div } Nv$.

Somewhat surprisingly, occasional eclipses do exist for which the measured electron concentration at the F2 peak is seen to increase. As mentioned in the preceding section of this chapter, this phenomenon has been attributed to a sudden collapse of the electron distribution which arises due to a rapid cooling of the plasma. Since the chemistry at the F-region maximum is presumably too sluggish to remove the descending electrons efficiently, a transient local enhancement is sometimes observed. Of course, this effect must be local, since the total electron content must diminish.

From Fig. 7.4, one sees that the estimated "time constants," which one is tempted to attribute to the ionosphere on the basis of the time difference ΔT between maximum phase and the subsequent isopleth extrema, are probably reasonable in the lower ionosphere but are questionable in the upper ionosphere. Of course, account must be taken of the fact that the rotational excursions in the upper ionosphere are related to those below. Hence, a "time constant" extracted from a contour at a particular height refers to the average behavior of the ionosphere below h but has greater significance at the so-called ionospheric mean height \bar{h} , which is simply defined by

$$\bar{h} = \frac{\int_0^h h' N(h') dh'}{\int_0^h N(h') dh'} \quad (7.3)$$

in view of the fact that the magnetic field parameter $\Psi = H \cos \theta \sec X$ is roughly linear with height. On this basis the time delay ΔT suggested by the rotational isopleths in Fig. 7.4 varies between approximately 10 and 25 minutes and refers to a mean height variation between ≈ 240 and ≈ 340 km. Naturally the total content (although it has a rather flat minimum) also exhibits a time delay which is close to the 25-minute upper limit.

It is also possible to deduce time delay ΔT directly upon inspection of the electron density contours shown in Fig. 7.5.* They appear to vary rather smoothly between ≈ 25 minutes at 275 km and ≈ 45 minutes at 375 km. Since the total content below 530 km has a time delay of ≈ 25 minutes, the losses below 275 km are dominating the picture. Stubbe [1970] suggests on theoretical grounds that ΔT should be ≈ 12 minutes at 300 km and ≈ 50 minutes at 600 km. The values of ΔT extracted from the present eclipse experiment, as well as the prediction of Stubbe, are plotted in Fig. 7.7. One immediately notes that the experimental values of ΔT are roughly twice the theoretical ones in the overlapping height region. One also sees that the values of ΔT deduced from the rotational isopleths follow a path which exhibits considerable curvature such that ΔT

*The term "time delay," denoted by the symbol ΔT , refers to the time difference between the obscuration maximum and the electron concentration minimum. The "time constant" is of course the e -folding time.

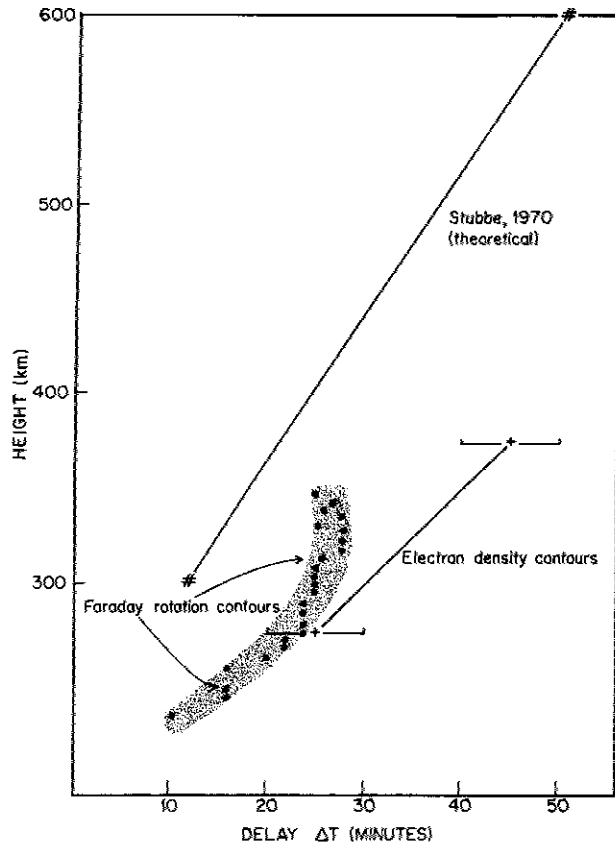


Fig. 7.7 - Time delay between maximum obscuration and electron concentration minimum

approaches a constant above 300 km. Several factors may contribute to this behavior. Of primary importance, however, is that the largest electron-content diminution occurs below 275 km, and so the Faraday effect at great heights will be heavily weighted toward the lower ionospheric response.

The values of ΔT discussed in this chapter are not exceedingly accurate, since no Faraday profiles were obtained between ≈ 1400 and ≈ 1422 EST, a rather crucial region of time. Nevertheless, due to the large temporal extent of the eclipse biteout, nine profiles were fortunately located within the region of interest. Referring to Fig. 7.4 and assuming that to first order the biteout at each altitude would be symmetrical, all questionable isopleths were appropriately smoothed. Thus more data points could help determine the shape of the rotational extrema in the biteout region. The general consistency of the data implies that the trend of the observed ΔT 's, suggested by the shaded area, represents Nature rather well, at least insofar as the Faraday rotational response is concerned. Although the values of ΔT are interesting, they are not directly useful in the determination of β , since (a) the electronic production term becomes significant for the larger values of ΔT and (b) they cannot be obtained with sufficient accuracy.

The electron continuity equation relates the rate of change of the electron density with certain loss and production processes. If one takes $q(t)$ to be the production of electrons and $L(t)$ to represent the loss of electrons, then in the absence of significant movement (given by $\text{div } N_v$), one has

$$dN/dt = q(t) - L(t) \quad (7.4)$$

Assuming that an attachmentlike process describes $L(t)$ and that in the neighborhood of maximum obscuration $q \approx 0$, then a simple differential equation to describe the electron concentration is

$$dN/dt \approx -\beta N, \quad (7.5)$$

to which the solution is of course

$$N = N_0 e^{-\beta t}. \quad (7.6)$$

Referring to Fig. 7.5, one notes that dN/dt is greatest in the vicinity of maximum phase, owing to the occurrence of a minimum in electron production. Using values of dN/dt and N in this region, it is possible to determine β as a function of height using Eq. (7.5). Fig. 7.8 is a plot of the electron density distributions obtained at maximum phase and at times preceding that time by 4 and 14 minutes. The distributions range between ≈ 250 and ≈ 500 km with the peak F-region densities naturally occurring prior to maximum phase. A triangular (three-point) smoothing function* was applied to points below 300 km and to points above 420 km, where the electron density slopes were greatest. Trapezoidal (five-point) smoothing was applied to points in the vicinity of the F2 maximum, since the data were more closely spaced in that region.

From the distributions given in Fig. 7.8, it is possible to deduce $(1/N)dN/dt$, and the results are plotted in Fig. 7.9. One notes that the present determination of β ,

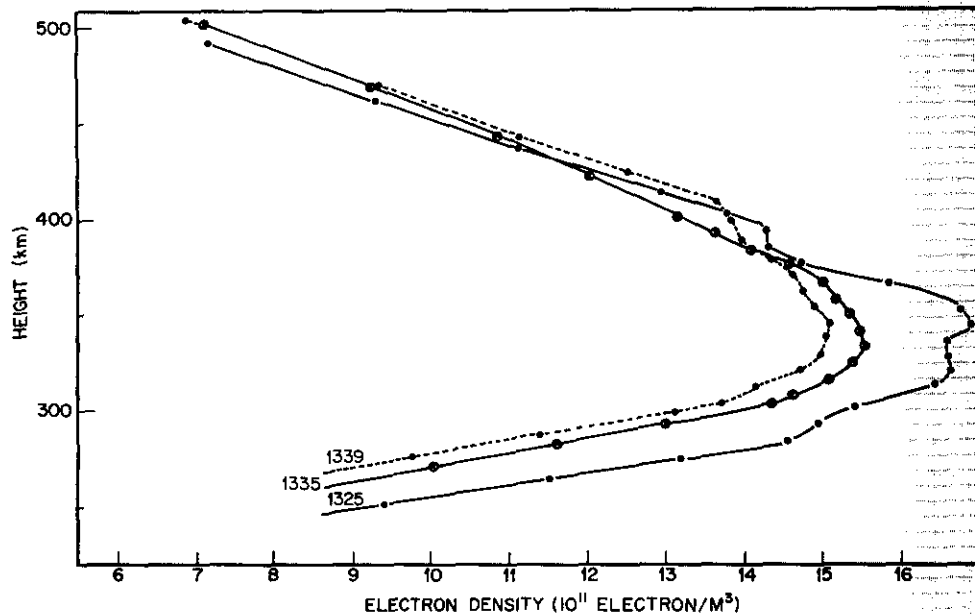


Fig. 7.8 - Electron density distributions in the temporal neighborhood of maximum phase

*Assuming $N_1, N_2, N_3, \dots, N_\zeta, \dots$ to be a set of unsmoothed electron densities, triangular smoothing of the ζ th value was accomplished as follows: $\hat{N}_\zeta = 0.25N_{\zeta-1} + 0.5N_\zeta + 0.25N_{\zeta+1}$. In like manner the five-point trapezoidal smoothing followed the prescription $\hat{N}_\zeta = 0.125N_{\zeta-2} + 0.25N_\zeta + 0.25N_{\zeta+1} + 0.125N_{\zeta+2}$. Data-point accuracy of the order of 5% was obtained after smoothing.

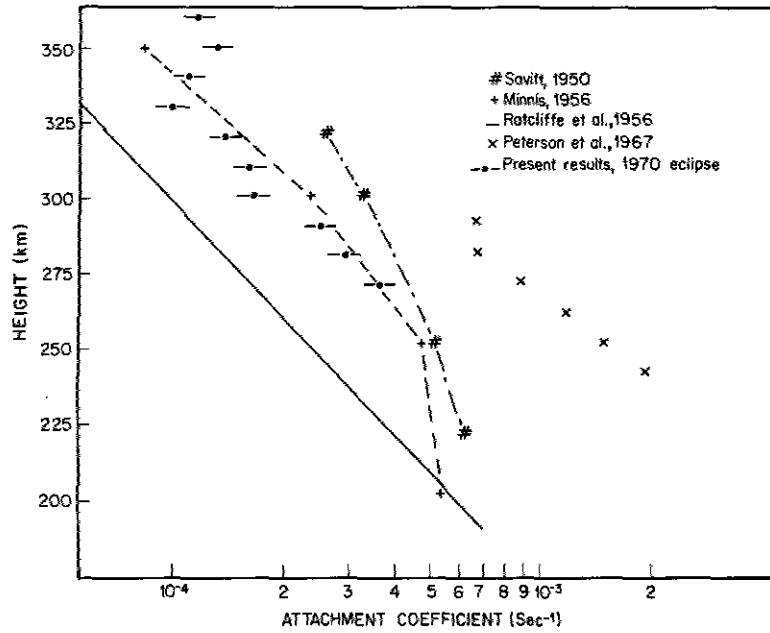


Fig. 7.9 - Attachment coefficient versus altitude

plotted with the horizontal error bars, are in close agreement with those of Minnis [1956], which were based on ionosonde data. Also shown are eclipse results obtained by Savitt [1950] using an ionosonde and a model proposed by Ratcliffe et al. [1956]. Although the Randle Cliff values are about twice as large as those due to Ratcliffe et al., the e -folding distance is roughly the same, namely, 50 km. Because the Ratcliffe model was based on nocturnal observations and the Randle Cliff values were obtained during the day, one would not look for especially good agreement between the two. Furthermore, a nonvanishing production term in the Randle Cliff analysis will increase the present values even more when taken into account. Clearly the discrepancy in the Randle Cliff values and the Ratcliffe model is real, and may be due to a temperature dependence of β . It might also result from the fact that the constitution of the ionosphere exhibits a diurnal variability. The movement term $\text{div } Nv$ might also play a substantial role in the nocturnal observations, since density changes are generally smaller and less rapid than corresponding changes during a solar eclipse.

The Randle Cliff determinations of β are thought to be the first obtained at a mid-latitude Thomson scatter using the solar eclipse method. The Thomson scatter-solar eclipse method has been employed over the magnetic equator, however, and somewhat larger values were obtained (Peterson et al. [1967]). No detailed comparison of the mid-latitude and equatorial results can be made, since the divergence terms, if important, would be expected to be quite dissimilar.

CONCLUDING REMARK

The solar eclipse occurred on a day which was moderately disturbed, ΣK_{F_2} being 33. This activity may have induced an additional perturbation taking the form of TID. In fact, a periodicity of ≈ 70 minutes was observed (Fig. 7.4) to be superimposed upon the eclipse excursion. Chimonas and Hines [1970] have proposed that the March eclipse should produce gravity waves, and these might result in observable TID. However, since the initial wavelike perturbation preceded the eclipse by several hours and since the perturbation would be expected to have the form of a bow wave (or wavelets), the

waves observed at Randle Cliff were probably unrelated to the eclipse excursion. Chimonas and Hines suggest that maximum energy associated with the gravity waves should be centered more or less in California. In this regard, Davis and Da Rosa [1970] have detected wave motions in the total content measured from Stanford; the wave period was about 20 minutes.

EPILOGUE

During the preceding decade the topside ionosphere has been examined by Thomson scatter radars, satellites, and infrequent rocket probes. Satellites yield excellent geographic coverage but inadequate local coverage. On the other hand, Thomson scatter radars, such as the Randle Cliff facility described herein, are able to examine the local ionosphere with great fidelity and are less expensive to operate per unit of information obtained. Furthermore, Thomson scatter systems are tailor-made for studies of traveling ionospheric disturbances (TID). The Randle Cliff Radar (RCR) is a unique system by virtue of its combined location and operating frequency. The Faraday rotation technique in conjunction with Thomson scatter has been adopted for deducing electron density profiles over Randle Cliff. This combination when employed at a frequency of 140 MHz is about optimum over middle latitudes and yields values of electron density which are unaffected by electron and ionic temperatures.

In this regard the RCR is the only midlatitude facility in the world engaged in studies using Faraday rotation. The only other facility in the world conducting similar Faraday rotation measurements on a routine basis is at Jicamarca, Peru, on the magnetic equator. However, since the ionospheric characteristics over the equator are far different from those over midlatitudes, there is little duplication of effort. The Jicamarca facility possesses greater antenna gain and presently has the more sophisticated data processing equipment. In addition the capability of the RCR to produce estimates of drift velocities and ionic temperatures has not been fully developed. Other major Thomson scatter facilities which do not employ Faraday rotation are Millstone Hill (Massachusetts), SRI (California), Arecibo (Puerto Rico), Malvern (Great Britain), and the French bistatic system at St. Santin.

In this report the potential of the Faraday rotation technique when used in conjunction with Thomson scatter at midlatitudes has been investigated. Constraints upon the method were explored and a new alternative scheme for deducing electron densities has been presented which involves Faraday dispersion. Although it is not clear how this procedure may be used in the solution of new problems in aeronomy, it will at least be useful as a backup procedure when more traditional methods fall or give questionable results. In addition a comparison of the rotational derivative and Faraday dispersion methods should yield estimates of statistical error which is encountered in the data analysis. Both methods may be refined by fitting a quasi-sinusoidal curve to the data and thereby extracting deviations from the average behavior. Although the computer routines required for this procedure are rather trivial, the interpretation of the results is not so apparent, and more work is required in this area.

Fluctuations in the contents $\int_0^{\infty} N dh$ and $\int_0^{400} N dh$ were compared by evaluating the Faraday rotation associated with ATS-5 transmission at 137 MHz as well as the 139-MHz RCR data. From the comparison, it was evident, not unexpectedly, that irregularities generally reside in the lower ionosphere. The most significant aspect of this type of experiment is that it represents the first step in comparing strictly ionospheric electron content with the exospheric electron content using the methods of Faraday rotation and Thomson scatter. Its relevance is secured by the fact that the upper limit of conventional Thomson scatter radars is 800 to 1000 km, except perhaps at Jicamarca, where $T_e/T_i \approx 1$ at great heights and profiles to almost an earth's radius have been obtained. Indications of electrodynamic drift, ionic diffusion, or particle precipitation through the

boundary defined by the Thomson scatter upper limit may be provided by further experiments of this type. It is remarked that the antenna elevation at which the experiment was conducted at Randle Cliff was about 38° and as a consequence the signal-to-noise ratio was reduced to an unacceptable level about 400 km. A future experiment might involve illumination of the moon at maximum declination to obtain the cislunar electron content at more appropriate elevation angles while simultaneously conducting Thomson scatter observations. In addition to polarization fading, the lunar signals will undergo rather rapid librational fluctuations associated with surface roughness, but these will average out for normal integration times. The only foreseeable troublesome feature of this proposal would be the lunar motion; however, since the RCR antenna is fully steerable, this motion may be compensated for.

In the chapter on traveling ionospheric disturbances (TID) several points were made. The TID were found to be a regular feature of the ionosphere, and one concludes, as have others, that one source of these wavelike disturbances is energy leakage from the auroral zone. The chapter emphasized that during the period of the present observations the magnetic activity was generally low; thus no obvious relationship between wave amplitude and magnetic index could be ascertained. Certain observable features of TID theory were elucidated in light of the RCR latitude, and special emphasis was placed upon the relationship between fluctuation amplitude (either in terms of rotational isopleths or electron densities directly), wave period, and wavelength. Experimental evidence to support some of these properties was presented. For example, one concluded that the electron-density wave amplitude is an increasing function of wave period and that the fluctuation is out of phase with layer height changes at least for the longer period disturbances. For a particular case a relation between layer height fluctuation and wave amplitude was deduced, and this information was used to estimate the vertical "wavelength" associated with the disturbances. The measurements of TID disclosed in this report represent the first midlatitude effort to detect wave motions in electron density using the Thomson scatter/Faraday rotation technique. Clearly the isopleth fluctuations which have been observed by this method are directly related to fluctuations in electron density alone; that is, the values of electron density obtained at Randle Cliff are not obscured by unknown variations in the ratio of T_e to T_i . A program to extract the ratio T_e/T_i is being initiated, and it is hoped that it will uncover the suspected interrelationship between fluctuations in T_e/T_i and electron density.

One of the most rewarding aspects of any research is that unexpected or anomalous behavior is sometimes uncovered. For example, a peculiar noontime decay in content was observed over Randle Cliff on December 16, 1969, not unlike the well known midday biteout. Although well known, the midday biteout still lacks an unassailable explanation. As mentioned in this report, some theoretical work by Kohl and King as well as an experimental effort by the French group at St. Santin suggest that neutral winds may play a role. However, the symmetry of Randle Cliff biteout about local noon and the apparent layer motion, its short duration, and its occurrence in winter imply that other mechanisms should be given equal consideration in the present case. Other candidates include electrodynamic drifts arising from horizontal E fields and atmospheric oscillations arising from solar thermal action. A long-term experiment designed to study this phenomenon in detail is being considered; it will involve the determination of electron density profiles, drift velocities, and ionic temperatures.

The solar eclipse of March 7, 1970, provided a unique opportunity to investigate the ionospheric response at sunspot maximum using the Randle Cliff approach. Among the effects observed was a decrease of $\approx 27\%$ in electron content and a time delay between maximum obscuration and minimum density, which increased with height, revealing an electronic delay controlled by an exponentially decreasing attachmentlike process. Although the vertical diffusion due to distribution collapse was not sufficient to produce a local enhancement in electron density, the electron density contours and other data suggest that a downdrift was in progress during the eclipse. It was found, however, that

this contribution to the subpeak content could be neglected to a good approximation, since the diminution above 530 km was only about 2% of the total ionospheric electron content. Both slab thickness and layer height were found to be enhanced during the period of bite-out; these enhancements imply that electron loss by attachment is dominant at least as high as the F2 maximum. Values of the attachment coefficient β were obtained by solving the continuity equation at maximum phase under the assumption that the electron production and movement terms are negligible. The height dependence for β obtained by this method is in agreement with values due to some workers but is in disagreement with values over Jicamarca. It is emphasized that this discrepancy may result from the very real differences between the midlatitude and equatorial ionospheres. For example, the two regions are subject to distinctly different forms of the movement term, and the ionic constitution may be quite dissimilar owing to seasonal effects and differing solar activity.

APPENDIX

DERIVATION OF POLARIZATION ROTATION IN A MAGNETOIONIC MEDIUM

The formulation for the index of refraction relevant to the earth's ionosphere is derived in this appendix. The so-called Faraday rotation of a linearly polarized radio-wave will be seen to result from the ionosphere being a magnetoionic medium with an anisotropy introduced by the magnetic field. It will turn out that the index of refraction is essentially double valued with one value corresponding to the ordinary mode and the other corresponding to the extraordinary mode. For the simple case in which the wave vector is parallel to magnetic field lines, the ordinary and extraordinary modes represent oppositely rotating circularly polarized radiowaves. The Faraday effect (polarization rotation) arises because these two modes travel with slightly different phase velocities in the ionosphere.

Before proceeding with the derivation, we assume that the medium is lossless, i.e., the electrons do not suffer collisions which would introduce a damping term into their equation of motion, and that the radiowave magnetic field B_γ is assumed negligible in comparison with the earth's field B . Thus the electronic motion is governed by

$$m\dot{\mathbf{x}} = e [\mathbf{E} + (\dot{\mathbf{x}} \times \mathbf{B})], \quad (\text{A1})$$

where e is the electronic charge (1.602×10^{-19} coulomb), m is the electronic mass (9.109×10^{-31} kg), and \mathbf{E} is the electric field associated with the electromagnetic wave, \mathbf{B} is the static geomagnetic field, \mathbf{x} is the electronic position vector, and the dot notation is used to represent time derivatives of various orders, with $\dot{\mathbf{x}}$ being the velocity and $\ddot{\mathbf{x}}$ being the acceleration. Furthermore, throughout this appendix, mks units will be used, to be consistent with other more detailed studies of radiowave propagation in the ionosphere. The term $e(\dot{\mathbf{x}} \times \mathbf{B})$ is the most important force in magnetoionic theory, since without it the anisotropy of the ionosphere would not exist. Clearly, both electronic and ionic motion is helical with respect to \mathbf{B} ; however, one is not concerned with the heavy ions, since in the present context they are completely unimportant in view of their sluggish response to high-frequency radiowaves.

Additionally it will be assumed for the sake of simplicity that the radiowave is directed parallel to local magnetic lines of force (the propagation will be said to be longitudinal). As a result both the \mathbf{E} and the \mathbf{B}_γ fields associated with the electromagnetic wave will have no components along the direction of propagation, and the two magnetoionic modes will be perfectly circular. In general, the two modes are elliptical, and the propagation under almost all reasonable conditions may be described as quasi-longitudinal. Conditions for quasi-longitudinal propagation are discussed at the end of this appendix. Finally, at the termination of the derivation it shall be most convenient to employ the high-frequency approximation, which in brief requires that $\omega \gg \omega_p$ and $\omega_p \gg \omega_g$, where ω is the radian radio frequency, and where ω_p and ω_g are the radian plasma and gyro frequencies respectively. Matrix representations will be used wherever possible to exhibit the tensorial character of certain quantities such as the dielectric permittivity and the ac conductivity.

The electric field oscillations and the electronic velocity are taken to have a harmonic time dependence of the form

$$\begin{bmatrix} \mathbf{E} \\ \dot{\mathbf{x}} \end{bmatrix} = \begin{bmatrix} E_0 \\ \dot{\mathbf{x}}_0 \end{bmatrix} e^{i\phi} e^{i\omega t} e^{-i\mathbf{k} \cdot \mathbf{s}}, \quad (\text{A2})$$

where \mathbf{k} is the wave vector whose magnitude is simply ω/v or $\omega n/c$ and whose direction is defined by the radiowave path. Using Eq. (A1) together with Maxwell's equations, one is now equipped to deduce the form of n , the index of refraction, through the solution Eq. (A2). Choosing a coordinate system as indicated by Fig. A1, one may write Eq. (A1) in component form as

$$i\omega \begin{pmatrix} \dot{x}_1 \\ \dot{x}_2 \\ \dot{x}_3 \end{pmatrix} = \frac{e}{m} \left\{ \begin{pmatrix} E_1 \\ E_2 \\ 0 \end{pmatrix} + \begin{bmatrix} \dot{x}_1 \\ \dot{x}_2 \\ \dot{x}_3 \end{bmatrix} \times \begin{pmatrix} 0 \\ 0 \\ B \end{pmatrix} \right\}. \quad (\text{A3})$$

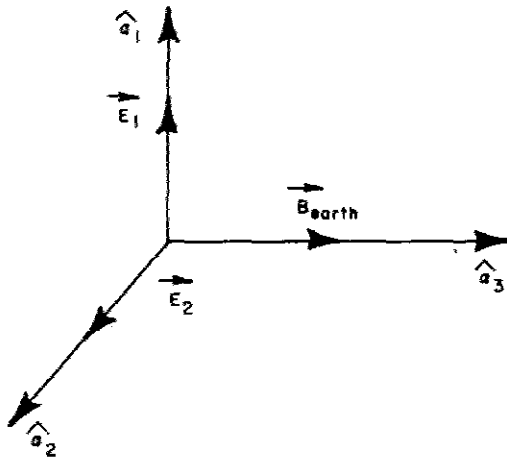


Fig. A1 - Coordinate System

In the above expression, the E_3 component has been excluded, since for a wave normal parallel to the earth's field ($\mathbf{B} \cdot \hat{a}_3 = B$), it may be shown to vanish (see for example Budden [1964]). To show that E_3 vanishes is simple, but it serves no purpose to introduce such a marginally instructive complication in the context of this derivation. Carrying out the cross product in Eq. (A3), one has

$$i\omega \begin{pmatrix} \dot{x}_1 \\ \dot{x}_2 \\ \dot{x}_3 \end{pmatrix} = \frac{e}{m} \begin{pmatrix} E_1 + x_2 B \\ E_2 - x_1 B \\ 0 \end{pmatrix}. \quad (\text{A4})$$

Clearly $\dot{x}_3 = 0$, and the other two components \dot{x}_1 and \dot{x}_2 are obtained by solving the first two component equations in Eq. (A4) simultaneously. One finds that

$$\begin{pmatrix} \dot{x}_1 \\ \dot{x}_2 \\ \dot{x}_3 \end{pmatrix} = \begin{pmatrix} \frac{i\omega E_1 \left(\frac{e}{m}\right) + E_2 B \left(\frac{e}{m}\right)^2}{\left(\frac{eB}{m}\right)^2 - \omega^2} \\ \frac{i\omega E_2 \left(\frac{e}{m}\right) - E_1 B \left(\frac{e}{m}\right)^2}{\left(\frac{eB}{m}\right)^2 - \omega^2} \\ 0 \end{pmatrix} \tag{A5}$$

Note that a resonance (gyroresonance) exists for $\omega = eB/m$. This is called the electron cyclotron frequency ω_g and represents the rate at which electrons spiral about magnetic lines of force. In the ionosphere, B is the order of 0.5 gauss (10^{-4} weber/m²), and since $e/m = 1.759 \times 10^{11}$ coulombs/kg, the electronic gyrofrequency $\omega_g/2\pi$ is about 1.42 MHz. The protonic gyrofrequency is similarly found to be only about 785 Hz and is immaterial at high frequencies and above (i. e., for $\omega/2\pi$ above 3 MHz).

Maxwell's second curl equation

$$\nabla \times \mathbf{H} = \dot{\mathbf{D}} = \epsilon_0 \dot{\mathbf{E}} + \mathbf{J}, \tag{A6}$$

where ϵ_0 is the permittivity of free space (8.85×10^{-2} farad/m), the dielectric constant being ϵ/ϵ_0 , and \mathbf{J} is the current density. This equation will be helpful in deducing the tensor permittivity ϵ_{jk} . (Alternatively, one could have written Eq. (A6) as $\nabla \times \mathbf{H} = \epsilon_0 \dot{\mathbf{E}} + \dot{\mathbf{P}}$ where \mathbf{P} is the polarization of the medium. This procedure is followed by Davies [1965] in his monograph.) Furthermore, since $\mathbf{J} = Ne\dot{\mathbf{x}}$, and $\dot{\mathbf{x}}$ is given in Eq. (A5), the job is almost done. First, one can write Eq. (A5) as a product of a three-by-three tensor with the vector \mathbf{E} :

$$\begin{pmatrix} \dot{x}_1 \\ \dot{x}_2 \\ \dot{x}_3 \end{pmatrix} = \left[\begin{matrix} \frac{e}{m} & \left(\frac{e}{m}\right)^2 \frac{B}{i\omega} & 0 \\ \omega_g^2 - \omega^2 & \omega_g^2 - \omega^2 & 0 \\ \frac{e}{m} & \left(\frac{e}{m}\right)^2 \frac{B}{i\omega} & 0 \\ \omega_g^2 - \omega^2 & \omega_g^2 - \omega^2 & 0 \\ 0 & 0 & \Delta \end{matrix} \right] \begin{pmatrix} E_1 \\ E_2 \\ 0 \end{pmatrix} \tag{A7}$$

where Δ will be determined. The tensor in Eq. (A7) must be proportional to the identity matrix as $B \rightarrow 0$ since in that instance Eq. (A7) obviously reduces to Eq. (A3) without the $\dot{\mathbf{x}} \times \mathbf{B}$ term. Thus, $\Delta = -e/m\omega^2$ to satisfy this condition. The electron current density $\mathbf{J} = Ne\dot{\mathbf{x}}$ is related to the electric field \mathbf{E} through a conductivity tensor σ_{jk} , which is essentially the bracketed term in Eq. (A7) apart from a factor Ne . Since one is ignoring collisions, σ_{jk} is especially simple. That is,

$$\mathbf{J} = Ne \dot{\mathbf{x}} = \sigma_{jk} \mathbf{E} = \begin{pmatrix} \sigma_{11} & -i\sigma_{12} & 0 \\ i\sigma_{12} & \sigma_{11} & 0 \\ 0 & 0 & \sigma_{33} \end{pmatrix} \begin{pmatrix} E_1 \\ E_2 \\ E_3 \end{pmatrix}, \quad (\text{A8})$$

where

$$\sigma_{11} = i\omega \epsilon_0 \frac{Ne^2/m\epsilon_0}{\omega_g^2 - \omega^2} = i\omega \epsilon_0 \frac{\omega_p^2}{\omega_g^2 - \omega^2},$$

$$\sigma_{12} = \frac{ieB}{m} \epsilon_0 \frac{Ne^2/m\epsilon_0}{\omega_g^2 - \omega^2} = i\epsilon_0 \frac{\omega_g \omega_p^2}{\omega_g^2 - \omega^2},$$

and

$$\sigma_{33} = -i \epsilon_0 \frac{Ne^2/m\epsilon_0}{\omega} = -i \epsilon_0 \frac{\omega_p^2}{\omega}$$

upon introduction of the so-called plasma frequency

$$\omega_p = \sqrt{Ne^2/m\epsilon_0}.$$

Thus, from Eqs. (A6) and (A8),

$$\nabla \times \mathbf{H} = \begin{pmatrix} i\omega \epsilon_0 + \sigma_{11} & -i\sigma_{12} & 0 \\ i\sigma_{12} & i\omega \epsilon_0 + \sigma_{11} & 0 \\ 0 & 0 & \sigma_{33} \end{pmatrix} \begin{pmatrix} E_1 \\ E_2 \\ 0 \end{pmatrix} \quad (\text{A9})$$

or for simplicity

$$\nabla \times \mathbf{H} = i\omega \epsilon_0 \mathbf{K}_{jk} \mathbf{E} = i\omega \epsilon_{jk} \mathbf{E},$$

where

$$\mathbf{K}_{jk} = \begin{pmatrix} 1 + \frac{\sigma_{11}}{i\omega \epsilon_0} & -\frac{\sigma_{12}}{\omega \epsilon_0} & 0 \\ \frac{\sigma_{12}}{\omega \epsilon_0} & 1 + \frac{\sigma_{11}}{i\omega \epsilon_0} & 0 \\ 0 & 0 & \frac{\sigma_3}{i\omega \epsilon_0} \end{pmatrix} \quad (\text{A10})$$

To illuminate certain features of the tensor $\epsilon_{jk} = \epsilon_0 K_{jk}$, which may be referred to as the dielectric permittivity tensor, it will be convenient to return to the notation involving ω_g and ω_p :

$$K_{jk} = \begin{pmatrix} 1 + \frac{\omega_p^2}{(\omega_g^2 - \omega^2)} & \frac{-i\omega_g \omega_p^2}{\omega(\omega_g^2 - \omega^2)} & 0 \\ \frac{i\omega_g \omega_p^2}{\omega(\omega_g^2 - \omega^2)} & 1 + \frac{\omega_p^2}{\omega_g^2 - \omega^2} & 0 \\ 0 & 0 & 1 - \frac{\omega_p^2}{\omega^2} \end{pmatrix} \quad (A11)$$

Note that if $B \rightarrow 0$, then $\omega_g = eB/m \rightarrow 0$, and

$$\lim_{B \rightarrow 0} \epsilon_{jk} = \epsilon_0 \left[1 - \left(\frac{\omega_p}{\omega}\right)^2 \right] \quad (A12)$$

which in turn goes to ϵ_0 for sufficiently large radio frequencies.

Maxwell's first curl equation

$$\nabla \times \mathbf{E} = -\dot{\mathbf{B}} = -i\omega \mathbf{B} = -i\omega \mu_0 \mathbf{H}, \quad (A13)$$

where the medium is assumed nonmagnetic (μ_0 being the magnetic permittivity of free space and equal to $4\pi \times 10^{-7}$ henrys/meter). This equation implies that $\mathbf{H} = (i\nabla \times \mathbf{E})/\omega\mu_0$. Thus $\nabla \times \mathbf{H} = i\omega \epsilon_{jk} \mathbf{E} = i/\omega \mu_0 (\nabla \times \nabla \times \mathbf{E})$ and

$$(\text{curl curl} - \omega^2 \mu_0 \epsilon_{jk}) \mathbf{E} = 0. \quad (A14)$$

Now $\nabla \times \nabla \times \mathbf{E} = \nabla(\nabla \cdot \mathbf{E}) - \nabla^2 \mathbf{E}$. Maxwell's divergence equation $\nabla \cdot \mathbf{E} = \rho$ implies $\nabla \times \nabla \times \mathbf{E} = -\nabla^2 \mathbf{E}$, since the ionosphere is considered to be electrically neutral, and no net space charge may exist ($\rho = 0$). The coordinate system was chosen so that derivatives of field quantities (such as \mathbf{E}) would be zero in the \hat{a}_1 and \hat{a}_2 directions, and from Eq. (A2):

$$\nabla \times \nabla \times \mathbf{E} = (-i)^2 \mathbf{k} \times \mathbf{k} \times \mathbf{E} = \left(\frac{\omega n}{c}\right) \mathbf{E}$$

where \mathbf{k} is parallel to a_3 by

$$\left[\begin{array}{c} \left(\frac{\omega}{c} \right)^2 \begin{pmatrix} n^2 & 0 & 0 \\ 0 & n^2 & 0 \\ 0 & 0 & 0 \end{pmatrix} \\ -\omega^2 \mu_0 \epsilon_0 \end{array} \right] \begin{pmatrix} 1 + \frac{\omega_p^2}{(\omega_g^2 - \omega^2)} & \frac{-i\omega_g \omega_p^2}{(\omega_g^2 - \omega^2)} & 0 \\ \frac{i\omega_g \omega_p^2}{(\omega_g^2 - \omega^2)} & 1 + \frac{\omega_p^2}{(\omega_g^2 - \omega^2)} & 0 \\ 0 & 0 & 1 - \frac{\omega_p^2}{\omega^2} \end{pmatrix} \begin{pmatrix} E_1 \\ E_2 \\ E_3 \end{pmatrix} = 0 \quad (\text{A15})$$

Since $\omega_g/2\pi \approx 1.4$ MHz, then if $\omega/2\pi \geq 50$ MHz, the term $\omega_g^2 - \omega^2 \approx -\omega^2$. At the radar frequency employed during this research (138.6 MHz) the difference between $\omega_g^2 - \omega^2$ and $-\omega^2$ is about 0.01% of ω^2 . Because ω_g^2 can be neglected with respect to ω_g^2 in the denominators of the components ϵ_{11} , ϵ_{12} , ϵ_{21} , and ϵ_{22} , Eq. (A15) is equivalent to

$$\begin{pmatrix} \left(\frac{\omega}{c} \right)^2 n^2 - \omega^2 \mu_0 \epsilon_0 \left[1 - \left(\frac{\omega_p}{\omega} \right)^2 \right] & i\omega^2 \mu_0 \epsilon_0 \left(\frac{\omega_p}{\omega} \right) \left(\frac{\omega_p}{\omega} \right)^2 & 0 \\ -i\omega^2 \mu_0 \epsilon_0 \left(\frac{\omega_g}{\omega} \right) \left(\frac{\omega_g}{\omega} \right)^2 & \left(\frac{\omega}{c} \right)^2 n^2 - \omega^2 \mu_0 \epsilon_0 \left[1 - \left(\frac{\omega_p}{\omega} \right)^2 \right] & 0 \\ 0 & 0 & -\omega^2 \mu_0 \epsilon_0 \left[1 - \left(\frac{\omega_p}{\omega} \right)^2 \right] \end{pmatrix} \begin{pmatrix} E_1 \\ E_2 \\ E_3 \end{pmatrix} = 0 \quad (\text{A16})$$

Since $E \neq 0$, the determinant of the coefficient matrix must be zero. Expanding this determinant, one obtains

$$\begin{aligned} & n^4 \left\{ -\omega^2 \mu_0 \epsilon_0 \left(1 - \frac{\omega_p^2}{\omega^2} \right) \left(\frac{\omega}{c} \right)^4 \right\} + \left\{ 2n^2 \left[\omega^2 \mu_0 \epsilon_0 \left(1 - \frac{\omega_p^2}{\omega^2} \right) \right]^2 \left(\frac{\omega}{c} \right)^2 \right\} \\ & + \left\{ \left[\omega^2 \mu_0 \epsilon_0 \left(1 - \frac{\omega_p^2}{\omega^2} \right) \right] \left[\omega^2 \mu_0 \epsilon_0 \left(\frac{\omega_g}{\omega} \right) \left(\frac{\omega_p}{\omega} \right)^2 \right]^2 - \left[\omega^2 \mu_0 \epsilon_0 \left(1 - \frac{\omega_p^2}{\omega^2} \right) \right]^3 \right\} = 0 \end{aligned} \quad (\text{A17})$$

Solving this, one finds that

$$n^2 = \left(\frac{c}{\omega} \right)^2 \left\{ \left[\omega^2 \mu_0 \epsilon_0 \left(1 - \frac{\omega_p^2}{\omega^2} \right) \right] \mp \left[\omega^2 \mu_0 \epsilon_0 \left(\frac{\omega_g}{\omega} \right) \left(\frac{\omega_p^2}{\omega^2} \right) \right] \right\} \quad (\text{A18})$$

Since the free-space velocity of light $c = (\mu_0 \epsilon_0)^{-1/2}$, one finds that

$$n^2 = 1 - \left(\frac{\omega_p^2}{\omega^2} \right) \mp \left(\frac{\omega_g}{\omega} \right) \left(\frac{\omega_p^2}{\omega^2} \right) \quad (\text{A19a})$$

where

$$n_o^2 = 1 - \left(\frac{\omega_p^2}{\omega^2} \right) \left[1 + \left(\frac{\omega_p}{\omega} \right) \right] \quad (\text{A19b})$$

and

$$n_x^2 = 1 - \left(\frac{\omega_p^2}{\omega^2} \right) \left[1 - \left(\frac{\omega_g}{\omega} \right) \right], \quad (\text{A19c})$$

in which n_o refers to the ordinary mode and n_x refers to the extraordinary mode. Since in the ionosphere the electron density is usually less than 3×10^{12} electrons/m³ at the F2 maximum, it follows that the corresponding plasma frequency $\omega_p = \sqrt{Ne^2/m\epsilon_0}$ is less than about $15.5 \text{ MHz}/2\pi = f_p/2\pi$. At a radar frequency of 138.6 MHz, ω_p^2/ω^2 is about 1.25×10^{-2} . Thus, one may expand Eqs. (A19b) and (A19c) in Taylor series, excluding all powers of $(\omega_p^2/\omega^2)[1 \pm (\omega_g/\omega)]$ higher than the first, that is

$$n_o = 1 - \frac{1}{2} \left(\frac{\omega_p}{\omega} \right)^2 \left[1 - \frac{\omega_g}{\omega} \right], \quad (\text{A20a})$$

and

$$n_x = 1 - \frac{1}{2} \left(\frac{\omega_p}{\omega} \right)^2 \left[1 + \left(\frac{\omega_g}{\omega} \right) \right]. \quad (\text{A20b})$$

The ordinary mode, whose index of refraction is n_o , is right-hand circularly polarized, and the extraordinary mode, whose index is n_x , is left-hand circularly polarized, assuming that the wave vector \mathbf{k} is parallel to \mathbf{B} . Note that the phase velocity $v_o = c/n_o$ associated with the ordinary mode is closer to the free-space value than is the extraordinary mode phase velocity $v_x = c/n_x$.

Using standard ionospheric terminology, that is,

$$\left(\frac{\omega_p}{\omega} \right)^2 = X, \quad \left(\frac{\omega_g}{\omega} \right) = Y,$$

one has that

$$n_o = 1 - \frac{1}{2} X (1 - Y), \quad (\text{A21a})$$

and

$$n_x = 1 - \frac{1}{2} X (1 + Y). \quad (\text{A21b})$$

It is clear that if \mathbf{B} were to vanish, both indices of refraction would be identical, and $n = n_o = n_x$ would describe the refractive index for an isotropic plasma. If N were to approach zero, then regardless of \mathbf{B} one sees that $n = n_o = n_x$ would approach the free space value of unity. The general Appleton-Hartree formula, for which \mathbf{B} makes an angle θ with the wave normal and for which a lossy medium is assumed (Appleton [1927], Hartree [1931]), is given by

$$n^2 = 1 - \frac{X}{1 - iZ - \frac{Y_T^2}{2(1-X-iZ)} \pm \left[\frac{Y_T^4}{4(1-X-iZ)^2} + Y_L^2 \right]^{1/2}} \quad (\text{A22})$$

where

$$X = \left(\frac{\omega_p}{\omega} \right)^2$$

$$Z = \left(\frac{\nu}{\omega} \right),$$

$$Y_L = \left(\frac{\omega_g}{\omega} \right) \cos \theta,$$

and

$$Y_T = \left(\frac{\omega_g}{\omega} \right) \sin \theta.$$

For $\theta = 0$ and $Z = 0$ (no collisions) this expression reduces to Eq. (A21) in the high-frequency approximation. When $\theta = 90^\circ$, one has transverse propagation and when $\theta = 0^\circ$ one has longitudinal propagation. The most useful relations for Faraday rotation studies arise upon consideration of the so-called quasi-longitudinal (QL) mode of propagation. The criterion for QL propagation is obtained on examination of Eq. (A22) for $Z = 0$ and may be written as

$$Y_T^4/4(1-X)^2 \ll Y_L \quad (\text{A23})$$

and

$$\frac{(\omega_g/\omega)^4 \sin^4 \theta}{4 [1 - (\omega_p/\omega)^2]^2} \ll (\omega_g/\omega)^2 \cos^2 \theta. \quad (\text{A24})$$

Inserting $f_p = 10\text{MHz}$, $f_g = 1\text{MHz}$, and $f = 100\text{MHz}$ into Eq. (A24) and carrying out the arithmetic, one finds that QL propagation prevails over approximately all θ . The constraint defined by Eq. (A24) breaks down when the wave normal (propagation path) and the magnetic field vector are within 2° of being orthogonal. Under QL propagation conditions the two characteristic modes become approximately circularly polarized; since n_o and n_x are both less than unity, it follows that the associated phase velocities are greater than the free-space velocity of light, but the extraordinary wave has a slightly greater phase velocity than does the ordinary wave. Faraday rotation results from the "addition" of the ordinary and extraordinary modes. Since $v_x > v_o$, the extraordinary wave appears to have rotated less rapidly than the ordinary wave after having traversed a given distance S . Thus, upon combination of the two modes (each assumed to have the same amplitude), one finds that the net rotation of the resultant linearly polarized radio wave is in the clockwise sense. One says that the medium is levorotatory whenever $\mathbf{B} \cdot \boldsymbol{\Gamma}$ and the ray path vector $\boldsymbol{\Gamma}$ have a nonvanishing positive dot product. If, however, $\mathbf{B} \cdot \boldsymbol{\Gamma} < 0$, one says that the medium is dextrorotatory, and the Faraday rotation is counterclockwise.

After traversing a distance ds in a magnetoionic medium, the magnitudes of the angles formed by the electric vectors of the two characteristic waves are given by

$$d\phi_i = (\omega/2c)n_i ds, \quad i = 0, x, \quad (\text{A25})$$

where ϕ_0 refers to the ordinary wave and is measured in the clockwise sense, and ϕ_x refers to the extraordinary wave and is measured in the counterclockwise sense. For radio frequencies in excess of 100 MHz the angle between the direction of phase propagation (wave normal) and the direction of energy propagation (ray direction) is negligibly small. As a consequence the distinction between the directions of phase and energy propagation may be neglected. In addition the ordinary and extraordinary waves may be expected to propagate over identical paths. If an equal amplitude is assumed for the two waves, the resultant electric vector will rotate by an amount $d\phi$, over the distance ds , given by

$$d\phi = d\phi_0/2 - d\phi_x/2 = (\omega_g/2c) (\omega_p/\omega)^2 \cos\theta ds. \quad (\text{A26})$$

In mks units the differential (Faraday) rotation is given by

$$d\phi = 2.97 \times 10^{-2} f^{-2} NH \cos\theta ds, \quad (\text{A27})$$

where $H = B/\mu_0$ is the magnetic field intensity, assuming free-space magnetic conditions.

Upon integration of Eq. (A27) over a distance S , one may obtain the total Faraday rotation angle

$$\Omega = \int_0^S d\phi = 2.97 \times 10^{-2} f^{-2} \int_0^S HN \cos\theta ds \quad (\text{A28})$$

where H , θ , and N are known functions of distance along the path of propagation, denoted by Γ . (For a superionospheric satellite radiating linearly polarized radio waves toward earth, one sometimes uses ∞ as the upper limit of Eq. (A28).) Surely, $\int H \cos\theta N ds \neq 0$ for the case of quasi-longitudinal propagation. However, Millman [1966] has shown that a nonvanishing amount of rotation may exist in the transverse region. This rotation amounts to about 1% of the maximum longitudinal rotation. To relate Ω to a vertical electron density distribution, one uses the relation

$$ds = dh \sec \chi, \quad (\text{A29})$$

where χ is the local zenith angle and dh is the differential altitude. Substituting $ds \sec \chi$ for ds in Eq. (A28), one obtains

$$\Omega = 2.97 \times 10^{-2} f^{-2} \int_0^h HN \cos\theta \sec \chi dh, \quad (\text{A30})$$

where h is the altitude corresponding to the upper limit in Eq. (A28).

This substitution enables one to discuss vertical electron density functions and is an obvious convenience for comparing results obtained over a variety of values of χ . It must be remembered, however, that any vertical density function $N(h, \Gamma)$ is also a function of the radio path Γ . In the limit of spherical stratification, $N(h)$ is independent of Γ . If one denotes $H \cos\theta \sec \chi$ by Ψ , Eq. (A30) becomes

$$\Omega = 2.97 \times 10^{-2} f^{-2} \int_0^h N \Psi \, dh. \quad (\text{A31})$$

Along each path of wave propagation Γ , Ψ is a continuous function of the measured distance s on Γ ; consequently, from Eq. (A29), Ψ is a continuous function of altitude h . Since $N(h)$ is everywhere positive and Ψ is continuous, one may apply the theorem of the mean to Eq. (A31), provided $N(h)$ is also continuous, and obtain

$$\Omega = 2.97 \times 10^{-2} f^{-2} \bar{\Psi} \int_0^h N \, dh, \quad (\text{A32})$$

where

$$\bar{\Psi} = \frac{\int_0^h \Psi N \, dh}{\int_0^h N \, dh}$$

and is called the magnetic field parameter. Eq. (A32) expresses the Faraday rotation as proportional to the product of $\bar{\Psi}$ and the electron content and inversely proportional to the square of the radio frequency. This implies that $\int N \, dh$ is readily obtainable, provided Ω may be measured unambiguously.

Furthermore, in radar studies one is concerned with the two-way path. Thus, a given electron content or population $\int N \, dh$ yields twice as much rotation as suggested by Eq. (A32) for the one-way path. Hence,

$$\Omega = 5.95 \times 10^{-2} f^{-2} \bar{\Psi} \int_0^h N \, dh \quad (\text{A33})$$

for two-way radar propagation. (Clearly, the rotation incurred following the reflection does not cancel the prereflection rotation, since, although the medium changes from levorotatory to dextrorotatory, the direction of Γ is correspondingly reversed.)

REFERENCES

- Almeida, O. G. , and Da Rosa, A. V. , "Observations of Ionospheric Electron Content During the March 7, 1970, Solar Eclipse, " *Nature* 226, 1115-1116 (1970)
- Appleton, E. V. , URSI Proc, Washington, D. C. , 1927
- Becker, W. , "The Ionosphere above Lindau During the Solar Eclipse on 30 June 1954"--- in "Solar Eclipses and the Ionosphere, " edited by W. J. G. Beynon, and G. M. Brown, London: Pergamon Press, 1956, pp. 36-39
- Becker, W. , Ruster, R. , and Klostermeyer, J. , "Experimental Results on the Dynamics of the F Region, " *Radio Sci.* 69D, 1083-1087 (1965)
- Belrose, J. S. , "The Ionospheric F Region, " in "Physics of the Earth's Upper Atmosphere, " edited by C. O. Hines, I. Paghis, T. R. Hartz, and J. A. Fejer, Englewood Cliffs, N. J. : Prentice-Hall, 1965, pp. 73-95
- Blake, L. V. , "A VHF-UHF Missile- and Space-Research Radar with a 150-foot Steerable Antenna, " NRL Report 5801, Aug. 1962
- Booker, H. G. and Gordon, W. E. , "A Theory of Radio Scattering in the Troposphere, " *Proc. IRE* 38, 401-412 (1950)
- Bowles, K. L. , "Observation of Vertical-Incidence Scatter from the Ionosphere at 41 Mc/sec, " *Phys. Rev. Letters* 1, 454 (1958)
- Browne, I. C. , Evans, J. V. , Hargreaves, J. K. , and Murray, W. A. S. , "Radio Echoes from the Moon, " *Proc. Phys. Soc.* 69B, 901 (1956)
- Budden, K. G. , "Radio Waves in the Ionosphere, " Cambridge, England, Cambridge University Press, 1961
- Budden, K. G. , "Lectures on Magnetoionic Theory, " New York: Gordon and Breach, 1964
- Buneman, O. , "Scattering of Radiation by the Fluctuations in a Nonequilibrium Plasma, " *J. Geophys. Res.* 67, 2050-2053 (1962)
- Chimonas, G. , and Hines, C. O. , "Atmospheric Gravity Waves Induced by a Solar Eclipse, " *J. Geophys.* 75, 875 (1970)
- Cohen, R. , "Determination of Electron Concentration and Magnetic Field Inclination from the Faraday Rotation of an Incoherently Scattered Signal, " (unpublished paper) ITSA ESSA, Boulder, Colorado, 57 pages (1967a)
- Cohen, R. , "Determination of Electron Concentration and Magnetic Field Inclination from the Faraday Rotation of an Incoherently Scattered Signal, " in *Univ. Illinois Aeronomy Rpt. 19*, edited by J. V. Evans, 1967b, pp. 184-188
- Carru, H. , "F2 Region Measurements at St. Santin including Winds", in *Univ. Illinois Aeronomy Report 19*, edited by F.V. Evans, 1967, pp. 149-157

- Davies, K. , "Ionospheric Radio Propagation," National Bureau of Standards Monograph 80, 1965
- Davis, M. J. and Da Rosa, A. V. , "Traveling Ionospheric Disturbances Originating in the Auroral Oval During Polar Substorms," J. Geophys. Res. 74, 5721-5735 (1969)
- Davis, M. J. , and Da Rosa, A. V. , "Possible Detection of Atmospheric Gravity Waves Generated by the Solar Eclipse," Nature 226, 1123 (1970)
- Dessler, A. J. , Nature 184:261 (1959)
- Dyson, P. L. , Newton, G. P. , and Brace, L. H. , "In Situ Measurements of Neutral and Electron Density Wave Structure from the Explorer 32 Satellite," J. Geophys. Res. 75, 3200-3210 (1970)
- Eccles, W. H. , "The Propagation of Long Electric Waves During the Solar Eclipse," Nature 89, 191 (1912)
- Elkins, T. J. , and Slack, F. F. , "Observations of Travelling Ionospheric Disturbances Using Stationary Satellites," J. Atmos. Terrest. Phys. 31, 421-439 (1969)
- Evans, J. V. , "The Measurement of the Electron Content of the Ionosphere by the Lunar Radio Echo Method," Proc. Phys. Soc. London 69B, 953 (1956)
- Evans, J. V. , "The Electron Content of the Ionosphere," J. Atmos. and Terrest. Phys. 11, 259 (1957)
- Evans, J. V. , "An F-Region Eclipse," J. Geophys. Research 70, 131-142 (1965)
- Evans, J. V. , (informal remarks on Thomson scatter studies of the ionosphere.) Univ. Illinois Aeronomy Rpt. 19, edited by J. V. Evans, 1967a, p. 187
- Evans, J. V. , "Design Considerations for a Thomson Scatter Radar," Univ. Illinois Aeronomy. Rpt. 17, 3 (1967b)
- Evans, J.V., "Diurnal and Seasonal Variations of the F Region Over Millstone at Sunspot Minimum", in Univ. Illinois Aeronomy Rpt. 19, edited by J.V. Evans, 1967c, pp. 161-169
- Evans, J. V. , Brockelman, R. A. , Julian, R. F. , and Reid, W. A. , "Determination of F-region Vertical Drifts at Millstone Hill," Radio Sci. 5, 27-38 (1970)
- Farley, D. T. , Jr. , "A Plasma Instability Resulting in Field-aligned Irregularities in the Ionosphere," J. Geophys. Res. 68, 6083-6097 (1963)
- Farley, D. T. , "A Theory of Incoherent Scattering of Radio Waves by a Plasma; 4. - The Effect of Unequal Ion and Electron Temperatures," J. Geophys. Res. 71, 4091-4098 (1966)
- Farley, D. T. , "Faraday Rotation Measurements Using Incoherent Scatter," Radio Sci. , 4(2): 143-152 (1969)
- Fejer, J. A. , "Scattering of Radio Waves by an Ionized Gas in Thermal Equilibrium," Can. J. Phys. 38, 1114-1133 (1960)
- Flaherty, B. J. , Cho, H. R. , and Yeh, K. C. , "Response of the F-Region Ionosphere to a Solar Eclipse," Nature 226, 1121-1123 (1970)

- Rutiser, S. J. , and Goodman, J. M. , "On the Scientific Use of a Satellite Radar System,"
NRL Memorandum Report 1768, Apr. 1967
- Savitt, J. , J. Geophys. Res. 55, 385 (1950)
- Schlederman, H. , "Effect of the Solar Eclipse on Wireless Telegraphic Signals,"
Nature 89, 329 (1912)
- Seddon, J. C. , "A Model of the Quiet Ionosphere," J. Geophys. Res. 68(5), 1339 (1963)
- Skolnik, M. I. , "Introduction to Radar Systems," New York: McGraw-Hill, 1962, pp. 3-4
- Sterling, D. L. , "Traveling Disturbances Observed at Jicamarca," in Univ. Illinois
Aeronomy Rpt. 19, edited by J. V. Evans, 1967, pp. 178-183
- Stubbe, P. "The F Region During an Eclipse--a Theoretical Study," J. Atmos. Terrest.
Phys. 32, 1109-1116 (1970)
- Taylor, G. N. , "Measurements of the Electron Content of the Ionosphere During Some
Magnetically Disturbed Periods in Winter," J. Atmos. Terrest. Phys. 27, 735-743
(1965)
- Thome, G. D. , "Incoherent Scatter Observations of Traveling Ionospheric Disturbances,"
J. Geophys. 69, 4047-4049 (1964)
- Thome, G. , "Long-period Waves Generated in the Polar Ionosphere During the Onset of
Magnetic Storms," J. Geophys. Res. 73, 6319-6336 (1968)
- Vasseur, G. , "Dynamics of the F Region Observed with Thomson Scatter-II. Influence
of Neutral Air Winds on the Ionospheric F Region," J. Atmos. Terrest. Phys. 32,
775-787 (1970)
- Whitten, R. C. , and Poppoff, I. G. , "Physics of the Lower Ionosphere," Englewood
Cliffs, N. J.: Prentice-Hall, 1965, pp. 155-157
- Yeh, K. C. and Gonzalez, V. H. , "Note on the Geometry of the Earth Magnetic Field
Useful to Faraday Effect Experiments," J. Geophys. Res. 65, 3209 (1960)